PNNL-31556 Rev 0
EWG-RPT-031 Rev 0

Enhanced Hanford Low-Activity Waste Glass Property Data Development: Phase 4

July 2021

V Gervasio
JD Vienna
JB Lang
BE Westman
SE Sannoh
RL Russell
DS Kim
SK Cooley
J George
DA Cutforth
SM Baird

Prepared for the U.S. Department of Energy
under Contract DE-AC05-76RL01830

PACIFIC NORTHWEST NATIONAL LABORATORY
operated by
BATTELLE
for the
UNITED STATES DEPARTMENT OF ENERGY
under Contract DE-AC05-76RL01830

Printed in the United States of America

Available to DOE and DOE contractors from the
Office of Scientific and Technical Information,
P.O. Box 62, Oak Ridge, TN 37831-0062;
ph: (865) 576-8401
fax: (865) 576-5728
email: reports@adonis.osti.gov

Available to the public from the National Technical Information Service
5301 Shawnee Rd., Alexandria, VA 22312
ph: (800) 553-NTIS (6847)
email: orders@ntis.gov <https://www.ntis.gov/about>
Online ordering: http://www.ntis.gov

PNNL-31556 Rev 0
EWG-RPT-031 Rev 0

Enhanced Hanford Low-Activity Waste Glass Property Data Development: Phase 4

July 2021

V Gervasio
JD Vienna
JB Lang
BE Westman
SE Sannoh
RL Russell
DS Kim
SK Cooley
J George
DA Cutforth
SM Baird

Prepared for
the U.S. Department of Energy
under Contract DE-AC05-76RL01830

Pacific Northwest National Laboratory
Richland, Washington 99354

Summary

This report presents the results of analyses of data collected on a fourth test matrix of 25 low-activity waste glass compositions intended to expand the composition-property database and to validate the Vienna et al. (2020) property-composition models. The 25 low-activity waste glass compositions were statistically designed to be within the composition region of the 2020 models. The analyses performed on these glasses include chemical composition (for target compositional verification), density, viscosity, electrical conductivity, crystal fraction, canister centerline cooling with crystal identification, product consistency test response, vapor hydration test response, and sulfur solubility. This report discusses the results obtained from these tests.

Acknowledgments

The authors gratefully acknowledge the financial support provided by the U.S. Department of Energy Office of River Protection Waste Treatment Plant Project managed by Tom Fletcher, with technical oversight by Albert Kruger. The authors thank Madison Hsieh of Savannah River National Laboratory for help in the analysis and testing of the glasses. The following Pacific Northwest National Laboratory staff members are acknowledged for their contributions: Tongan Jin for his technical review, Cary Counts for his editorial review, David MacPherson for quality assurance, and Veronica Perez and Chrissy Charron for programmatic support during the conduct of this work.

Acronyms and Abbreviations

AD	acid dissolution
BNI	Bechtel National, Inc.
CCC	container centerline cooling (heat treatment)
CF	crystal fraction
CUA	The Catholic University of America
DI	deionized water
DOE	U.S. Department of Energy
DWPF	Defense Waste Processing Facility
EA	Environmental Assessment
EC	electrical conductivity
EWG	Enhanced Waste Glass
ε	electrical conductivity
η	viscosity
GCR	glass composition region
GFA	glass formulation algorithm
HDI	“How Do I…?”
HLW	high-level waste
IA	image analysis
IC	ion chromatography
ICP-OES	inductively coupled plasma–optical emissions spectroscopy
IHLW	immobilized high-level waste
IL	inner layer
ILAW	immobilized low-activity waste
KH	potassium hydroxide digestion
LAW	low-activity waste
MCC	multiple-component constraints
MSE	mean squared error
NQAP	Nuclear Quality Assurance Program
OL	outer layer
OM	optical microscopy
ORP	Office of River Protection
ρ	density
PCT	Product Consistency Test
PF	sodium peroxide fusion
PL	prediction limit
PNNL	Pacific Northwest National Laboratory

PQM	partial quadratic mixture model
QGCR	qualified glass composition region
SCC	single-component constraints
SFD	space-filling design
SRNL	Savannah River National Laboratory
T_L	liquidus temperature
VHT	Vapor Hydration Test
vol%	volume percent
VFT	Vogel-Fulcher-Tammann
wt%	weight percent
WTP	Hanford Tank Waste Treatment and Immobilization Plant
XRD	x-ray diffraction

Contents

Figures

Tables

1.0 Introduction

The U.S. Department of Energy's (DOE's) Hanford Site in Washington State has roughly 56 million gallons of radioactive wastes managed as high-level waste stored in 177 underground tanks. The Hanford Tank Waste Treatment and Immobilization Plant (WTP) will provide DOE with a capability to treat the waste by vitrification for subsequent disposal. The tank waste will be partitioned into low-activity waste (LAW) and high-level waste (HLW) fractions, which will then be vitrified, respectively, into immobilized low-activity waste (ILAW) and immobilized high-level waste (IHLW) products. The ILAW product will be disposed of in the Integrated Disposal Facility on the Hanford Site, while the IHLW product will be temporarily stored on-site prior to disposal at a national deep geological disposal facility for high-level nuclear waste. The ILAW and IHLW products must satisfy a variety of requirements with respect to regulatory compliance and protection of the environment before they can be accepted for disposal. Additionally, to be efficiently processed in the WTP, the LAW melts must satisfy process-related properties.

Current plans for the WTP envision vitrifying LAW prior to startup of the WTP HLW Facility using a Direct Feed Low-Activity Waste approach (Bernards et al. 2020). The WTP LAW Facility will be operated and controlled using a LAW glass formulation algorithm (GFA), which requires several inputs based on research and development results, plant operations data, and analyzed compositions. Currently, it is envisioned that the preliminary LAW GFA discussed by Kim and Vienna (2012) and the LAW glass property-composition models recommended in Piepel et al. (2007) will be used for commissioning and initial radioactive operations of the LAW Facility under the Direct Feed Low-Activity Waste approach. After commissioning and initial operations, it is intended that an updated LAW GFA will be developed at Pacific Northwest National Laboratory (PNNL) and using the models in Vienna et al. (2020) it will be implemented by the WTP operations contractor in the WTP LAW Facility. The new models represent a significant increase in model validity range, which directly translates to the size of the processing envelope, compared to previously published models (Piepel et al. 2007). An updated LAW GFA will be developed to implement Vienna et al. (2020) models along with several inputs, including the 1) LAW glass formulation methods and constraints, 2) LAW glass property constraints, 3) plant related uncertainties and operating data, and 4) model validity constraints.

The purposes of the present task, Low-Activity Waste (LAW) Phase 4 Matrix Glass Testing, are to improve glass-property/composition data coverage and to validate the composition-property models.

This report presents the glass compositions and glass property data developed in Phase 4 of the enhanced Hanford LAW glass property data development effort as well as how well these data fit to the new models.

This work was performed in accordance with the *Pacific Northwest National Laboratory (PNNL) Nuclear Quality Assurance Program (NQAP)*. The NQAP complies with DOE Order 414.1D, *Quality Assurance*, and 10 CFR 830, *Nuclear Safety Management*, Subpart A, *Quality Assurance Requirements*. NQAP uses NQA-1-2012, *Quality Assurance Requirements for Nuclear Facility Application*, as its consensus standard and NQA-1-2012, Subpart 4.2.1, as the basis for its graded approach to quality.

The NQAP works in conjunction with PNNL's laboratory-level Quality Management Program, which is based on the requirements as defined in DOE Order 414.1D and 10 CFR 830 Subpart A, *Quality Assurance Requirements*.

The work of this report was performed to the QA level of applied research with a technology readiness level of 4.

2.0 Test Methods

This section describes how the 25 LAW test-matrix glasses were designed and data were obtained. The descriptions include the methods for 1) glass matrix design, 2) glass fabrication, 3) chemical composition analysis, 4) secondary phase identification from container centerline cooling (CCC) treatment, 5) crystal fraction (CF) as a function of temperature and liquidus temperature (T_L) measurement, 6) density (ρ) determination, 7) viscosity (η) measurement, 8) electrical conductivity (EC, ε) measurement, 9) product consistency test (PCT) measurement, 10) vapor hydration test (VHT) measurement, and 11) sulfur solubility measurement.

2.1 Glass Matrix Design

The LAW Phase 4 Matrix Glass Testing matrix was generated to augment the previous LAW Phases 1, 2, and 3 by using a space-filling design (SFD) technique with JMP® version 14.3.0 (SAS Institute Inc. 2019) software. This experimental design was chosen to spread the glasses evenly for each of the 16 components that were selected to vary throughout the composition region. Twenty-two glasses of unique compositions were generated. Table 2.1 lists the single- and multiple-component constraints used in matrix design.

Table 2.1. Single- and Multiple-Component Constraints for Matrix Design (in mass fraction unless otherwise indicated)

Single-/Multi-Component	Lower	Upper
Al_2O_3	0.035	0.1385
B_2O_3	0.06	0.1375
CaO	0	0.1224
Cr_2O_3	0	0.006
Fe_2O_3	0	0.015
K_2O	0	0.0575
Li_2O	0	0.05
MgO	0	0.035
Na_2O	0.1	0.26
SiO_2	0.34	0.47
SO_3	0.001	0.015
SnO_2	0	0.045
TiO_2	0	0.02
V_2O_5	0	0.04
ZnO	0	0.035
ZrO_2	0.025	0.065
Others*	0.0036	0.03
$Na_2O+0.66K_2O+2.07Li_2O$	0.15	0.265
$ZrO_2 + SnO_2$	0.03	0.1
Viscosity ($\eta_{1150°C}$, Pa-s)	1	10
$19.9Li_2O + 99.67SnO_2 + 10.15(Al_2O_3+ZrO_2) - 5.38(1 - Li_2O - SnO_2 - Al_2O_3 - ZrO_2)$	0	1.5
$Na_2O+0.66K_2O+2.07Li_2O-ZrO_2-0.82SnO_2-1.54TiO_2$	0	0.2

*Others are Cl, F, and P_2O_5

The multi-component constraint for viscosity was taken from Vienna et al. (2016). JMP® 14.3.0 was used to generate 25,000 candidate points to fill the space defined by the set of constraints listed in Table 2.1 using SFD with the fast flexible filling option. A set of 95 glasses, previously tested at PNNL were identified within the same set of constraints and were used as "existing glasses to be backfilled." JMP® SFD with the fast flexible filling option was used to select a new set of 22 compositions from the 25,000 candidate points to efficiently backfill the 95 existing glasses. Three glasses were selected from previous LAW studies and added to the current matrix: LAW-ORP-LD1 from Russel et al. (2017) as LP4-05 and LP2-IL-10 and LP2-OL-25 from Russel et al. (2021) as LP4-15 and LP4-01.

The batching sheets were calculated based the use of $ZrO(NO_3)_2$-$2H_2O$ as a ZrO_2 source material but the source material actually used was $ZrO(NO_3)_2$-xH_2O at x = 8. This batching error resulted in target glass compositions different from the intended or designed. Table 2.2 reports the lower and upper bounds of component concentrations as designed and as batched. The relative percentage difference (RPD) for all other components were less than 2%. The significant deviation in ZrO_2 concentration range is not expected to be an issue if the actually batched target glass compositions meet the following two design success criteria that are used when designing the matrix glasses:

1. The dispersion value of each component must be below 1.0.
2. The relative range of individual components across the glasses in the matrix should be greater than or equal to 0.90.

With the batching error, the three compositions selected from previous studies and intended as triplicates resulted in three new compositions.

The multiple-component constraints applied to the matrix as designed and as batched are listed in Table 2.3 together with the RPD.

The 25 LAW glasses making up the test matrix are listed in Table 2.4.

Table 2.2. Lower and Upper Bounds of Component Concentrations (mass fractions) for LAW Phase 4 Glasses as Designed and as Batched. Relative Percentage Difference (RPD) is Reported

	As designed		Batched		RPD	
Component	Lower Bound	Upper Bound	Lower Bound	Upper Bound	Min.	Max
Al_2O_3	0.0366	0.1364	0.0372	0.1376	1.6%	0.9%
B_2O_3	0.0605	0.1371	0.061	0.1401	0.8%	1.5%
CaO	0.0011	0.1213	0.0011	0.1223	1.2%	0.8%
Cr_2O_3	0.0001	0.0059	0.0001	0.006	1.2%	1.9%
Fe_2O_3	0.0005	0.0148	0.0005	0.0153	1.8%	1.0%
K_2O	0.0008	0.0574	0.0008	0.0583	0.8%	1.5%
Li_2O	0.0047	0.0498	0.0048	0.0505	1.8%	1.3%
MgO	0.0023	0.0348	0.0023	0.0353	1.6%	1.5%
Na_2O	0.101	0.2026	0.1025	0.2649	1.5%	1.2%
SiO_2	0.341	0.4654	0.3463	0.4729	1.6%	1.6%
SO_3	0.0011	0.0144	0.0011	0.0146	1.0%	1.6%
SnO_2	0.0008	0.044	0.0008	0.0447	1.6%	1.6%
TiO2	0.0029	0.02	0.0029	0.0202	1.2%	0.8%
V_2O_5	0.0005	0.0398	0.0005	0.0405	1.5%	1.6%
ZnO	0.0002	0.0347	0.0002	0.0367	1.3%	1.3%
ZrO_2	0.0251	0.064	0.018	0.0472	−32.9%	−31.8%
Others*	0.005	0.1364	0.005	0.038	1.0%	1.6%

*Others are Cl, F, and P_2O_5

Table 2.3. Lower and Upper Bounds of Multiple-Component Constraints for LAW Phase 4 Glasses as Designed and as Batched. Relative Percentage Difference (RPD) is Reported

	As designed		Batched		RPD	
Expression (units)	Lower Bound	Upper Bound	Lower Bound	Upper Bound	Min	Max
$Na_2O+0.66K_2O+2.07Li_2O$	0.1644	0.2649	0.1671	0.2690	1.6%	1.5%
$ZrO_2 + SnO_2$	0.0318	0.0999	0.0232	0.0852	−31.2%	−15.9%
Viscosity ($\eta_{1150^{\circ}C}$, Pa-s)	1.00	9.26	0.89	8.88	−11.6%	−4.1%
950 Cassiterite: $19.9Li_2O + 99.67SnO_2 + 10.15(Al_2O_3+ZrO_2) - 5.38(1 - Li_2O - SnO_2 - Al_2O_3 - ZrO_2)$	NA	1.43	NA	1.29	NA	−10.0%
VHT 80%: $Na_2O+0.66K_2O+2.07Li_2O-ZrO_2-0.82SnO_2-1.54TiO_2$	NA	0.1778	NA	0.1957	NA	9.6%

Table 2.4. Targeted Compositions (mass fractions) for the Low-Activity Waste Glasses Study

Components	LP4-01	LP4-02	LP4-03	LP4-04	LP4-05	LP4-06	LP4-07	LP4-08	LP4-09	LP4-10	LP4-11	LP4-12	LP4-13
SiO_2	0.3557	0.4331	0.3711	0.3809	0.3747	0.3740	0.3463	0.3979	0.3662	0.4485	0.4337	0.4655	0.3576
Al_2O_3	0.0611	0.1376	0.0986	0.1325	0.1025	0.1290	0.0945	0.1086	0.0445	0.0408	0.0917	0.0391	0.0388
B_2O_3	0.1401	0.0722	0.1391	0.0624	0.1215	0.1157	0.0731	0.0610	0.1296	0.0834	0.1275	0.1036	0.1067
Na_2O	0.2649	0.1025	0.1079	0.1073	0.2118	0.1272	0.1447	0.1552	0.1496	0.1393	0.1447	0.1148	0.1767
Fe_2O_3	0.0153	0.0111	0.0028	0.0016	0.0101	0.0073	0.0017	0.0147	0.0005	0.0118	0.0006	0.0036	0.0099
CaO	0.0263	0.0152	0.0575	0.0711	0.0809	0.0024	0.1165	0.0115	0.0033	0.0478	0.0063	0.0074	0.0830
SnO_2	0.0357	0.0013	0.0217	0.0034	0.0000	0.0368	0.0408	0.0250	0.0316	0.0085	0.0377	0.0447	0.0212
V_2O_5	0.0000	0.0261	0.0074	0.0277	0.0101	0.0333	0.0334	0.0221	0.0354	0.0005	0.0077	0.0405	0.0016
ZnO	0.0367	0.0304	0.0045	0.0002	0.0303	0.0327	0.0057	0.0289	0.0276	0.0021	0.0101	0.0074	0.0338
ZrO_2	0.0472	0.0219	0.0368	0.0331	0.0216	0.0198	0.0386	0.0200	0.0437	0.0377	0.0244	0.0405	0.0413
TiO_2	0.0000	0.0078	0.0035	0.0180	0.0000	0.0046	0.0083	0.0202	0.0174	0.0187	0.0168	0.0068	0.0175
Cl	0.0006	0.0051	0.0015	0.0047	0.0033	0.0051	0.0011	0.0053	0.0022	0.0058	0.0060	0.0013	0.0057
Cr_2O_3	0.0031	0.0017	0.0055	0.0002	0.0050	0.0006	0.0013	0.0044	0.0005	0.0058	0.0046	0.0026	0.0011
K_2O	0.0000	0.0340	0.0481	0.0544	0.0016	0.0509	0.0116	0.0538	0.0577	0.0583	0.0433	0.0556	0.0319
Li_2O	0.0000	0.0466	0.0446	0.0505	0.0000	0.0132	0.0126	0.0315	0.0351	0.0441	0.0144	0.0215	0.0259
MgO	0.0000	0.0206	0.0072	0.0304	0.0101	0.0323	0.0312	0.0076	0.0172	0.0353	0.0218	0.0297	0.0083
P_2O_5	0.0020	0.0171	0.0192	0.0062	0.0029	0.0082	0.0169	0.0191	0.0212	0.0047	0.0059	0.0057	0.0175
F	0.0010	0.0106	0.0091	0.0014	0.0017	0.0040	0.0104	0.0011	0.0082	0.0046	0.0017	0.0049	0.0094
SO_3	0.0103	0.0051	0.0139	0.0140	0.0107	0.0029	0.0113	0.0121	0.0085	0.0023	0.0011	0.0048	0.0121
Cs_2O	0.0000	0.0000	0.0000	0.0000	0.0007	0.0000	0.0000	0.0000	0.0000	0.0000	0.0000	0.0000	0.0000
NiO	0.0000	0.0000	0.0000	0.0000	0.0004	0.0000	0.0000	0.0000	0.0000	0.0000	0.0000	0.0000	0.0000
PbO	0.0000	0.0000	0.0000	0.0000	0.0001	0.0000	0.0000	0.0000	0.0000	0.0000	0.0000	0.0000	0.0000
Total	1.0000	1.0000	1.0000	1.0000	1.0000	1.0000	1.0000	1.0000	1.0000	1.0000	1.0000	1.0000	1.0000

Table 2.4. Targeted Compositions (mass fractions) for the Low-Activity Waste Glasses Study (continued)

Components	LP4-14	LP4-15	LP4-16	LP4-17	LP4-18	LP4-19	LP4-20	LP4-21	LP4-22	LP4-23	LP4-24	LP4-25
SiO_2	0.3620	0.3924	0.4498	0.4174	0.4437	0.3651	0.3509	0.4731	0.4044	0.4164	0.3494	0.3950
Al_2O_3	0.0599	0.1012	0.0552	0.0372	0.0416	0.1249	0.0684	0.0430	0.0947	0.0607	0.1326	0.0742
B_2O_3	0.1335	0.0961	0.1190	0.1091	0.0640	0.0740	0.1353	0.1341	0.1282	0.0646	0.0960	0.0877
Na_2O	0.1146	0.2327	0.1332	0.1109	0.1541	0.1993	0.1801	0.1026	0.2051	0.1657	0.1605	0.1073
Fe_2O_3	0.0144	0.0061	0.0050	0.0059	0.0048	0.0073	0.0144	0.0111	0.0134	0.0083	0.0094	0.0150
CaO	0.1081	0.0506	0.0044	0.0858	0.1223	0.0295	0.0187	0.0543	0.0011	0.0440	0.0234	0.0938
SnO_2	0.0088	0.0152	0.0398	0.0008	0.0328	0.0015	0.0395	0.0390	0.0110	0.0435	0.0028	0.0375
V_2O5	0.0129	0.0101	0.0386	0.0392	0.0090	0.0128	0.0387	0.0005	0.0316	0.0250	0.0188	0.0103
ZnO	0.0150	0.0283	0.0053	0.0024	0.0005	0.0046	0.0066	0.0056	0.0085	0.0022	0.0351	0.0020
ZrO_2	0.0307	0.0288	0.0230	0.0401	0.0198	0.0464	0.0180	0.0400	0.0311	0.0231	0.0314	0.0260
TiO_2	0.0029	0.0000	0.0198	0.0121	0.0195	0.0161	0.0151	0.0156	0.0100	0.0185	0.0183	0.0099
Cl	0.0061	0.0021	0.0054	0.0028	0.0016	0.0032	0.0016	0.0023	0.0043	0.0041	0.0020	0.0045
Cr_2O_3	0.0057	0.0046	0.0008	0.0058	0.0020	0.0060	0.0058	0.0036	0.0001	0.0011	0.0025	0.0014
K_2O	0.0347	0.0101	0.0207	0.0292	0.0008	0.0339	0.0390	0.0147	0.0040	0.0412	0.0466	0.0262
Li_2O	0.0320	0.0000	0.0470	0.0313	0.0183	0.0048	0.0111	0.0264	0.0105	0.0299	0.0290	0.0422
MgO	0.0287	0.0066	0.0133	0.0243	0.0337	0.0329	0.0351	0.0023	0.0041	0.0263	0.0242	0.0322
P_2O_5	0.0173	0.0068	0.0032	0.0206	0.0212	0.0147	0.0061	0.0137	0.0200	0.0132	0.0089	0.0186
F	0.0022	0.0032	0.0102	0.0111	0.0036	0.0086	0.0070	0.0035	0.0076	0.0027	0.0059	0.0097
SO_3	0.0105	0.0051	0.0063	0.0140	0.0067	0.0144	0.0086	0.0146	0.0103	0.0095	0.0032	0.0065
Cs_2O	0.0000	0.0000	0.0000	0.0000	0.0000	0.0000	0.0000	0.0000	0.0000	0.0000	0.0000	0.0000
NiO	0.0000	0.0000	0.0000	0.0000	0.0000	0.0000	0.0000	0.0000	0.0000	0.0000	0.0000	0.0000
PbO	0.0000	0.0000	0.0000	0.0000	0.0000	0.0000	0.0000	0.0000	0.0000	0.0000	0.0000	0.0000
Total	1.0000	1.0000	1.0000	1.0000	1.0000	1.0000	1.0000	1.0000	1.0000	1.0000	1.0000	1.0000

2.2 Glass Fabrication

Glass fabrication was performed according to the PNNL procedure, *Glass Batching and Melting* (WFDL-GBM-1, Rev. 2).[1] Single-metal oxides, single-metal carbonates, sodium salts, and boric acid were mixed in the appropriate masses to form the target composition for each glass. After thoroughly mixing in the plastic bag for at least 30 seconds until uniform color developed, the powders were transferred to an agate milling chamber and milled for 4 minutes in a vibratory mill (AngstromTE110). The powders were then transferred to a clean platinum (Pt)-10% rhodium (Rh) crucible for melting. Initial melting was performed at 1150°C for 1 hour ±10 minutes.

After the first melt was air quenched on a stainless-steel pouring plate, the glass was observed under the optical microscope (OM) and the presence of undissolved particles and/or salts was reported. The glass was then ground to a fine powder for 5 minutes in a tungsten carbide vibratory mill and a second melt was performed. The temperature of the second melt varied depending on the outcome of the first melt. If the first melt was homogeneous or had only a small amount of undissolved particle observed by OM, then the second melt was performed again at 1150 °C ± 10 °C for 1 hour ± 10 minutes. If undissolved particle were particularly abundant after the first melt, then the temperature of the second melt was increased. In some cases, more than two melts were necessary to fully dissolve the undissolved particles in the glass matrix and obtain a homogeneous glass. A detailed list of the number of melts and temperatures is reported in Table 2.5. All melts were 1 hour long ± 10 minutes. Re-batched glasses were given a replicate number starting from the value of “1” after the glass ID (e.g., LP4-04-1 in Table 2.5). Compositions that required more than 4 melts to yield an uniform glass, were re-batched, given a replicate number starting from the value of “1” after the glass ID, and started the first melt at higher temperatures than 1150 °C (e.g., LP4-07-1 in Table 2.5).

Three glasses—LP4-04-1, LP4-08-1, and LP4-19—presented a superficial sulfate salt layer that was not being incorporated into the glass and was therefore washed before undergoing the final melt. This sulfate wash consisted of crushing the glass using a tungsten carbide vibratory mill. The powder was then collected in a clean beaker and deionized water (DI) water was added about double the sample mass. The sample was mixed in the DI water using a spatula for 2 minutes and then using a sonic bath for 20 minutes. The solution was left to settle overnight and then was decanted. The excess water was extracted using a vacuum set with 0.45 µm membrane filter. The process was repeated twice. The wet powder then was poured in a large container and let dry for 1 hour in an oven at 90 °C. The filters were also dried for 10 minutes in the 90 °C oven to recover the glass powder that was attached to them. The dry glass powder was finally melted one last time as reported in Table 2.5.

The use of higher melting temperature is deemed to be an acceptable method of fabricating challenging glass compositions. Laboratory crucible-scale fabrication of glasses is not intended to mimic the actual melter process or feed processability; rather, it is intended to fabricate a glass sample with a controlled composition for property testing.

The morphology and color of each quenched glass is shown in Appendix A.

---

[1] Russell RL. 2016. *Glass Batching and Melting.* WFDL-GBM-1, Rev. 2, Pacific Northwest National Laboratory, Richland, Washington.

Table 2.5. Melt History of the Low-Activity Waste Glasses

Glass ID	First Melt Temperature (°C)	Second Melt Temperature (°C)	Third Melt Temperature (°C)
LP4-01	1150	1150	
LP4-02	1150	1150	1200
LP4-03	1150	1150	1200
LP4-04-1*	1150	1250	
LP4-05	1150	1150	
LP4-06-2	1300	1350	1350
LP4-07-1	1350	1350	
LP4-08-1*	1150	1300	1300
LP4-09	1150	1150	
LP4-10	1150	1150	
LP4-11	1150	1150	1200
LP4-12	1150	1200	1200
LP4-13	1150	1150	1150
LP4-14	1150	1150	
LP4-15	1150	1150	
LP4-16	1150	1200	
LP4-17	1150	1150	
LP4-18	1150	1150	1150
LP4-19*	1150	1200	1150
LP4-20	1150	1150	1200
LP4-21	1150	1150	1150
LP4-22	1150	1150	1150
LP4-23-1	1250	1350	
LP4-24	1150	1150	
LP4-25-1	1250	1350	

* Glasses LP4-04-1, LP4-08-1 and LP4-19 were washed to eliminate excess sulfate before undergoing the final melt.

2.3 Chemical Analysis of Glass Composition

To confirm that the “as-fabricated” glasses corresponded to the specified target compositions, a representative sample of each glass was chemically analyzed at the Savannah River National Laboratory (SRNL) Process Science Analytical Laboratory. The samples were sent in two separated batches—Batch 1 and Batch 2 (Table 2.6). Three dissolution techniques, including sodium peroxide fusion (PF), acid dissolution (AD), and potassium hydroxide fusion (KH), were used to prepare glass samples, in duplicate, for analysis. Descriptions of the dissolution processes can be found in Hsieh (2020a).

Duplicate samples (two each for the preparation techniques) were analyzed twice for each element of interest by inductively coupled plasma-optical emission spectroscopy (ICP-OES) or ion chromatography (IC). Glass composition standards also were intermittently prepared and analyzed to assess the performance of the ICP-OES and IC instruments over the course of these analyses. Specifically, several samples of the analytical reference glass-1 (Smith 1993) and the low-level reference material (Ebert and Wolfe 1999) were included as part of the SRNL Process Science Analytical Laboratory analysis plan. The preparation and measurement methods used for each of the reported glass analytes are listed in Table 2.7.

A detailed data analysis of the chemical composition measurements was published elsewhere (Hsieh 2020a). A short summary of these data analyses is included in Section 3.2.

Table 2.6. LAW Phase 4 Glasses Batches Identifier

Batch 1	Batch 2
LP4-01-Q	LP4-04-1-Q
LP4-02-Q	LP4-06-2-Q
LP4-03-Q	LP4-07-1-Q
LP4-05-Q	LP4-08-1-Q
LP4-09-Q	LP4-13
LP4-10-Q	LP4-19
LP4-11-Q	LP4-22-Q
LP4-12-Q	LP4-23-1-Q
LP4-14-Q	LP4-24-Q
LP4-15-Q	LP4-25-1-Q
LP4-16-Q	
LP4-17-Q	
LP4-18-Q	
LP4-20-Q	

Table 2.7. Preparation and Measurement Methods Used in Reporting the Analyte Concentrations of the Study Glasses

Analyte	Measurement Method	Preparation Method Batch 1	Preparation Method Batch 2
Al	ICP-OES	PF	PF
B	ICP-OES	PF	PF
Ca	ICP-OES	AD	AD
Cl	IC	KH	KH
Cr	ICP-OES	AD	AD
F	IC	KH	KH
Fe	ICP-OES	AD	AD
K	ICP-OES	AD	AD
Li	ICP-OES	AD	PF
Mg	ICP-OES	AD	PF
Na	ICP-OES	AD	AD
Ni	ICP-OES	AD	AD
P	ICP-OES	AD	AD
Pb	ICP-OES	AD	
Sn	ICP-OES	PF	PF
S	ICP-OES	AD	AD
Si	ICP-OES	PF	PF
Ti	ICP-OES	AD	AD
V	ICP-OES	AD	AD
Zn	ICP-OES	AD	AD
Zr	ICP-OES	AD	AD

2.4 Container Centerline Cooling and Crystal Identification

A portion (~100 g) of each test glass was subjected to the simulated CCC temperature profile shown in Table 2.8 and Figure 2.1.

This profile is the temperature schedule of CCC treatment for Hanford LAW glasses planned for use at WTP.(1) Pieces of quenched glass, <3 cm in diameter, were placed in a Pt-alloy crucible and covered with a Pt-alloy lid. The glass samples were placed in a furnace preheated to the glass melting temperature. After 30 minutes at the melting temperature, the furnace temperature was quickly dropped to 1114 °C, and the cooling profile was started. It progressed down to about 400 °C based on seven cooling segments shown in Table 2.8. The starting temperature for the seven segments of cooling were 1114 °C, 1000 °C, 900 °C, 825 °C, 775 °C, 725 °C, and 600 °C.

Table 2.8. Temperature Schedule during CCC Treatment of Hanford LAW Glasses

Segment	Time (min)	Start Temperature (°C)	Rate (°C/min)
1	-30	Melt temperature	0
2	0	1114	-7.125
3	0–16	1000	-1.754
4	16–73	900	-0.615
5	73–195	825	-0.312
6	195–355	775	-0.175
7	355–640	725	-0.130
8	640–1600	600	-0.095
9	1600–3710	Room temperature	NA

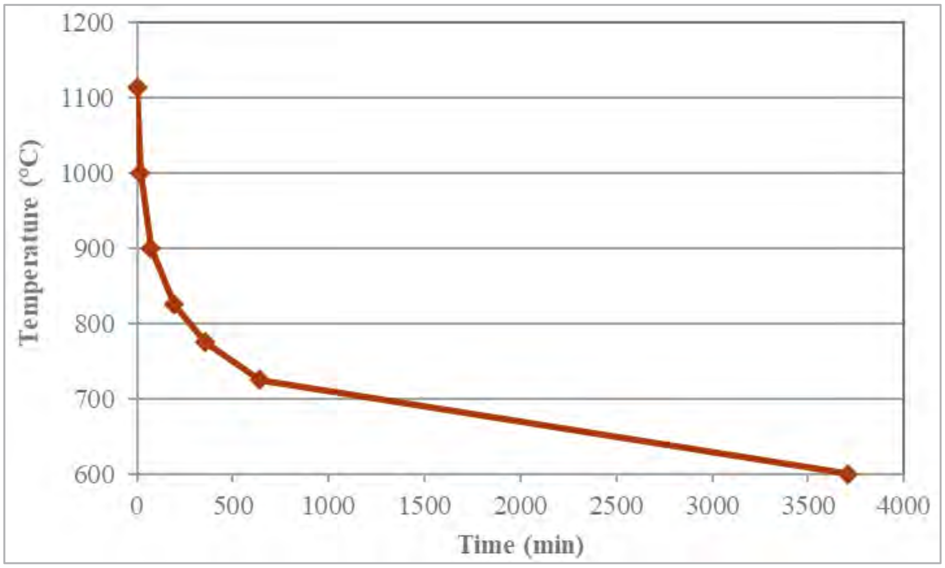

Figure 2.1. Plot of Temperature Schedule During CCC Heat-Treatment of Hanford LAW Glasses

---

[1] Memorandum, Low Activity Container Centerline Cooling Data, CCN: 074181, RPP-WTP, October 16, 2003.

The amount and type of crystalline phases that formed during CCC treatment were analyzed by X-ray diffraction (XRD) according to Section 12.4.4 of the standard ASTM International procedure, *Standard Test Method for Determining Liquidus Temperature of Immobilized Waste Glasses and Simulated Waste Glasses* (ASTM C1720). Powdered glass samples were prepared using ~1.5 g of glass milled for 1 minute in a 10 cm^3 vibratory mill with a tungsten carbide cup and disc. Roughly 5 wt% CeO_2 was added to the powder as an internal standard and milled together with the glass for additional 30 seconds. The powdered glass samples were loaded into XRD sample holders and scanned at a 0.015° 2θ step size, 1.5 second dwell time, from 5° to 75° 2θ scan range. XRD spectra were analyzed with DIFFRAC.EVA software (Bruker AXS GmbH, Karlsruhe, Germany) for phase identification. Full-pattern Rietveld refinement using TOPAS 4.2 (Bruker AXS GmbH, Karlsruhe, Germany) was performed to quantify the amounts of crystal phases on samples with crystalline content. These results are discussed in Section 3.3.

2.5 Crystal Fraction in Isothermal Heat-treated Glasses

Isothermal CF as a function of temperature and T_L were measured in Pt-alloy boats (~2 g of glass per boat) with tight fitting lids to minimize volatility according to the standard ASTM International procedure, “Standard Test Method for Determining Liquidus Temperature of Immobilized Waste Glasses and Simulated Waste Glasses” (ASTM C1720). The heat treatments were performed at temperatures of 800 °C, 850 °C, 900 °C, and 950 °C. The period for treatment at each temperature was 24 hours for temperatures ≥ 900 °C and 48 hours for temperatures <900 °C. Prior to measuring the CF, the furnace temperature accuracy was verified using two glasses with T_Ls traceable to a round-robin study, analytical reference glass-1 (Smith 1993), and a replicate of the original AmCm2-19 prepared and verified by Gervasio et al. (2019). Attempts to measure the T_L of the test-matrix glasses were done using the *Crystal Fraction Extrapolation Method* in ASTM C1720 where T_L is calculated by extrapolating CF as a function of temperature to zero crystals. These results are discussed in Section 3.4.

2.6 Glass Density

The room temperature density of each glass was measured according to PNNL procedure, *Density Using a Gas Pycnometer* (EWG-OP-045)(1) using an AccuPyc II 1340 gas pycnometer (MicroMeritics, Norcross, Georgia) with approximately 1 g of glass pieces. The glass was loaded into a vial and placed within the instrument. The instrument then determined the density by the difference in amount of helium gas needed to fill the vial with glass versus the amount needed without glass. The pycnometer was calibrated within 6 months of the testing and the calibration was checked before and after measurements for that day using a National Institute of Standards and Technology traceable standard tungsten carbide ball. These results are discussed in Section 3.5.

---

[1] Russell RL. 2017. *Density Using a Gas Pycnometer*. EWG-OP-0045, Rev. 0.0, Pacific Northwest National Laboratory, Richland, Washington.

2.7 Glass Viscosity

The viscosities of the glass melts were measured as functions of temperature with a fully automated Anton Parr FRS 1600 Furnace Rheometer System according to the PNNL procedure, *High-Temperature Viscosity Measurement Using Anton Paar FRS1600* (EWG-OP-0046).(1) Approximately 25 to 30 mL or ~70 g of glass was placed into a Pt-alloy cylindrical cup. It was then heated to ~1150 °C and maintained at that temperature until thermal equilibrium was reached. A Pt-alloy spindle then was lowered into the cup of molten glass. An initial torque reading (at a constant spindle speed) was taken at ~1150 °C with subsequent measurements at target temperatures of 1050 °C, 950 °C, 1150 °C, 1250 °C, and then 1150 °C using a hysteresis approach. The hysteresis approach allows for the potential impacts of crystallization (at lower temperatures) to be assessed via reproducibility with duplicate measurements being taken at approximately the melting temperature. Also, volatilization (at higher temperatures) is minimized by measuring viscosity at temperatures above the melting temperature as the final viscosity measurement(s). The soak time was 30 minutes at each temperature. Prior to glass viscosity measurements, halfway through the sample measurements and after sample measurements, the test instrumentation was checked for accuracy using a standard glass (Defense Waste Processing Facility [DWPF] Startup Frit) as discussed in the literature (Crum et al. 2012). These results are discussed in Section 3.6.

2.8 Electrical Conductivity

The EC of glass melts was determined with an Anton Parr FRS 1600 Furnace Rheometer System by the high-temperature furnace and a Solartron impedance analyzer according to PNNL procedure, *High-Temperature Electrical Conductivity Measurement* (EWG-OP-0047).(2) Platinum plates (1.3 inches long by 0.28 inches wide) were placed parallel to each other with a separation of 0.367 inches. About 30 mL of glass sample was used for EC measurements in a Pt-alloy crucible. Before measuring ε of the test-matrix glasses, calibration was conducted at room temperature with reference solutions of KCl (0.1 M and 1 M) by measuring the resistance values at three frequencies (1, 10, and 100 kHz). Four readings were taken at each frequency over a period of 2 to 5 minutes. For high temperatures, calibration was conducted with DWPF glass. The averaged values of the four readings were then used to calculate the cell constant. For glass measurement, the probe was lowered into the molten glass to a depth of 12.7 mm and the sample was first heated to 1250 °C for 30 minutes. After the temperature was stabilized, a scan from 1 MHz to 0.1 Hz in 3 minutes was conducted and resistance at 1 kHz was used to calculate the ε. The ε was measured at four different temperatures in a range around the melting temperature of the glass: 1250 °C, 1150 °C, 950 °C, and 1150 °C. Two scans were made for each temperature after the glass was held 10 minutes at each temperature before measurement for temperature stabilization. These results are discussed in Section 3.7.

---

[1] McCarthy BP. 2017. *High-Temperature Viscosity Measurement Using Anton Paar FRS1600*. EWG-OP-0046, Rev. 0, Pacific Northwest National Laboratory, Richland, Washington.

[2] McCarthy BP. 2017. *High-Temperature Electrical Conductivity Measurement*. EWG-OP-0047, Rev. 0, Pacific Northwest National Laboratory, Richland, Washington.

2.9 Product Consistency Test

PCT responses were measured in triplicate for quenched and CCC samples of each glass using Method A of the standard ASTM International procedure *Standard Test Methods for Determining Chemical Durability of Nuclear, Hazardous, and Mixed Waste Glasses and Multiphase Glass Ceramics: The Product Consistency Test (PCT)* (ASTM C1285). The PCT test matrix also included the DWPF Environmental Assessment (EA) glass (Jantzen et al. 1993) and blanks. All measurements (including DWPF-EA and blanks) were performed in triplicate. Glass samples were ground, sieved to -100+200 mesh, washed, and prepared according to the standard ASTM C1285 procedure. The prepared glass was added to water in a 1.5 g:15 mL ratio, to obtain a glass surface area:solution volume ratio of approximately 2000 m^{-1}. The ratio was not adjusted to account for measured glass density. The vessels used were desensitized Type 304L stainless steel. The vessels were closed, sealed, and placed into an oven at 90 °C ± 2 °C for 7 days ± 3 hours.

After 7 days at 90 °C, the vessels were removed from the oven and allowed to cool to room temperature. The final mass of the vessel and the solution pH were recorded on a data sheet. Each test solution was then filtered through a 0.45-µm filter and acidified with HNO_3 to assure that the cations remained in solution. The resulting solutions were analyzed by ICP-OES for Si, Na, B, and Li. Samples of multi-element, standard solutions were also analyzed as a check on the accuracy of the ICP-OES. Normalized releases (g/L) were calculated based on target and measured glass composition. The former was used for data evaluation and analysis. Results are included in Section 3.8.

2.10 Vapor Hydration Test

In the VHT, monolithic glass samples were exposed to water vapor at 200 °C in sealed stainless-steel vessels according to the ASTM International standard procedure, *Standard Test Method for Measuring Waste Glass or Glass Ceramic Durability by Vapor Hydration Test* (ASTM C1663). Roughly 1.5 mm × 10 mm × 10 mm samples were cut from annealed or CCC-treated LAW glass bars using a diamond-impregnated saw. All sides of the cut sample were polished to 600-grit surface finishes with silicon carbide paper.

Polished samples were hung from stainless-steel supports with Pt wire within a stainless-steel container (see Figure 2.2). DI water was added to the bottom of the vessel so that enough water was present to react with the specimen but without enough water to reflux during testing (~0.20 g). The samples were heated and held at 200 °C in a convection oven for either 7 or 24 days. All samples were initially tested for 24 days. Samples found to have fully reacted in 24 days were then tested for shorter times to enable estimating a numerical alteration rate (as opposed to “greater-than” values).

After removal from the oven, vessels were weighed and then quenched in cold water. The specimens were removed from the vessels and cross-sectioned with or without epoxy (depending on the stability of each sample) for analysis by optical microscopy-image analysis to determine the amount of glass altered during the test. The solution in the vessel was tested for pH to ensure reflux did not occur. Any test with a pH >10 was not used due to reflux.

The remaining glass thickness of the VHT specimen was determined by performing at least 10 measurements distributed (roughly equally) across the crack-free cross section of the sample. Then, the average and standard deviation of the 10 thickness measurements of the remaining glass were calculated. The amount of glass altered per unit surface area of specimen was determined from the average thickness of unaltered glass according to Equation (2.1):

$$m = \frac{1}{2}\rho(d_i - d_r) \qquad (2.1)$$

where: d_i, = initial thickness of the specimen (m)

d_r = average thickness of remaining glass layer (m)

m = mass of glass converted to alteration products per unit surface area (g/m^2)

ρ = glass density (g/m^2).

The average rate of corrosion was calculated as $r_a = m/t$, where t is the corrosion time. Vienna et al. (2001) showed that, if the average rate of corrosion at 200 °C is:

$$r_a = m \,/\, t < 50\ g/(m^2 \cdot d) \qquad (2.2)$$

then the final rate of corrosion, r_a <50 g/(m^2·d), meets the current ORP requirement for LAW glass performance. Although the contract limit for VHT response is stated in rates (50 g/m^2/d), the test directly measures alteration depth (D) in µm at different times. In previous studies (Piepel et al. 2007 and Muller et al. 2014), the directly measured parameter of D in µm after 24 days was modeled. This value can be converted to a rate by: D (µm) *10^{-6} (m/µm) *density (g/cm^3) *10^6 (cm^3/m^3) /t(d). Assuming a density of 2.65 g/cm^3, the limit of 50 g/m^2/d is equivalent to a D of 453 µm for a 24-d test duration. In the present study the density was assumed to be 2.65 g/cm^3.

The apparatus used to conduct VHT is shown in Figure 2.2, and the results are discussed in Section 3.9.

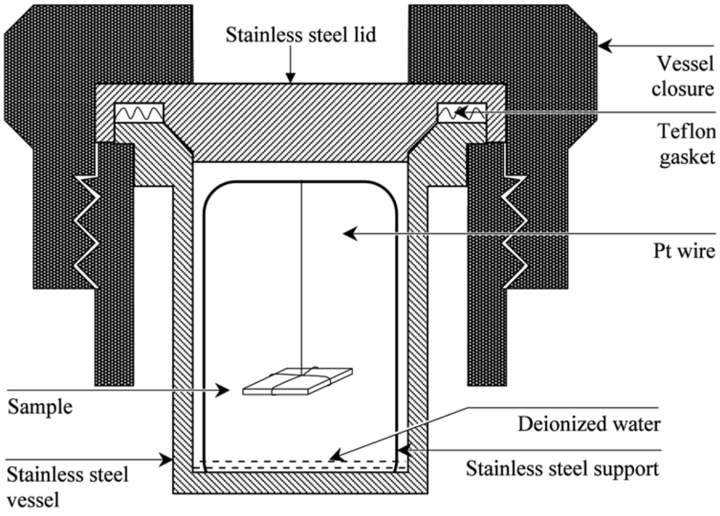

Figure 2.2. Apparatus used to Conduct VHTs

2.11 Sulfur Solubility Procedure

Sulfur solubility was measured on the quenched glass samples. The procedure was developed by PNNL and is described in Jin et al. (2019). There are three primary phases of testing with each glass: 1) saturation with sodium sulfate, 2) washing with de-ionized water, and 3) analysis. Each phase is described below.

2.11.1 Phase 1 Testing

Saturation with sodium sulfate was performed by taking 50 g of each glass, grinding it, and then sieving through a #120 sieve (125 µm). Then, 7.64 g of Na_2SO_4 per 100 g of glass was added to the sieved powdered glass to maintain 4 mass% SO_3 added to the glass/salt system, and the combination was mixed to achieve homogeneity. The mixture of baseline glass and Na_2SO_4 was melted at 1150 °C for 1 hour in a Pt-10%Rh crucible with a tight-fitting lid. After melting, the mixture was poured onto a steel plate and quenched. The mixture was again mixed by crushing and sieving through a #120 sieve (125 µm) and placed back into the Pt 10%Rh crucible to melt at 1150 °C for 1 hour the second time. After the second melting, the mixture was quenched by pouring onto a steel plate, mixed by crushing and sieving, and melted under the same conditions for the third time. After three re-melting and re-mixing cycles, the glass was crushed and sieved through the #120 sieve (125 µm).

2.11.2 Phase 2 Testing

After the third melt, the sieved samples were washed with DI water to remove excess salt prior to further analysis. This was done by adding 2 g of glass/salt mixture to a centrifuge filter in a centrifuge tube and adding 20 g of DI water to the tube. The tube was capped and shaken by hand for 2 minutes. Samples were placed in a balanced centrifuge that was set to 3175 rpm for 5 minutes. The solution was decanted into a bottle through a low-density polyethylene filter.

The filter was removed, and then was reinserted into the centrifuge tube. A second wash was performed following the same steps, and then the glass was weighed and dried at 80 °C overnight. To assure there was enough sample for analysis, a fresh 2 g of the same glass was obtained, the procedure described above was repeated, and the resulting solutions combined.

2.11.3 Phase 3 Testing

The washed and filtered glasses and the wash solutions recovered from filtering were then analyzed by ICP-OES and IC by Hsieh (2020c). A representative sample was taken from each of the wash solutions generated from the preparation of the sulfate saturated melt samples. The sample was diluted according to expected concentrations of the species of interest in each of the solutions, and each sample was analyzed in triplicate by ICP-OES and IC. Blanks and standards were used intermittently to assess the performance of each of the instruments and procedures. Methods of measurement are shown in Table 2.9.

The results are discussed in Section 3.10.

Table 2.9. Measurement Methods Used in Reporting Wash Solutions Analytes Concentrations (Hsieh, 2020c).

Analyte	Measurement Method	Analyte	Measurement Method
Al	ICP-OES	Ni	ICP-OES
B	ICP-OES	P	ICP-OES
Ca	ICP-OES	Pb	ICP-OES
Cl	IC	Sn	ICP-OES
Cr	ICP-OES	S	ICP-OES
F	IC	Si	ICP-OES
Fe	ICP-OES	Ti	ICP-OES
K	ICP-OES	V	ICP-OES
Li	ICP-OES	Zn	ICP-OES
Mg	ICP-OES	Zr	ICP-OES
Na	ICP-OES		

3.0 Results and Discussion

This section describes the results for the chemical composition, CCC, CF and T_L, ρ, η, EC, PCT, VHT, and sulfur solubility. As the present task aimed to improve glass property-composition data coverage and to validate the new composition-property models developed by Vienna et al. (2020), both collected data and their comparison to model predictions are presented.

3.1 Property Prediction Models Validation

The present task aimed to improve glass property-composition data coverage and to validate the new composition-property models developed by Vienna et al. (2020). The recommended model types are in the form of a partial quadratic mixture (PQM) model for viscosity, electrical conductivity, and melter SO_3 tolerance, bias-corrected PQM model for PCT, and logistic PQM model for VHT.

A 90% confidence criterion has been chosen for model validation investigations. The 90% confidence criterion approach considers intervals that describe uncertainty in both measured and model predicted property values. Intervals used to describe measured property values were one- or two-sided 90% confidence intervals having confidence limits of the form:

$$CLs = y \pm z_{1-\alpha/2} \cdot u_y \tag{3.1}$$

where: y = the measured property value (transformed to match units of model predicted property values) for a given glass from the model validation set
α = the significance level for the interval = 1 minus the confidence level for the interval
$z_{1-\alpha/2}$ = the multiplying factor taken from a standard normal distribution to represent the selected confidence level for the interval (for a 90% confidence level, $z_{1-\alpha/2}$ = 1.644854)
u_y = the assumed measurement uncertainty associated with the measured property value for a given glass and property.

Measurement uncertainties were taken from replicate glass standard deviations reported in Vienna et al. (2020).

Intervals used to describe predicted property values were two-sided 90% prediction intervals have prediction limits (PLs) of the form:

$$PLs = \hat{y} \pm z_{1-\alpha/2} \cdot \sqrt{MSE(1 + g^T(G^TG)^{-1}g)} \tag{3.2}$$

where: $\hat{y}$ = the model predicted property value for a given glass from the model validation set
$z_{1-\alpha/2}$ is as defined above
MSE = the mean squared error calculated for the given property model
g = the composition for a given glass, expanded to match the model form
G = the matrix of glass compositions used to generate the property model, with compositions expanded to match the model form (note, $MSE \cdot (G^TG)^{-1}$ is the variance-covariance matrix associated with the given property model).

A *z*-multiplier was used instead of a *t*-multiplier (typically used for confidence and prediction intervals) because the validation glasses were not used for model generation and because the number of glasses used to develop the different 2020 LAW models differed by property but was always adequately large for the *t*-multiplier to have adequate degrees of freedom to be essentially equal to a corresponding *z*-multiplier.

Prediction intervals for PCT were slightly different because the PCT models involved a bias correction for certain glasses. For glasses that required a bias correction for PCT models, the difference in the prediction interval formula involved the use of error propagation when calculating the prediction uncertainty for the glass, the $MSE \cdot g^T(G^TG)^{-1}g$ part of the formula. This will this be discussed further in the Section 3.8.

Measured and predicted property values for a given glass composition are considered to be in agreement (from a confidence-based point of view which takes measurement and prediction uncertainties into account) if the measured property value falls within the corresponding prediction interval or if the predicted property value falls within the measurement confidence interval. Visually, this means that the confidence rectangle for the given glass (formed using the measurement confidence interval and prediction interval) intersects the 45° line in a predicted versus measured plot.

A particular property model is considered to have good validation performance if at least 90% of the glasses in the model validation set are found to have confidence-based agreement between measured and corresponding predicted property values. That is, if at least 90% of the confidence rectangles intersect the 45° line in the predicted versus measured plot for that property.

Another metric that describes model validation performance is R^2-validation. R^2-validation for a given property model was calculated as follow:

$$R_{val}^2 = 1 - \frac{\sum_{i=1}^{n}(y_i - \hat{y}_i)^2}{\sum_{i=1}^{n}(y_i - \bar{y})^2} \tag{3.3}$$

where: y_i = the measured property value (transformed to match units of model predicted property values) for a given glass from the model validation set
$\hat{y}_i$ = the model predicted property value for a given glass from the model validation set
$\bar{y}$ = the mean measured property value (transformed) for glasses in the model validation set
n = number of glasses in the model validation set.

Figure 3.1 shows an example predicted versus measured plot with measurement confidence intervals and prediction intervals depicted for several hypothetical validation glasses. The figure also includes confidence rectangles for two hypothetical validation glasses; one confidence rectangle intersects the 45° line, the other does not. Again, for model validation performance purposes, if any part of a given confidence rectangle intercepts the 45° line, then the measured and predicted values are considered to be in agreement for the corresponding glass from the validation set.

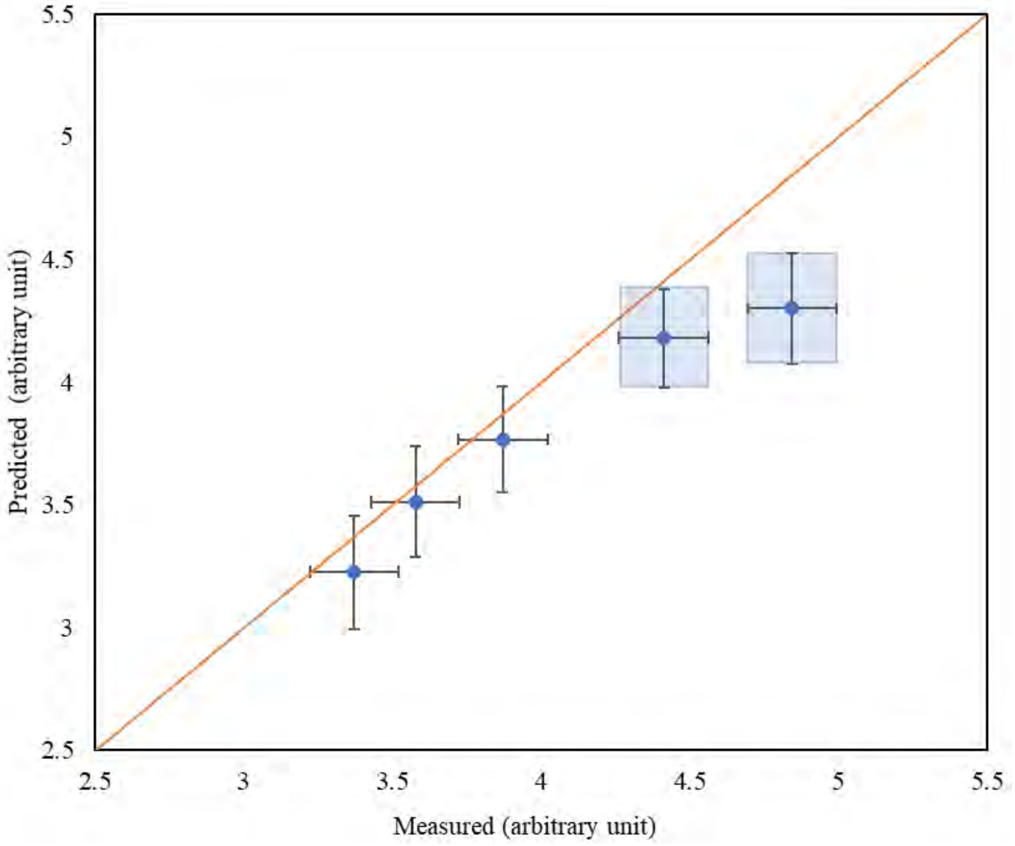

Figure 3.1. Visualization of the 90% Probability Area Represented by the Blue Shaded Rectangular Shapes

A different approach was used to validate the VHT response model because it was a logit function of probability to pass or fail the VHT limit. Because the methods used for that comparison are specific to VHT model, they are described in the Section 3.9.

3.2 Chemical Analysis of Glass Composition

The targeted and average of duplicate measured components in weight percent in the quenched glasses are presented in Appendix B along with the percent differences of components with targeted concentrations of 5 wt% or more. The composition analyses of the glass samples were performed as described in Section 2.3. All the measurements for each oxide in each glass were averaged to determine a representative chemical composition for each glass.

The following was observed in the samples from Batch 1 (see Section 2.3 for sample IDs):

- Measured concentrations of B_2O_3 and SiO_2 were higher than the targeted values for most of the glasses.
- Measured concentrations for MgO and P_2O_5 were generally low.
- Measured concentrations of ZrO_2 were both below and above the targeted values.
- Measured concentrations of chlorine and fluorine were below the targeted values for most of the study glasses, likely because of volatility during melting.

The following was observed in the samples from Batch 2 (see Section 2.3 for samples ID):

- Measured concentrations of Al_2O_3, B_2O_3 and P_2O_5, and SiO_2 were low relative to the targeted values for some of the glasses.
- Measured concentrations of ZrO_2 were below the targeted values for most glasses.
- Measured concentrations of Cl, Fl, and SO_3 were below the targeted values for most of the study glasses, likely because of volatility during melting.

As expected, the three glasses that were washed before the final melt showed losses of sulfur above the average, with the absolute percentage difference between target and measured SO_3 > 42%. Overall, the measured sums of oxides for all glasses fell within the interval of 95 to 105 wt%, indicating acceptable recovery of the glass components. For more details, see Hsieh (2020a).

3.3 Crystal Identification in Container Centerline Cooling Glasses

The formation of crystals during the slow cooling of the molten ILAW core in the final containers might have an adverse impact in glass durability by sequestering valuable glass forming chemicals (Kim et al. 1995). Property-composition models were developed by using quenched glass data, therefore any differences in PCT and VHT responses upon slow cooling need to be evaluated.

Not all crystals affect glass durability the same way, the identification of crystalline phases that form during the CCC process is the first step in predicting glass durability. This section presents and discusses the CF results from the CCC glasses obtained using the methods discussed in Section 2.4. The effect of CCC on PCT and VHT is reported in Sections 3.8 and 3.9, respectively.

The crystal content and weight percent of crystallinity from XRD scans of CCC glass samples are summarized in Table 3.1. Of the 25 glasses, 11 formed some crystals with crystal content ranging from 0 to 10.9 wt%. The main crystalline phases observed were $Ca_4Na_6(SO_4)_6F_2$, alinite ($Ca_{11}Si_3AlO_{18}Cl$), nosean ($Na_8Al_6Si_6O_{24}(SO_4)$), nepheline ($Na_3K_{0.55}(AlSiO_4)_4$), metathenardite (Na_2SO_4), anhydrite $CaSO_4$, Al, Mg orthosilicate, and Zr_3O. Of these, nepheline, nosean, and Zr_3O are likely to affect glass durability. Nepheline and nosean have the potential to impact glass durability by sequestering glass-forming chemicals. The formation of nepheline has been observed to increase PCT boron release when present at concentrations ≥ 10 wt% (Kim et al. 1995; Lonergan et al. 2021). Zr_3O is an unlikely phase to form in LAW glasses melted in air. It is known to be stable in highly reducing environments but not stable in air (Zhang et al. 2015). It is likely that the actual crystal composition which matched this structure file is not Zr_3O, however, the phase corresponding to that XRD structure file has not yet been identified. Because it was only present in very small concentrations (~0.1 wt%), it’s unlikely to impact glass properties.

These data were used in crystal constraint development by Lonergan et al. (2021b) so were not used in model validation.

Table 3.1. Primary and Secondary Crystalline Phases in CCC LAW Phase 4 Glasses

Glass ID	Primary Phase	Wt%	Secondary phase	Wt%	Third Phase	Wt%
LP4-02	Grossular $Ca_3Al_2(SiO_4)_3$	1.6	SiO_2	0.5	Zr_3O	0.1
LP4-03	$Ca_4Na_6(SO_4)_6F_2$	3.3	Alinite $Ca_{11}Si_3AlO_{18}Cl$	1.1		
LP4-04-1	Nepheline $Na_3K_{0.55}(AlSiO_4)_4$	4.1				
LP4-05	Nosean $Na_8Al_6Si_6O_{24}(SO_4)$	0.5				
LP4-08-1	Grossular $Ca_3Al_2(SiO_4)_3$	1.8	SiO_2	0.8	Zr_3O	0.1
LP4-13	trace					
LP4-14	$Ca_4Na_6(SO_4)_6F_2$	3.3	Alinite $Ca_{11}Si_3AlO_{18}Cl$	0.4	Anhydrite $CaSO_4$	0.2
LP4-17	$Ca_4Na_6(SO_4)_6F_2$	4.0	Alinite $Ca_{11}Si_3AlO_{18}Cl$	1.1	Al,Mg Orthosilicate	0.5
LP4-19	Nosean $Na_8Al_6Si_6O_{24}SO_4$	10.9				
LP4-21	$Ca_4Na_6(SO_4)_6F_2$	2.5	Alinite $Ca_{11}Si_3AlO_{18}Cl$	0.7	Al,Mg Orthosilicate	0.2
LP4-22	trace					

trace = crystals were observed by OM, but the quantity was not enough to be detectable by XRD

3.4 Crystal Fraction in Isothermal Heat-Treatment

The long idling of the left-over glass in the melter at low temperatures might promote crystal formation impacting both glass durability by sequestering glass components that increase durability, and/or glass processability by settling in the melter clogging the pour sprout (Vienna et al. 2001). Therefore, the study of crystalline phases, quantities and T_L in isothermal heat-treatments is part of the regular investigation of LAW glasses.

Crystal fraction as a function of temperature was measured as described in Section 2.5 at 800 °C, 850 °C, 900 °C, and 950 °C. Only one glass—LP2-06-2—needed higher temperature heat treatments because of the presence of SnO. Results are reported in Table 3.2 and pictures of the 950 °C samples are shown in Appendix D. The main crystalline phases were $Ca_4Na_6(SO_4)_6F_2$, alinite ($Ca_{11}Si_3AlO_{18}Cl$), nosean ($Na_8Al_6Si_6O_{24}(SO_4)$), nepheline ($Na_3K_{0.55}(AlSiO_4)_4$) and an Al Mg Orthosilicate phase. Two samples, LP2-06-2 and LP2-25-1 formed cassiterite (SnO_2). In LP2-06-2, cassiterite was the primary phase; whereas, in LP4-25-1, it appeared after the 950 °C heat treatment when the crystalline phases present at lower temperatures disappeared. The CF at 1000 °C was not performed on LP4-25-1 because it was likely where T_L was and the quantity of crystals, if any, would have been too low to be detected by XRD.

Of the crystals formed, nepheline, nosean and cassiterite have the highest potential to affect glass durability and/or processability. As discussed previously, nepheline, nosean, and cassiterite could reduce glass durability by sequestering glass components that improve durability (Kim et al. 1995, Lonergan et al. 2021). In addition, with a density of 6.95 g/cm^3, cassiterite is the perfect candidate to have negative consequences for the melter (i.e., it could clog the pour spout) (Lonergan et al. 2021b). In the baseline WTP glass formulation, cassiterite crystal formation is not a concern because SnO_2 is not added. However, in the enhanced waste glass formulations SnO_2 has been added to improve VHT performance due to the higher waste loading.

T_L is defined as the highest temperature at which the glass is thermodynamically in equilibrium with the main crystalline phase (Riley et al. 2011). Therefore, one way to avoid crystal settling in the melter, is to use glass compositions that will not form crystals at the melter idling temperature or the coolest spot within the pour-spout riser. One of the methods to measure T_L is to extrapolate the temperature at which the content of crystal is zero using at least three CFs taken at temperature below T_L. In the current study, not all samples had three measurable CF data points, in which case the following assumption were made. When a glass had no visible crystals after the 800 °C heat treatment, the T_L was assumed to be below 800 °C and the glasses are not reported in Table 3.2. When a glass had a main measurable crystalline phase only in one or two heat treated samples, T_L was reported as less than the next higher heat treatment temperature examined in which no crystals were found. For example, for glass LP4-03 the last crystals were observed by OM at 900 °C; however, the quantity was too low to be detected by XRD. Therefore, T_L was reported as < 950 °C. When it was possible to extrapolate the T_L, the data are reported. In all other cases, T_L was calculated (Table 3.2).

Table 3.2. Crystalline Phases Recognized by XRD in CF LAW Phase 4 Glasses and Suggested Liquidus Temperature

Glass ID	Temperature (°C)						Crystalline Phases
	800	850	900	950	1000	1100	
LP4-01	trace						
LP4-03	2.5	2.6	trace				$Ca_4Na_6(SO_4)_6F_2$
	0.7	0.6					Alinite $Ca_{11}Si_3AlO_{18}Cl$
	0.2	0.1					$Al_{0.5}Mg_{0.25}\ Si_{0.5}O_2$
LP4-04-1	8.5	trace					Nepheline [$Na_3K_{0.55}(AlSiO_4)_4$ and $K(Na,K)_3Al_4Si_4O_{16}$]
LP4-05	14.9	0.9	trace				Nosean $Na_8Al_6Si_6O_{24}SO_4$
LP4-06-2				1.9	2.0	1.8	SnO_2
LP4-07-1	3.7	4.1	3.2				Alinite $Ca_{11}Si_3AlO_{18}Cl$
	2.1						$Ca_4Na_6(SO_4)_6F_2$
	0.1	0.4					Anhydrite $Ca(SO_4)$
		3.0	0.3	0.5			SnO_2
			0.5				$Al_{0.5}Mg_{0.25}\ Si_{0.5}O_2$
LP4-08-1	trace						
LP4-13	trace						
LP4-14	1.8	trace					Alinite $Ca_{11}Si_3AlO_{18}Cl$
	1.1						$Ca_4Na_6(SO_4)_6F_2$
	0.2						$Al_{0.5}Mg_{0.25}\ Si_{0.5}O_2$
LP4-17	2.8	2.7	1.6	0.8			$Ca_4Na_6(SO_4)_6F_2$
	1.4	1.4	0.5	0.3			Alinite $Ca_{11}Si_3AlO_{18}Cl$
	0.5	0.4	0.2				$Al_{0.5}Mg_{0.25}\ Si_{0.5}O_2$
LP4-18	trace						
LP4-19-1	15.6	16.2	10.0				Nosean $Na_8Al_6Si_6O_{24}SO_4$
LP4-20							
LP4-21	2.1	2.2	1.3	1.0			$Ca_4Na_6(SO_4)_6F_2$
	0.9	1.1	0.6	0.3			Alinite $Ca_{11}Si_3AlO_{18}Cl$
	0.4	0.4	0.3				$Al_{0.5}Mg_{0.25}\ Si_{0.5}O_2$
LP4-22	trace						
LP4-23-1	trace	0.6					$Al_{0.5}Mg_{0.25}\ Si_{0.5}O_2$
LP4-24	2.9	trace					Nepheline $Na_3K_{0.55}(AlSiO_4)_4$
LP4-25-1	1.3	trace					$Ca_4Na_6(SO_4)_6F_2$
	0.5						Alinite $Ca_{11}Si_3AlO_{18}Cl$
	0.1						$Al_{0.5}Mg_{0.25}\ Si_{0.5}O_2$
				0.3			SnO_2

trace = crystals were observed by OM, but the quantity was not enough to be detectable by XRD

These data were used in development of crystal constraints for plant operation reported by Lonergan (2021b) and so were not used to validate any models.

3.5 Density

This section discusses the results of the glass density measurements obtained using the methods discussed in Section 2.6. The results of the glass density measurements ranged from 2.561 g/cm^3 to 2.769 g/cm^3 and are shown in Table 3.3. The glasses have an average density of 2.645 g/cm^3.

Table 3.3. Measured Densities in LAW Phase 4 Glasses

Glass ID	Measured Density (g/cm^3)	Glass ID	Measured Density (g/cm^3)
LP4-01	2.73	LP4-14	2.66
LP4-02	2.59	LP4-15	2.63
LP4-03	2.61	LP4-16	2.61
LP4-04-1	2.60	LP4-17	2.63
LP4-05	2.64*	LP4-18	2.71
LP4-06-2	2.62	LP4-19	2.59
LP4-07-1	2.77	LP4-20	2.65
LP4-08-1	2.62	LP4-21	2.63
LP4-09	2.67	LP4-22	2.56
LP4-10	2.64	LP4-23-1	2.67
LP4-11	2.59	LP4-24	2.62
LP4-12	2.64	LP4-25-1	2.73
LP4-13	2.73		

* Average of two measurements

Two models were used to predict the density of LAW Phase 4 glasses: the molar-volume-based density model (Vienna et al. 2002) and the specific volume-based density model (Vienna et al. 2009).

The molar-volume based model (Vienna et al. 2002) predicts density, ρ, using the following equation:

$$\rho = \frac{\sum_{i=1}^{N} M_i x_i}{V} \tag{3.4}$$

where M_i is the molecular weight of the i^{th} component, x_i is the mole fraction of the *i*-th component, and V is the partial molar volume of the i^{th} component as listed in Table S.5 of Vienna et al. (2002).

The specific volume-based density model (Vienna et al. 2009) predicts density by using the partial-specific volume of oxides with the following formula:

$$\rho = \frac{1}{\sum_{i=1}^{N} v_i x_i} \tag{3.5}$$

where v_i is the partial-specific volume of the i^{th} glass component, x_i is the mass fraction of the i^{th} component, and N is the total number of glass components.

Measured versus predicted density (g/cm^3) is plotted in Figure 3.2.

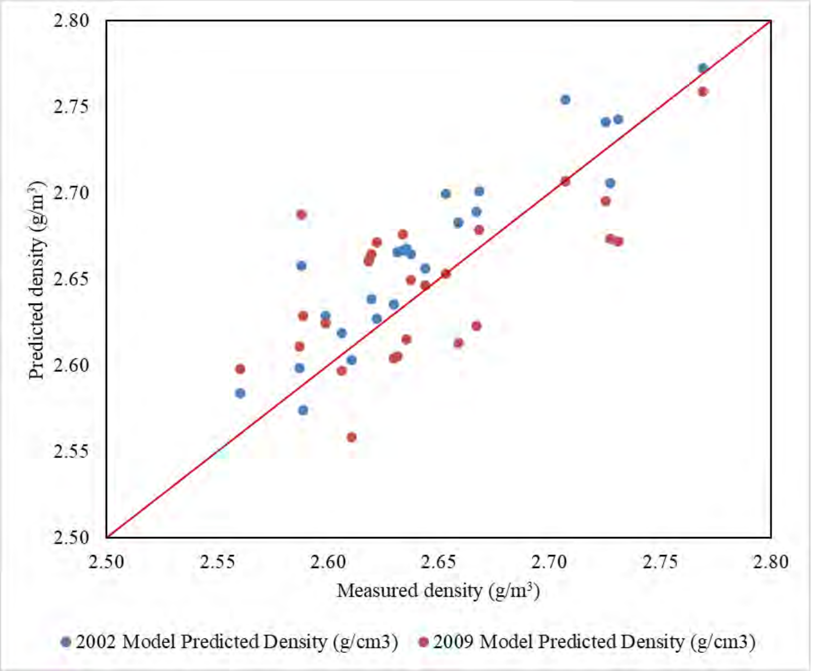

Figure 3.2. Plot of Predicted versus Measured Densities in LAW Phase 4 using the 2002 and 2009 Models. Note, the 2002 model is not compliant with the Nuclear Quality Assurance Requirements and Descriptions requirements (Daudt 2015)

The molar volume density model should be considered for interim use only because it was not developed according to the Nuclear Quality Assurance Requirements and Descriptions requirements (Daudt 2015). However, it has the advantage of leading to a better understanding of the relation between the model coefficients and the effect of each component on glass structure. As expected, this model showed the best fit clustering close to the 45° line (Figure 3.2).

3.6 Viscosity

This section presents and discusses the viscosity results obtained using the methods discussed in Section 2.7. The results of the viscosity measurements are listed in Appendix F and summarized in Table 3-4.

At the melting temperature of 1150 °C, the optimal viscosity of LAW glass melts should be maintained between 2 and 8 Pa-s to avoid processing issues (Vienna et al. 2020). Of the 25 glasses, eight had measured viscosity at 1150 ºC outside this range with most of them being less than 2 Pa-s and just two above 8 Pa-s (see Table 3-4).

Table 3-4. Measured η (Pa-s) Values Versus Target Temperature (in the sequence of measurement) for the LAW Phase 4

Target Temperature (°C)	1150	1050	950	1150	1250	1150
Glass ID	ln *η* (Pa-s)					
LP4-01	0.101	1.011	2.144	0.0900	-0.436	0.156
LP4-02	1.898	2.833	3.979	1.897	1.277	1.90
LP4-03	0.650	1.469	2.485	0.542	0.043	0.691
LP4-04-1	1.130	1.986	3.218	1.111	0.327	1.119
LP4-05	0.975	1.850	3.038	0.920	0.396	1.007
LP4-06-2	2.626	3.569	4.767	2.530	2.031	2.455
LP4-07-1	1.199	2.322	3.597	1.127	0.240	1.282
LP4-08-1	1.687	2.642	3.899	1.681	0.890	1.678
LP4-09	0.523	1.196	2.284	0.508	-0.155	0.586
LP4-10	0.630	1.442	2.498	0.593	-0.134	0.584
LP4-11	2.184	3.225	4.617	2.216	1.743	2.178
LP4-12	1.972	3.016	4.377	1.994	1.202	1.958
LP4-13	0.118	0.952	1.985	0.212	-0.126	0.120
LP4-14	0.168	1.0920	2.247	0.208	-0.143	0.161
LP4-15	1.535	2.524	3.786	1.637	1.295	1.572
LP4-16	1.041	1.927	3.078	1.194	0.833	1.058
LP4-17	0.718	1.589	2.782	0.755	0.371	0.714
LP4-18	1.244	2.218	3.591	1.294	0.922	1.240
LP4-19	2.103	3.170	4.562	2.122	1.593	2.089
LP4-20	0.606	1.434	2.610	0.598	0.245	0.566
LP4-21	2.053	3.170	4.691	2.067	1.536	2.010
LP4-22	1.583	2.453	3.606	1.590	1.220	1.582
LP4-23-1	1.252	2.189	3.421	1.261	0.857	1.223
LP4-24	1.100	1.978	3.074	1.112	0.715	1.102
LP4-25-1	0.861	1.711	2.945	0.900	0.473	0.851

Two model forms are used here to fit viscosity-temperature data for each waste glass. The first model form is the Arrhenius equation:

$$\ln(\eta) = A + \frac{B}{T_K} \tag{3.6}$$

where A and B are coefficients independent of temperature (T_K), expressed in Kelvin (T(°C) + 273.15). The values for the A and B coefficients are reported in Table 3.5 for each glass.

The second model is the Vogel-Fulcher-Tamman (VFT) model:

$$\ln(\eta) = E + \frac{F}{T_k - T_0} \tag{3.7}$$

where E, F, and T_0 are temperature independent coefficients and T_K is the temperature in Kelvin (T(°C) + 273.15). This model can be used to estimate the effect of temperature on viscosity over a wide range of temperatures for silicate-based glasses. Therefore, this model also was applied to the data for each glass; the E, F, and T_0 coefficients for each glass are shown in Table 3.5. Furthermore, Table 3.5 summarizes the viscosity results at 1150 °C (η_{1150}) calculated using both the Arrhenius and the VFT equations for these glasses.

Table 3.5. Fitted Coefficients of Arrhenius and VFT Models for Viscosity of LAW Phase 4

	Arrhenius Coefficients		VFT Coefficients			Calculate η_{1150} (Pa-s)	
	A	B	E	F	T_0 (K)	Arrhenius	VFT
Glass ID	(ln Pa·s)	(ln Pa-s·K)	(ln Pa-s)	(ln Pa-s K)			
LP4-01	-11.85	17063	-6.167	5166	601.8	1.15	1.13
LP4-02	-10.45	17620	-6.483	8526	408.1	6.88	6.80
LP4-03	-10.69	16105	-9.507	13073	132.8	1.87	1.87
LP4-04-1	-11.41	17832	-6.820	7548	470.3	3.06	3.01
LP4-05	-11.39	17600	-6.049	6140	547.1	2.65	2.61
LP4-06-2	-11.31	19673	44.678	155860*	5122.2	12.41	12.72
LP4-07-1	-14.06	21657	211.200	3645100*	18780.0	3.17	3.29
LP4-08-1	-11.47	18744	-6.300	7332	504.0	5.47	5.35
LP4-09	-9.91	14846	-5.745	5693	512.2	1.69	1.66
LP4-10	-10.87	16332	-8.706	10980	242.7	1.83	1.81
LP4-11	-12.37	20729	-5.544	6467	586.5	8.98	8.90
LP4-12	-12.28	20314	-6.314	7371	533.6	7.34	7.18
LP4-13	-11.16	16065	-7.912	8562	357.9	1.14	1.13
LP4-14	-12.36	17847	-8.122	8310	421.7	1.20	1.19
LP4-15	-11.80	19032	-5.724	6258	565.0	4.81	4.80
LP4-16	-11.05	17252	-5.656	5855	552.6	2.91	2.91
LP4-17	-11.54	17472	-5.015	4351	664.9	2.08	2.06
LP4-18	-12.29	19327	-3.182	2603	839.1	3.65	3.58
LP4-19	-12.46	20761	-5.020	5572	641.7	8.40	8.26
LP4-20	-11.57	17300	-5.518	4887	621.6	1.80	1.79
LP4-21	-13.76	22502	-5.752	6146	634.6	7.81	7.70
LP4-22	-10.56	17293	-5.003	5601	572.4	4.89	4.86
LP4-23-1	-11.84	18630	-6.155	6509	543.3	3.49	3.47
LP4-24	-10.81	16959	-7.006	8297	400.0	3.03	3.01
LP4-25-1	-11.40	17480	-4.052	3307	750.3	2.41	2.37

Vienna et al. (2020) model used a reduced PQM to predict viscosity at the melter operating temperature of 1150 °C. Predicted versus measured η_{1150}, calculated using the VFT equation (Equation 3-7), are illustrated in Figure 3.3. The model slightly underpredicted at lower η_{1150} and matched the measured data very well at higher values, except for LP4-06-2, a glass with 12.9 wt% aluminum oxide (Figure 3.3). The model validation R^2 value (R^2_{val}) was 0.9057 compared to the model fit R^2 of 0.9487. After applying prediction and measurement uncertainties, 24 of the 25 validation glasses had confidence rectangles that intersected 45° line, for a success proportion of 96%. Thus the 90% validation criterion was met for the viscosity model.

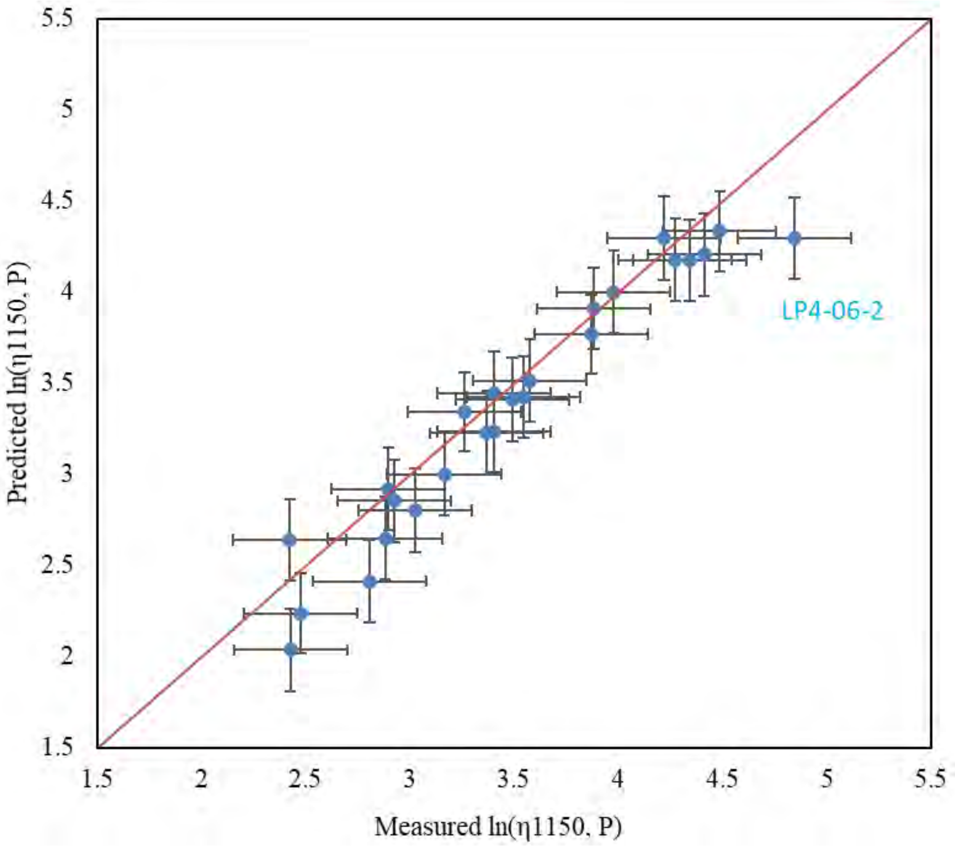

Figure 3.3. Measured Versus Predicted η_{1150} in in Natural Log Scale of LAW Phase 4 Glasses Using the Vienna et al. (2020) Model. Prediction uncertainties (vertical error bars) and measurement uncertainties (horizontal error bar) are added.

3.7 Electrical Conductivity

This section presents and discusses the ε results obtained using the methods discussed in Section 13. Table 3.6 lists the ε versus temperature data for each glass, and Appendix G shows plots for the ε versus temperature data obtained from the ε testing.

The Arrhenius equation (Equation 3.6) was used. The values for the A and B coefficients obtained by fitting the equation to the ε-temperature data for each glass (using least squares regression) are shown in Table 3.7 for each glass along with the calculated ε at 1150 °C (ε_{1150}) using Equation 3.6 fit to each glass measured data.

Figure 3.4 shows measured ε_{1150}, calculated using the Arrhenius equation, versus predicted values using the PQM for electrical conductivity from Vienna et al. (2020). The model appears to predict fairly well with some expected scatter. The R2-validation was 0.5231 compared to the model fit R2 of 0.8563. The low validation R-squared is largely due to the three outliers labeled in the plot (Figure 3.4). Removing the three data points would produce an R2-validation of 0.8786. Further research is needed to identify all the possible reasons behind the low R2-validation value. After applying prediction and measurement uncertainties, confidence rectangles intercepted the 45° line for all 25 validation glasses. Thus the 90% validation criterion was met for the electrical conductivity model.

Table 3.6. Measured Electrical Conductivity (S/m) Values Versus Temperatures for the LAW Phase 4 Glasses

Target Temperature	950°C	950°C	1250°C	1250°C	1150°C	1150°C	1050°C	1050°C
Glass ID	Electrical Conductivity (S/m)							
LP4-01	34.53	34.50		48.55		62.76	76.62	76.51
LP4-02	17.06	17.03	26.55	26.52	36.86	36.82		47.82
LP4-03	15.71	15.67		26.02	37.85	37.78	50.57	50.62
LP4-04-1	11.13	11.00	18.68	18.64		28.52	39.32	39.22
LP4-05	21.54	21.53	32.36	32.28	43.59	43.48		57.01
LP4-06-2	11.47	11.45	18.70	18.69		27.07		35.94
LP4-07-1	7.99	7.97	14.30	14.27	22.66	22.61	32.23	32.18
LP4-08-1	14.25	14.22		21.91	30.86	30.83	41.02	41.02
LP4-09	25.45	25.40	38.16	38.14	51.92	51.79	64.39	64.32
LP4-10	25.93	25.81	36.97	36.89	47.46	47.36	55.66	55.06
LP4-11	11.93	11.87	18.23	18.20		25.16		32.53
LP4-12	13.12	13.06	20.66	20.60		29.28	38.37	38.48
LP4-13	26.27	26.19	39.21	39.10		52.42	65.75	65.76
LP4-14	27.09	27.01	40.36	40.25		54.11	68.07	68.05
LP4-15	27.95	27.90	38.76	38.64	49.67	49.62	60.27	60.27
LP4-16	21.25	21.20	31.17	31.08		42.29	53.68	53.69
LP4-17	15.56	15.50	24.92	24.84	35.51	35.45	46.56	46.70
LP4-18	13.45	13.40	22.32	22.28	33.24	33.11	45.39	45.52
LP4-19	23.00	22.91	33.26	33.10	44.01	43.96	54.67	54.71
LP4-20	23.65	23.57	34.76	34.64		46.58		59.06
LP4-21	9.22	9.18	15.92	15.89	24.31	24.29	32.93	33.02
LP4-22	25.09	25.02	34.93	34.83		44.93	54.95	54.88
LP4-23-1	21.45	21.37	32.56	32.49		44.60	57.18	57.20
LP4-24	23.07	23.00	33.92	33.74	45.06	45.08	56.43	56.45
LP4-25-1	12.57	11.91	22.71	22.53		35.38	49.32	49.45

Table 3.7. Fitted Coefficients of Arrhenius Model for ε_{1150} of LAW Phase 4 Glasses

Glass ID	Arrhenius Coefficients		Calculated
	A, ln[S/m]	B, ln[S/m]-K	ε_{1150} (S/m)*
LP4-01	7.60	-4954.7	61.61
LP4-02	8.16	-6486.3	36.54
LP4-03	8.74	-7304.9	36.97
LP4-04-1	8.86	-7871.4	27.78
LP4-05	8.02	-6045.9	43.65
LP4-06-2	8.33	-7178.1	26.64
LP4-07-1	9.20	-8689.1	22.13
LP4-08-1	8.05	-6585.7	30.57
LP4-09	8.00	-5795.2	50.61
LP4-10	7.17	-4756.5	46.00
LP4-11	7.64	-6302.3	24.91
LP4-12	8.05	-6680.3	28.71
LP4-13	7.94	-5689.8	51.47
LP4-14	7.99	-5715.2	53.16
LP4-15	7.26	-4784.8	49.06
LP4-16	7.78	-5762.1	41.63
LP4-17	8.36	-6838.1	34.82
LP4-18	8.82	-7584.9	32.66
LP4-19	7.57	-5401.2	43.37
LP4-20	7.87	-5739.2	46.22
LP4-21	8.76	-7967.1	23.58
LP4-22	7.21	-4865.0	44.37
LP4-23-1	8.06	-6088.0	43.85
LP4-24	7.71	-5569.2	44.46
LP4-25-1	9.61	-8644.9	34.17

*ε_{1150} calculated using the measured coefficients as reported in the table

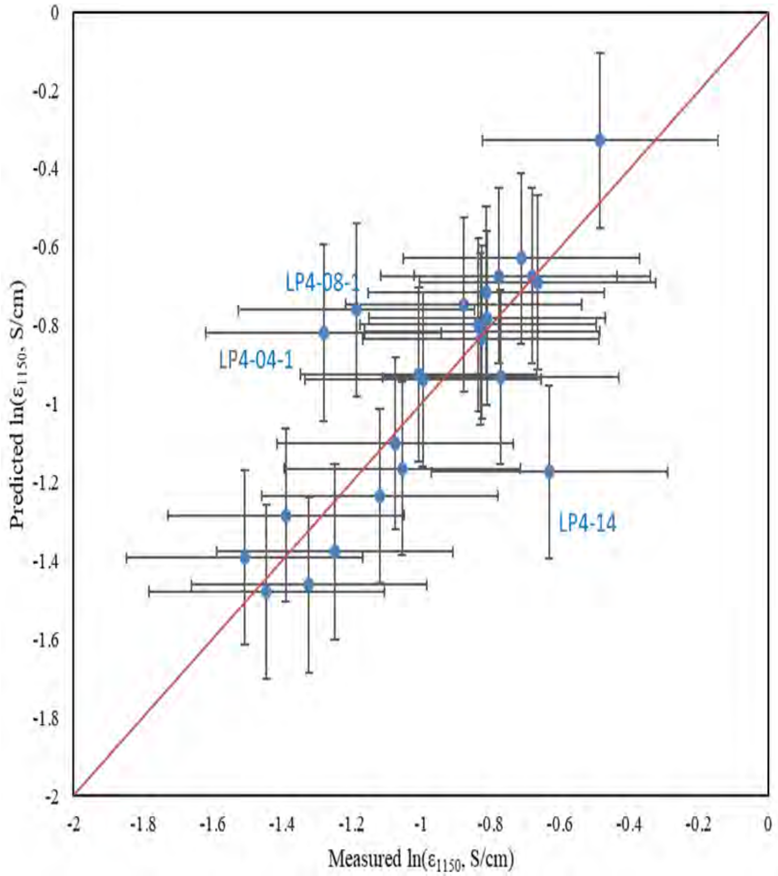

Figure 3.4. Measured Versus Predicted ε1150 in Natural Log Scale of LAW Phase 4 Glasses using the Vienna et al. (2020) Model. Prediction uncertainties (vertical error bars) and measurement uncertainties (horizontal error bar) are added.

3.8 °Product Consistency Test

PCTs were performed at PNNL, and the PCT leachates were analyzed at SRNL (Hsieh 2020b). Each sample was run in triplicate, and the relative standard deviation for B, Na, and Li was found to be less than 10% in all samples, thus suggesting no significant issues with the analytical outcomes for the measurements of the PCT leachates.

The normalized PCT release (NR) for B, Na, Li and Si are reported in Table 3.8 and Table 3.9 for quenched and CCC glasses, respectively. Per WTP contract (DOE 2000), the NR for B, Na, and Si must be below 2.0 g/m^2. Overall, 28% of quenched glasses exceeded the NR_B limit, 40% exceeded NR_{Na} limit and 4% exceeded NR_{Si} limit. Of the CCC samples, 36% exceeded NR_B limit, 32% NR_{Na} limit and 4% NR_{Si} limit.

Table 3.8. Normalized PCT Releases for Quenched LAW Phase 4 Glasses. Missing values were below the analytical laboratory detection limit

Glass ID	NR_B, g/m^2	NR_{Li}, g/m^2	NR_{Na}, g/m^2	NR_{Si}, g/m^2
LP4-01	2.815		2.353	0.327
LP4-02	0.197	0.294	0.220	0.122
LP4-03	0.586	0.617	0.561	0.113
LP4-04-1	0.428	0.679	0.595	0.170
LP4-05	0.589		0.700	0.165
LP4-06-2	0.277	0.565	0.365	0.135
LP4-07-1	0.313	0.613	0.529	0.111
LP4-08-1	0.283	0.387	0.497	0.202
LP4-09	15.010	9.601	11.263	0.638
LP4-10	14.959	9.953	11.983	2.345
LP4-11	0.431	0.426	0.434	0.120
LP4-12	4.903	4.208	3.747	0.402
LP4-13	14.459	10.403	11.932	1.580
LP4-14	4.929	4.697	4.871	0.493
LP4-15	0.490		0.612	0.176
LP4-16	3.273	2.832	2.192	0.458
LP4-17	12.542	11.141	11.303	0.760
LP4-18	0.955	1.141	1.187	0.363
LP4-19	0.252	1.122	0.410	0.130
LP4-20	4.479	3.985	3.332	0.279
LP4-21	0.501	0.568	0.498	0.168
LP4-22	3.819	2.666	2.227	0.140
LP4-23-1	0.614	0.754	0.865	0.292
LP4-24	0.673	0.621	0.637	0.163
LP4-25-1	0.666	0.820	0.754	0.225

Table 3.9. Normalized PCT Releases for CCC LAW Phase 4 Glasses

Glass ID	NR_B, g/m^2	NR_{Li}, g/m^2	NR_{Na}, g/m^2	NR_{Si}, g/m^2
LP4-01	3.012		2.489	0.306
LP4-02	0.159	0.366	0.228	0.123
LP4-03	0.964	0.958	0.831	0.127
LP4-04-1	1.138	1.464	0.927	0.264
LP4-05	0.457		0.595	0.146
LP4-06-2	0.281	0.408	0.307	0.120
LP4-07-1	0.374	0.548	0.569	0.115
LP4-08-1	0.246	0.391	0.427	0.186
LP4-09	12.815	8.250	9.551	0.593
LP4-10	11.903	8.167	10.022	2.052
LP4-11	0.123	0.374	0.210	0.102
LP4-12	4.307	3.969	3.373	0.381
LP4-13	8.223	7.114	6.713	1.251
LP4-14	2.081	2.333	2.068	0.343
LP4-15	0.484		0.630	0.186
LP4-16	1.981	1.800	1.381	0.363
LP4-17	5.355	5.536	4.761	0.647
LP4-18	0.758	0.994	0.964	0.298
LP4-19	0.651	1.122	0.603	0.141
LP4-20	4.278	3.746	3.318	0.266
LP4-21	0.549	0.647	0.498	0.171
LP4-22	2.067	1.707	1.224	0.144
LP4-23-1	0.683	0.849	0.850	0.285
LP4-24	1.394	1.311	1.024	0.206
LP4-25-1	0.500	0.660	0.584	0.178

The glasses were divided into three groups depending on the quantity of crystals observed by OM or found by XRD after CCC: crystallinity <1wt% and crystallinity >1wt%. All other glasses with crystal content above 1 wt% were grouped under the label "crystallinity >1wt%" (see Section 3.3 for details on crystals). Quenched versus CCC normalized NR_B and NR_{Na} were plotted in Figure 3.5 and Figure 3.6, respectively.

To determine if the difference between quenched and CCC heat treated glasses was within experimental error, the following hypothesis was tested (Rieck 2018):

$$p_Q - p_C = 0 \tag{3.9}$$

where p_Q and p_C are the true but unknown values of quenched and the CCC NR_B or NR_{Na}.

To test this hypothesis, we considered $\hat{p}_C - \hat{p}_Q \pm k \cdot SD(\hat{p}_C - \hat{p}_Q)$ to see if:

$$0 \in \left(\hat{p}_c - \hat{p}_Q - k \cdot SD(\hat{p}_C - \hat{p}_Q),\ \hat{p}_c - \hat{p}_Q + k \cdot SD(\hat{p}_C - \hat{p}_Q)\right) \tag{3.10}$$

where $\hat{p}_Q$ and $\hat{p}_c$ are the measured values of the quenched and the CCC NRB or NRNa, k is a multiplying factor based on the assumed normal distribution of $\hat{p}_C - \hat{p}_Q$ and intended confidence level for the test (in the present study set at 95%), and $SD(\hat{p}_C - \hat{p}_Q)$ is the estimated standard deviation of $\hat{p}_c - \hat{p}_Q$. Assuming SD($\hat{p}_C$) = SD($\hat{p}_Q$) = SD, then:

$$\hat{p}_c - \hat{p}_Q \pm kSD(\hat{p}_c - \hat{p}_Q) = \hat{p}_c - \hat{p}_Q \pm k\sqrt{2}SD \tag{3.11}$$

That is, the measured property of CCC glass is considered the same as that of quenched glass within the experimental error if the following condition is satisfied:

$$\hat{p_Q} \epsilon \left(\hat{p_c} - k\sqrt{2}\ SD, \hat{p_c} + k\sqrt{2}\ SD\right) \tag{3.12}$$

Of 25 glasses, 20 NR_B (80%) and 22 NR_{Na} (88%) satisfied the condition. Most of the samples lay on the 45° line for NR_B and all for NR_{Na} (Figure 3.5 and Figure 3.6). Three values did not lay on the 45° line and were overpredicted by the NR_B model: LP4-04-1, LP4-19, and LP4-24. Of these samples, LP4-04-1 and LP4-10 had crystal contents > 1 wt%, 4.1 wt% and 10.9 wt%, respectively, with formation of nepheline and nosean. Lonergan et al. (2021) suggests that crystals in the Na-Al-silicate and Na-Ca-silicate families tend to have a significant impact over PCT responses usually if in concentrations of ≥10 wt%. LP4-24, did not form crystals during CCC (Figure 3.5).

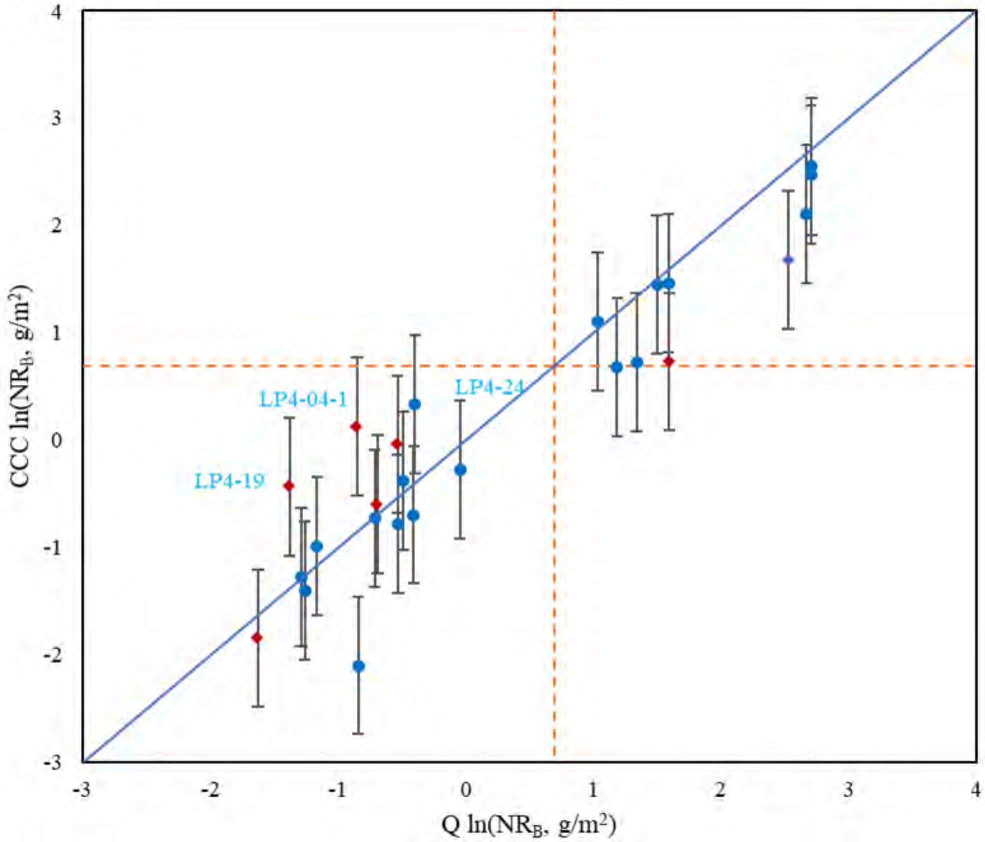

Figure 3.5. Normalized NR_B Release in Natural Logarithm Scale of Quenched Versus CCC LAW Phase 4 Glasses. Samples that formed >1 wt% of crystal after CCC are shown as red diamond symbols. Vertical Lines are the 95% standard deviation. Dashed lines are the natural logarithmic scale of the constraint = 2 g/m^2.

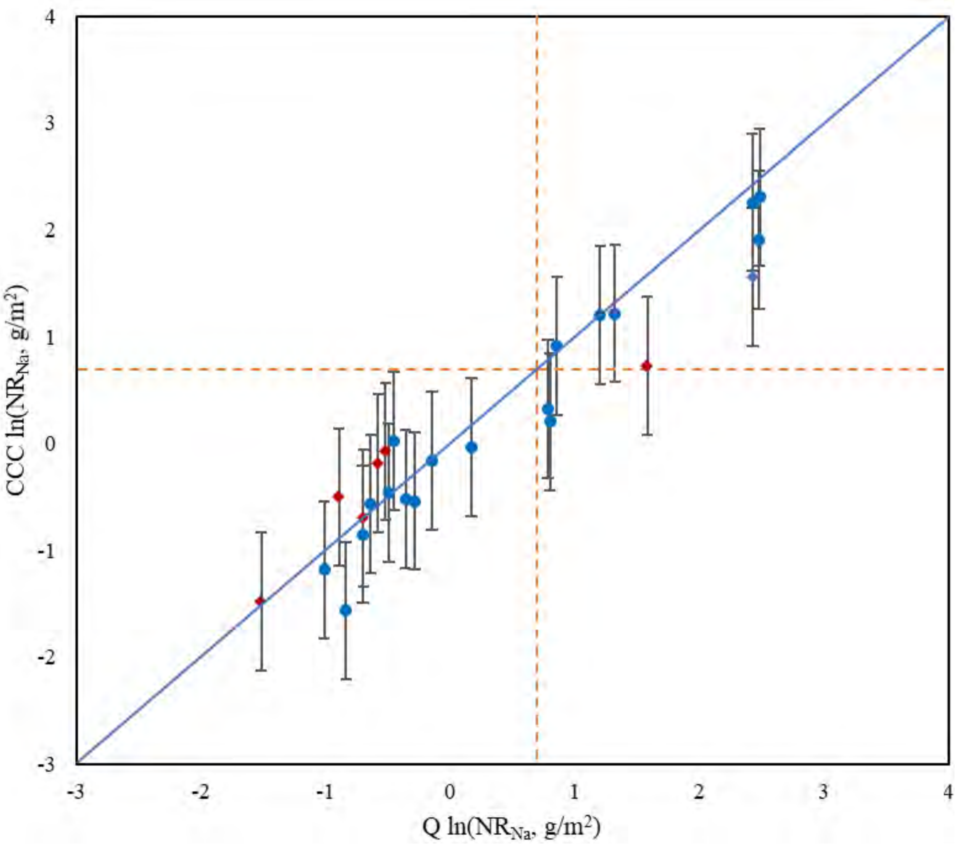

Figure 3.6. Normalized NR$_{Na}$ Release in Natural Logarithm Scale of Quenched Versus CCC LAW Phase 4 Glasses. Samples that formed >1wt% of crystal after CCC are shown as red diamond symbols. Dashed lines are the natural logarithmic scale of the PCT constraint = 2 g/m^2.

Figure 3.7 compares the predicted and measured ln[NRB] values using the model recommended by Vienna et al. (2020) model. The NRB model clearly underpredicted boron release values above 2 g/m^2 as well as showing a slightly larger scatter data about the 45° line in the same region of the predicted versus measured plot. The underprediction at higher NRB values was expected because it was observed during the model generation as well (Vienna et al. 2020). The R2-validation was 0.6311, which is lower than the model fit R2 of 0.7762. After applying prediction and measurement uncertainties, 80% (20 of 25) of the confidence rectangles for validation glasses intercepted the 45° line. Thus the 2020 model failed the 90% validation criterion.

Figure 3.8 compares the predicted and measured ln[NRNa] values. The NRNa model significantly underpredicts values above the 2 g/m^2 limit, whereas better results were observed at lower values. The authors observed similar results during the model generation (Vienna et al. 2020). The R2-validation was 0.7043, which is similar to the model fit R2 of 0.7621. The percentage of confidence rectangles intercepting the 45° line after applying prediction and measurement uncertainties to validation glasses was 88% (22 of 25), nearly meeting the 90% validation criterion.

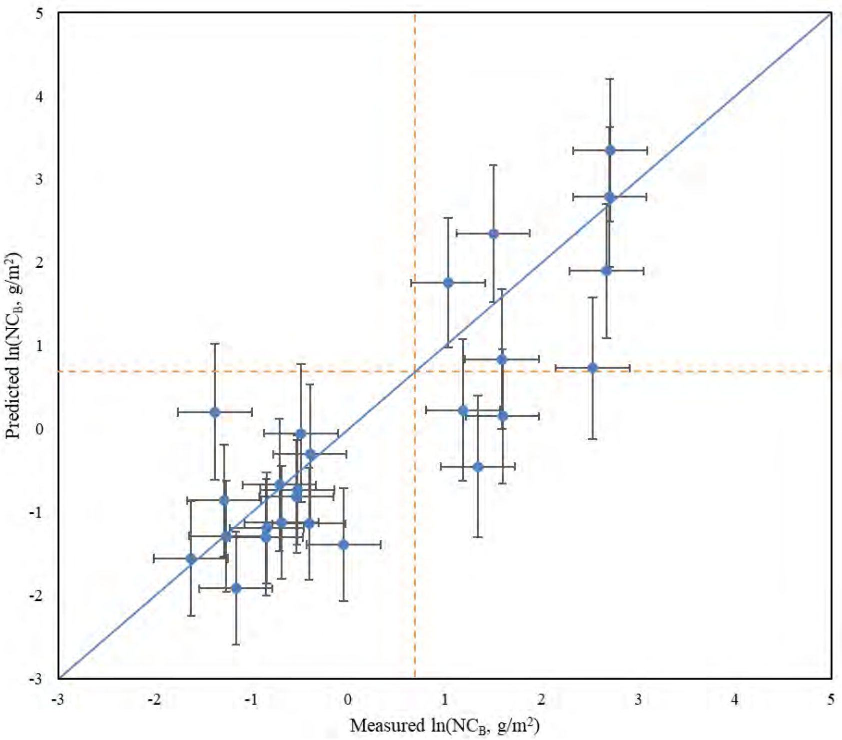

Figure 3.7. Natural Log Scale NR_B Versus Predicted Releases with Uncertainties using the 2020 Model. Orange dotted lines are the WTP limit

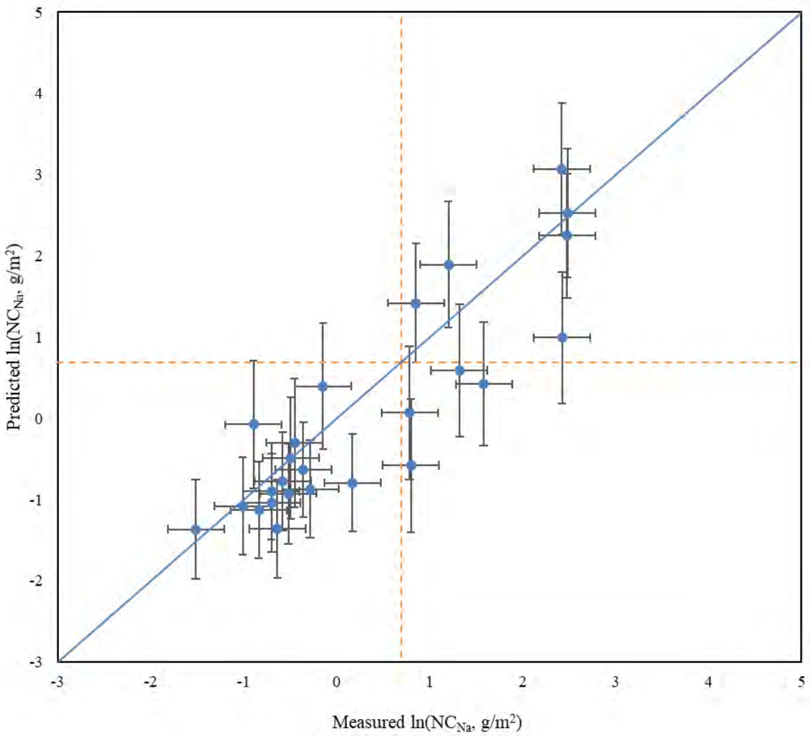

Figure 3.8. Natural Log Scale NRNa Versus Predicted Releases using the NRB 2020 Model. Orange dotted lines are the WTP limit

3.9 Vapor Hydration Test

In accordance with the WTP contract, the alteration rates (r) of LAW glasses subjected to >7-day VHT shall be less than 50 g/m^2/d (DOE 2000).

One of the 25 glasses was removed from the data analysis because of an error in the initial coupon measurements. Three quenched and two CCC samples were fully corroded after 24 days. VHT alteration rates for the remaining glasses varied from zero to >245 g/m^2/d for the quenched glasses and from 0.29 to >225 g/m^2/d for the CCC glasses. A total of seven quenched and five CCC glasses exceeded the WTP contract limit (Table 3.10).

Table 3.10. Alteration Depth and Rate for Quenched and CCC LAW Phase 4 Glasses after 24 Day VHT

	Quenched		CCC	
Glass ID	Alteration depth (µm)	Alteration rate (g/m^2/day)	Alteration depth (µm)	Alteration rate (g/m^2/day)
LP4-01	145.7	16.09	315.5	34.8
LP4-02	4.8	0.53	580.0	64.0
LP4-03	12.1	1.34	138.2	15.3
LP4-04-1	94.4	10.43	296.3	32.7
LP4-05	197.3	21.79	87.1	9.6
LP4-06-2	45.9	5.07	241.5	26.7
LP4-07-1	3.5	0.39	219.8	24.3
LP4-08-1	Fully corroded		636.7	70.3
LP4-09	0.0	0.00	57.0	6.3
LP4-10	512.9	56.63	Fully corroded	
LP4-11	Test failed		Test failed	
LP4-12	282.0	31.14	88.2	9.7
LP4-13	503.4	55.58	158.2	17.5
LP4-14	307.1	33.91	305.4	33.7
LP4-15	686.5	75.80	12.6	1.4
LP4-16	675.6	74.60	Fully corroded	
LP4-17	9.7	1.07	34.7	3.8
LP4-18	43.1	4.76	8.8	1.0
LP4-19*	41.6	4.59	0.0	0.0
LP4-20	Fully corroded		126.8	14.0
LP4-21	8.0	0.88	2.6	0.3
LP4-22	296.5	32.73	577.1	63.7
LP4-23-1	Fully corroded		3.5	0.4
LP4-24	19.2	2.12	274.0	30.2
LP4-25-1	48.8	5.38	221.6	24.5

* Extrapolated from the 7-day test to a 24-day test equivalent.

The Vienna et al. (2020) VHT model is in the form of a logistic model. Logistic models are often used to predict binary responses, in this case expressed as Pass/Fail for VHT. The predictor variables in the model represents glass compositions in the form of a PQM model while the response is a logit of the binary response. The model is used to calculate the probability that a given glass will fail the VHT.

$$\hat{y} = ln\left[\frac{P(g)}{1-P(g)}\right] = \sum_{i=1}^{q} b_i \cdot g_i = g^T b \tag{3.13}$$

where $\hat{y}$ = the model predicted logit value for a given glass
g = the composition for a given glass, expanded to match the model form
b = the vector of model coefficients
P(g) = the model predicted 'score' or probability that the binary response for a given glass composition (*g*) is 'success' (in this case, suggesting that the glass will fail the VHT)
q = the number of model parameters.

Note that the predicted probability or 'score' for a given glass, P(g), is calculated by inverting the logit transformation:

$$P(g) = \frac{e^{\hat{y}}}{1+e^{\hat{y}}} \tag{3.14}$$

As part of the development of the 2020 VHT model, the suggested threshold for predicted model 'scores' when classifying a given glass as pass or fail with respect to the VHT was set at 0.19. Thus, a glass having P(g) <0.19 is predicted to pass the VHT, whereas a glass having P(g) ≥0.19 is predicted to fail the VHT (Vienna et al. 2020).

Because of the binary nature of the model, only prediction uncertainties were applied. The measured alteration rate was converted to an observed 'pass'/'fail' status for each glass, and measurement uncertainty was not included in this process. Thus, validation agreement for a given glass was determined based on whether the prediction interval for that glass captured the designated threshold.

Figure 3.9 illustrates results comparing VHT model predictions to corresponding observed pass/fail binary responses determined from measured alteration rates for validation quenched glasses. The x-axis in this figure indicates the actual Pass/Fail status of the validation glasses, the y-axis shows model predicted logit values for the validation glasses. The red horizontal line in Figure 3.9 denotes the designated classification threshold for the VHT model, represented by its corresponding logit value.

The "as calculated" (i.e., without uncertainties) false positive rate was 10 ÷ 17 = 0.59. This means that of the 17 validation glasses that actually passed the VHT, the model predicted that 10 would fail the VHT (i.e., they had scores above the 0.19 threshold). When prediction uncertainties were applied, the false positive rate drops to 5 ÷ 17 = 0.29. These values are larger than the those observed during model development (0.24).

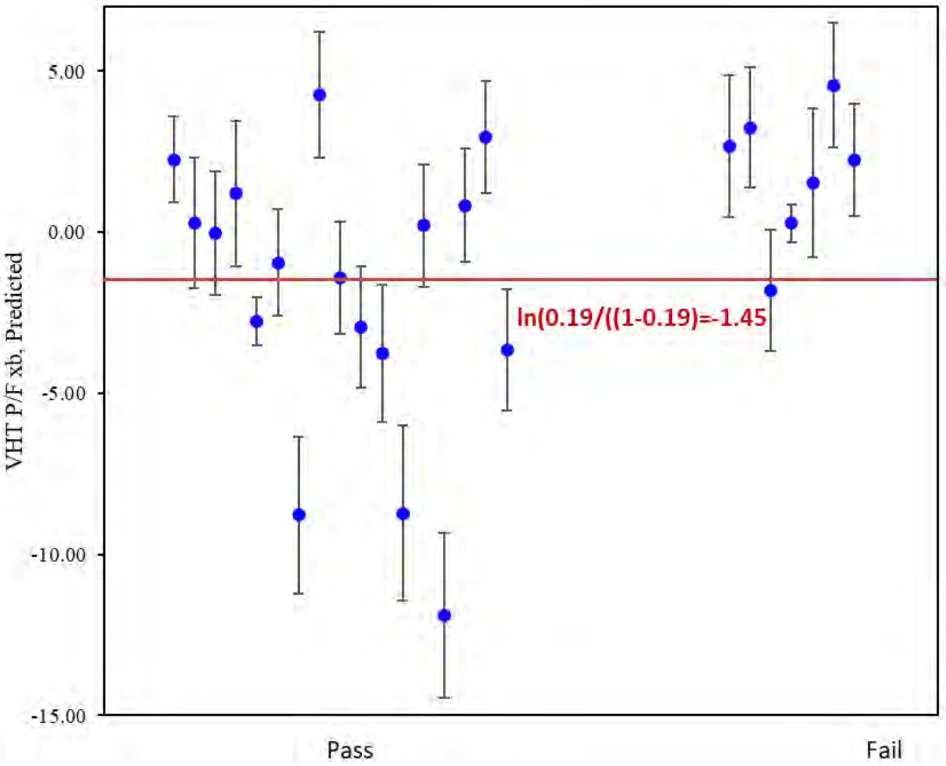

Figure 3.9. Predicted Versus Measured VHT Responses the 2020 Model. The orange line represents the threshold value of 0.19 for predicted model “scores” when classifying a given glass as pass or fail. A glass having *P*(*g*) <0.19 is predicted to pass. xb = ln[P(g)/(1-P(g)].

The “as calculated” (i.e., without uncertainties) false negative rate was 1 ÷ 7. This means that of the 7 validation glasses that actually failed the VHT, the VHT model predicted that only 1 would pass the VHT (i.e., had a score below the 0.19 threshold). This false negative rate is very close to the model expected false negative percentage of 10%. When prediction uncertainties were applied, the model succeeded in predicting all failed VHT glasses for the model validation set. It is worth noting that for this one glass, when uncertainty is applied, the threshold is exceeded, meaning that it would not be a successful formulation.

3.10 Sulfur Solubility

Melter SO_3 tolerance is the feed SO_3 concentration above which a salt phase accumulates in the melter. The melter SO_3 tolerance at the processing temperature of 1150 °C must exceed the weight percent of SO_3 in the feed to avoid risk of excessive corrosion of melter construction materials and increased radionuclide volatility (Vienna et al. 2014, Muller et al. 2015b). A preliminary constraint used to plan the Hanford cleanup mission (Vienna et al. 2013, 2016) has been that the SO_3 target concentration in melter feed (after converting to oxides/halogens) must be lower than the predicted melter SO_3 tolerance at 1150 °C.

There is a good correlation between the melter SO_3 tolerance and SO_3 solubility (i.e., the saturated SO_3 concentrations) at 1150 °C (Vienna et al. 2014, Jin et al. 2019, Skidmore et al. 2019). Hence, SO_3 solubility data developed primarily from crucible scale tests can be used to predict the melter SO_3 tolerance that can only be obtained from costly melter tests.

Sulfur solubility of each glass was determined experimentally by measuring SO_3 retention after 3× saturation (see Section 2.11 for procedure). Results are reported in Table 3.11. For more details, see Hsieh (2020c).

Table 3.11. Saturated SO_3 Concentrations in LAW Phase 4 Glasses after Sulfate Saturation Procedure

		SO_3 wt%	
Glass ID	Targeted SO_3 (wt%)	Initial Measured SO_3 (wt%)	Sulfate Saturated (wt%)
LP4-01	1.03	1.05	1.78
LP4-02	0.51	0.46	1.03
LP4-03	1.39	1.27	1.61
LP4-04-1*	1.40	0.81	1.24
LP4-05	1.07	1.05	1.35
LP4-06-2	0.29	0.19	0.91
LP4-07-1#	1.13	0.62	1.48
LP4-08-1*	1.21	0.62	1.09
LP4-09	0.85	0.87	1.91
LP4-10	0.23	0.31	1.36
LP4-11	0.11	0.15	0.80
LP4-12	0.48	0.42	1.12
LP4-13	1.21	1.16	1.74
LP4-14	1.05	1.03	1.92
LP4-15	0.51	0.54	1.24
LP4-16	0.63	0.62	1.56
LP4-17	1.40	1.33	2.60
LP4-18	0.67	0.69	1.73
LP4-19*	1.44	0.60	0.89
LP4-20	0.86	0.85	1.44
LP4-21	1.46	1.08	1.22
LP4-22	1.03	0.91	1.02
LP4-23-1	0.95	0.77	1.53
LP4-24	0.32	0.33	1.04
LP4-25-1	0.65	0.32	1.72

*Glass was washed before the final melt to help remove superficial sulfate.
#SO_3 loss most likely due to volatilization due to high melting temperatures.

Measured SO_3 solubility at 1150 °C as reported in Table 3.11 was converted into melter SO_3 tolerance by subtracting an offset of 0.33 wt%, and measured versus predicted SO_3 melter tolerance are plotted in Figure 3.10 (Skidmore et al. 2019).

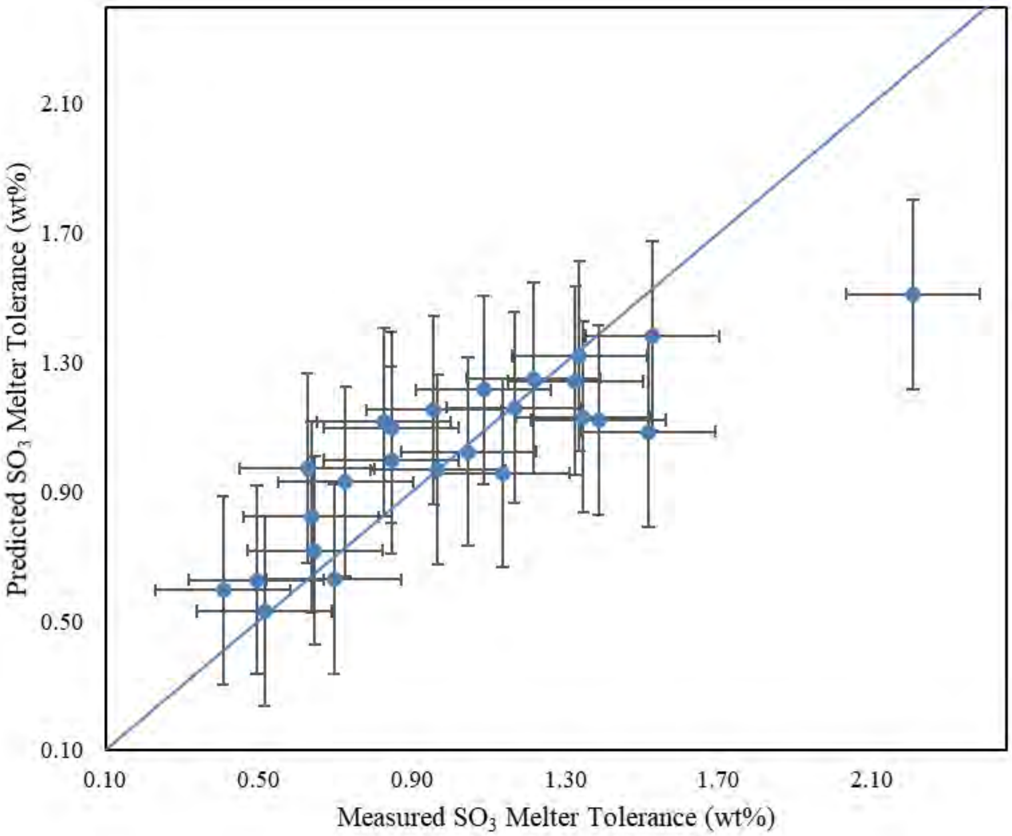

Figure 3.10. Measured Versus Predicted SO_3 Solubility (wt%) Using the SO_3 2020 Model

The Vienna et al. (2020) model appears to predict very well for validation glasses except for one outlier, LP4-17, a glass with the highest SO_3 content. Similar results were observed during the model generation where the highest SO_3 responses were underpredicted (Vienna et al. 2020). The R2-validation was 0.6732 and was lower than the model fit R2 of 0.8303. The percentage of validation glasses with confidence rectangles intercepting the 45° line after applying prediction and measurement uncertainties was 96%, which is well above the 90% model validation criterion for the SO_3 melter tolerance model.

4.0 Conclusions

This report summarizes the data collected and analyzed on the fourth test matrix of 25 LAW glass compositions intended to fill the enhanced LAW glass composition region over which glass property-composition data and models are available and to validate the Vienna et al. (2020) property-composition models. The results are summarized in Table 4.1, and our conclusions are described below.

Measured density ranged from approximately 2.6 g/cm^3 to 2.8 g/cm^3 (Section 3.5). The new composition-property models by Vienna et al. (2020) did not include a new density model; therefore, two previously developed models were applied to the current matrix data (Vienna et al. 2002, 2009). The best fit between measured and predicted property was found for the molar volume-based model (Vienna et al. 2002). Indeed, as expected, the molar volume model yields better predictions of the density over a variety of compositional space other than the one used to generate the model.

Viscosity at 1150 °C ranged from 1.13 to 12.72 Pa-s with eight glasses having viscosity at 1150 ºC outside optimum range of 2 to 8 Pa-s (Section 3.6). The new viscosity model showed very good predictive capabilities with all samples on or tightly around the 45° line, except for one outlier. The confidence rectangles of 24 of 25 glasses crossed the 45° line for 96%, suggesting adequate prediction at the 90% confidence level.

The ε_{1150} was between 3.097 and 4.121 S/m (Section 3.7). The 2020 model appeared to have some scatter, with slight underprediction at lower ε_{1150} values, and overpredicting at higher ε_{1150} values. After applying prediction and measurement uncertainties, the confidence rectangles of all 25 glasses crossed the 45° line for 100%, suggesting adequate prediction at the 90% confidence level.

PCT NR_B and NR_{Na} are described in Section 3.8. The values ranged from 0.197 to 15.010 g/m^2. Roughly one-third of the glasses exceeded the PCT limit of 2 g/m^2. CCC heat treatment did not appear to significantly increase PCT responses except for three glasses. Both PCT models for B and Na appeared to underpredict at PCT values above 2 g/m^2 (Section 3.8). The confidence rectangles of 20 of 25 glasses crossed the 45° line for NR_B for 80% while 22 of 25 glasses crossed the 45° line for NR_{Na} for 88%, suggesting inadequate prediction at the 90% confidence level.

VHT alteration rates (r) varied from zero to >245 g/m^2/d for the quenched glasses and from 0.29 to >225 g/m^2/d for the CCC. A total of 9 quenched and 6 CCC glasses exceeded the WTP contract limit. The reported thickness for each glass was transformed into a pass/fail binary response (i.e., fail is classified as $r \geq 50$ g/m^2/d) and the VHT model validity was verified. (Section 3.9). False negative predictions of 1 ÷ 7 = 14% was close to the 10% model target while the false negative predictions of 5 ÷ 17 = 29% also was close to the model results of 24%.

Sulfur solubility (i.e., the saturated SO_3 concentrations) was measured for each glass and converted into SO_3 melter tolerance (Section 3.9. The VHT model predicted very well except for the expected underprediction at high sulfur content in the glass. The confidence rectangles of 24 of 25 glasses crossed the 45° line for 96%, suggesting adequate prediction at the 90% confidence level.

Table 4.1. Statistics of Property Models

Statistics	η_{1150}	ε_{1150}	NR_B	NR_{Na}	Melter SO_3 Tolerance	VHT		
R^2	0.9487	0.8563	0.7762	0.7621	0.8303		False Positive Rate	False Negative Rate
RMSE	0.1304	0.1318	0.3954	0.3529	0.1747	Per Model	0.24	0.07
R^2 validation	0.9057	0.5231	0.6311	0.7044	0.6732	Measured	0.29	0.14
PI	0.96	1.00	0.80	0.88	0.96			

5.0 Bibliography

ASTM. "Standard Test Methods for Determining Chemical Durability of Nuclear, Hazardous, and Mixed Waste Glasses and Multiphase Glass Ceramics: The Product Consistency Test (PCT)." ASTM C1285, ASTM International, West Conshohocken, Pennsylvania.

ASTM. "Standard Test Method for Measuring Waste Glass or Glass Ceramic Durability by Vapor Hydration Test." ASTM C1663, ASTM International, West Conshohocken, Pennsylvania.

ASTM. "Standard Test Method for Determining Liquidus Temperature of Immobilized Waste Glasses and Simulated Waste Glasses." ASTM C1720, ASTM International, West Conshohocken, Pennsylvania.

Bernards GA, GA Hersi, TM Hohl, RT Jasper, PD Mahoney, NK Pak, SD Reaksecker, AJ Schubick, and EB West. 2020. *River Protection Project System Plan*. ORP-11242, Rev. 9, U.S. Department of Energy, Office of River Protection, Richland, Washington.

Crum JV, TB Edwards, RL Russell, PJ Workman, MJ Schweiger, RF Schumacher, DE Smith, DK Peeler, and JD Vienna. 2012. "DWPF Startup Frit Viscosity Measurement Round Robin Results," *Journal of the American Ceramic Society*, 95(7):2196-2205.

Daudt RD. 2015. *Nuclear Quality Assurance Program (NQAP) Manual*. Pacific Northwest National Laboratory, Richland, Washington.

Ebert WL and SF Wolfe. 1999. *Round-Robin Testing of a Reference Glass for Low-Activity Waste Forms*. ANL-99/22, Argonne National Laboratory, Argonne, Illinois.

Hsieh MC. 2020a. *Composition Measurements of the LAW Phase 4 Glasses*. SRNL-STI-2020-00276, Rev.0. Savannah River National Laboratory, Aiken, South Carolina.

Hsieh MC. 2020b. *Product Consistency Test Results for the LAW Phase 4 Glasses*. SRNL-STI-2020-00402, Rev.0. Savannah River National Laboratory, Aiken, South Carolina.

Hsieh MC. 2020c. *Characterization of the Sulfur-Saturated Melt Versions of the LAW Phase 4 Glasses*. SRNL-STI-2020-00591, Rev.0. Savannah River National Laboratory, Aiken, South Carolina.

Jantzen CM, NE Bibler, DC Beam, CL Crawford, and MA Pickett. 1993. *Characterization of the Defense Waste Processing Facility (DWPF) Environmental Assessment (EA) Glass Standard Reference Material (U)*. WSRC-TR-92-346, Rev. 1, Westinghouse Savannah River Company, Aiken, South Carolina.

Jin T, D Kim, LP Darnell, BL Weese, NL Canfield, M Bliss, MJ Schweiger, JD Vienna, and AA Kruger. 2019. "A crucible salt saturation method for determining sulfur solubility in glass melt." *International Journal of Applied Glass Science* 10(1):92-102.

Kim DS, D Peeler, P Hrma. 1995. “Effect of Crystallization on the Chemical Durability of Simulated Nuclear Waste Glasses.” *Environmental issues and waste management technologies in the ceramic and nuclear industries* 177-186.

Kim DS, JD Vienna, PR Hrma, MJ Schweiger, J Matyas, JV Crum, DE Smith, GJ Sevigny, WC Buchmiller, JS Tixier, JD Yeager, and KB Belew. 2003. *Development and Testing of ICV Glasses for Hanford LAW*. PNNL-14351, Pacific Northwest National Laboratory, Richland, Washington.

Kim DS and JD Vienna. 2012. *Preliminary ILAW Formulation Algorithm Description*. 24590 LAW-RPT-RT-04-0003, Rev. 1, River Protection Project, Hanford Tank Waste Treatment and Immobilization Plant, Richland, Washington.

Lonergan CE, JL George, D Cutforth, T Jin, P Cholsaipant, SE Sannoh, CH Skidmore, BA Stanfill, SK Cooley, GF Piepel, R Russell, and JD Vienna. 2020. *Enhanced Hanford Low-Activity Waste Glass Property Data Development: Phase 3*. PNNL-29847, Rev. 0, EWG-RPT-026, Pacific Northwest National Laboratory, Richland, Washington.

Lonergan CE, E Rivers, D Bellofatto, DS Kim, and JD Vienna. 2021. *Crystallization Constraints for WTP LAW Operations: Assessment of CCC Impacts on VHT and PCT*. PNNL-31138, Rev. 0, EWG-RPT-032, Pacific Northwest National Laboratory, Richland, Washington.

Lonergan CE, E Rivers, SM Baird, SE Sannoh, DS Kim, and JD Vienna. 2021b. *Glass Crystallization Constraints for WTP LAW Operations: Assessment of Isothermal Treatments on Crystal Formation*. EWG-RPT-033, Pacific Northwest National Laboratory, Richland, Washington.

Matlack KS, M Chaudhuri, H Gan, IS Muller, WK Kot, W Gong, and IL Pegg. 2005a. *Glass Formulation Testing to Increase Sulfate Incorporation*. VSL-04R4960-1, Vitreous State Laboratory, The Catholic University of America, Washington, D.C.

Matlack KS, W Gong, and IL Pegg. 2005b. *Glass Formulation Testing to Increase Sulfate Volatilization from Melter*. VSL-04R4970-1, Vitreous State Laboratory, The Catholic University of America, Washington, DC.

Matlack KS, W Gong, IS Muller, I Joseph, and IL Pegg. 2006a. *LAW Envelope C Glass Formulation Testing to Increase Waste Loading*. VSL-05R5900-1, Vitreous State Laboratory, The Catholic University of America, Washington, D.C.

Matlack KS, W Gong, IS Muller, I Joseph, and IL Pegg. 2006b. *LAW Envelope A and B Glass Formulations Testing to Increase Waste Loading*. VSL-06R6900-1, Vitreous State Laboratory, The Catholic University of America, Washington, D.C.

Matlack KS, I Joseph, W Gong, IS Muller, and IL Pegg. 2007. *Enhanced LAW Glass Formulation Testing*. VSL-07R1130-1, Vitreous State Laboratory, The Catholic University of America, Washington, D.C.

Matlack KS, I Joseph, W Gong, IS Muller, and IL Pegg. 2009. *Glass Formulation Development and Dm10 Melter Testing with ORP LAW Glasses*. VSL-09R1510-2, Vitreous State Laboratory, The Catholic University of America, Washington, D.C.

Muller IS, WK Kot, HK Pasieka, K Gilbo, FC Perez-Cardenas, I Joseph, and IL Pegg. 2012. *Compilation and Management of ORP Glass Formulation Database*. VSL-12R2470-1, Vitreous State Laboratory, The Catholic University of America, Washington, D.C.

Muller, IS, K Gilbo, I Joseph, and IL Pegg. 2014. *Enhanced LAW Glass Property-Composition Models—Phase 1*. VSL-13R2940-1, Vitreous State Laboratory, The Catholic University of America, Washington, D.C.

Muller IS, M Chaudhuri, H Gan, AC Buechele, X Xie, IL Pegg, and I Joseph. 2015a. *Improved High-Alkali Low-Activity Waste Formulations.* VSL-15R3290-1, Rev. 0, Vitreous State Laboratory, The Catholic University of America, Washington, DC.

Muller IS, H Gan, K Gilbo, IL Pegg, and I Joseph. 2015b. *LAW Glass Property-Composition Models for K-3 Refractory Corrosion and Sulfate Solubility*. VSL-15R3270-1, Vitreous State Laboratory, The Catholic University of America, Washington, D.C.

Muller, IS, KS Matlack, IL Pegg, and I Joseph. 2017. *Enhanced LAW Glass Correlation-Phase 3*. VSL-17R4230-1, Vitreous State Laboratory, The Catholic University of America, Washington, D.C.

Piepel GF, SK Cooley, IS Muller, H Gan, I Joseph, and IL Pegg. 2007. *ILAW PCT, VHT, Viscosity, and Electrical Conductivity Model Development*. VSL-07R1230-4, Rev. 0, ORP-56502, Vitreous State Laboratory, The Catholic University of America, Washington, D.C.

Piepel GF, SK Cooley, IS Muller, H Gan, I Joseph, and IL Pegg. 2007. *ILAW PCT, VHT, Viscosity, and Electrical Conductivity Model Development*. VSL-07R1230-1, Rev. 0, Vitreous State Laboratory, The Catholic University of America, Washington, D.C.

Russell RL, T Jin, BP McCarthy, LP Darnell, DE Rinehart, CC Bonham, V Gervasio, JM Mayer, CL Arendt, JB Lang, MJ Schweiger, and JD Vienna. 2017. *Enhanced Hanford Low-Activity Waste Glass Property Data Development: Phase 1*. PNNL-26630, EWG-RPT-012, Pacific Northwest National Laboratory, Richland, Washington.

Russell R.L., B.P. McCarthy, S.K. Cooley, E. Scott K, Cordova, S.E. Sannoh, V. Gervasio, M.J. Schweiger, J Lang, CH Skidmore, CE Lonergan, BA Stanfill, JD Vienna. 2021. *Enhanced Hanford Low-Activity Waste Glass Property Data Development: Phase 2*. PNNL-28838, Rev 2, Pacific Northwest National Laboratory, Richland, Washington.

Rieck B.T. 2018. *ILAW Product Qualification Report – Waste Forming Testing*. 24590-LAW-RPT-PENG-17-008-05, Rev 1, River Protection Project, Waste Treatment Plant. Richland, Washington.

Riley BJ, Hrma PR, Vienna JD, Schweiger MJ, Rodriguez CP, Crum JV, Lang JB. 2011. “The Liquidus Temperature of Nuclear Waste Glasses: An International Round-Robin Study. *International Journal of Applied Glass Science* 2(4):321-333.

Russell, RL, T Jin, BP McCarthy, LP Darnell, DE Rinehart, CC Bonham, V Gervasio, JM Mayer, CL Arendt, JB Lang, MJ Schweiger, and JD Vienna. 2017. *Enhanced Hanford Low-Activity Waste Glass Property Data Development: Phase 1.* PNNL-26630, Rev. 0, Pacific Northwest National Laboratory, Richland, Washington.

Skidmore, C. H., J. D. Vienna, T. Jin, D. Kim, B. A. Stanfill, K. M. Fox, and A. A. Kruger. 2018. “Sulfur solubility in low activity waste glass and its correlation to melter tolerance.” *International Journal of Applied Glass Science* (10):558-68.

Smith, G. L. 1993. *Characterization of Analytical Reference. Glass-1 (ARG-1)*. PNL-8992, Pacific Northwest Laboratory, Richland, Washington.

U.S. Department of Energy (DOE). 2000. *Design, Construction, and Commissioning of the Hanford Tank Waste Treatment and Immobilization Plant*. Contract DE-AC27-01RV14136, as amended, U.S. Department of Energy, Office of River Protection, Richland, Washington.

Vienna JD. 2002. *The Effects of Temperature and Composition on the Solubility of Chromium in Multi-component Alkali-borosilicate Glass Melts*. Ph.D. Dissertation, Washington State University, Pullman, Washington.

Vienna, JD, P Hrma, A Jiricka, DE Smith, TH Lorier, IA Reamer, and RL Schultz. 2001. *Hanford Immobilized LAW Product Acceptance Testing: Tanks Focus Area Results*. PNNL-13744, Pacific Northwest National Laboratory, Richland, Washington.

Vienna, JD, DS Kim, and DK Peeler. 2003a. “Glass Formulation for INEEL Sodium Bearing Waste.” *Ceramic Transactions* 143:169-176.

Vienna JD, DS Kim, and P Hrma. 2003b. "Interim Models Developed to Predict Key Hanford Waste Glass Properties Using Composition." *Ceramic Transactions* 143:151-157, American Ceramic Society, Westerville, Ohio.

Vienna JD, DS Kim, MJ Schweiger, P Hrma, J Matyas, JV Crum, and DE Smith. 2004a. "Preliminary Glass Development and Testing for in-Container Vitrification of Hanford Low Activity Waste," *Ceramic Transactions* 97(10):261-268, American Ceramic Society, Westerville, Ohio.

Vienna, JD, P Hrma, WC Buchmiller, and JS Ricklefs. 2004b. *Preliminary Investigation of Sulfur Loading in Hanford LAW Glass*. PNNL-14649, Pacific Northwest National Laboratory, Richland, Washington.

Vienna, J.D., A. Fluegel, D. Kim, and P. Hrma. 2009. *Glass Property Data and Models for Estimating High-Level Waste Glass Volume*. PNNL-18501, Pacific Northwest National Laboratory, Richland, Washington.

Vienna JD, DC Skorski, D Kim, J Matyas, 2013. *Glass Property Models and Constraints for Estimating Glass to be Produced at Hanford by Implementing Current Advanced Glass Formulation Efforts.* PNNL-22631, Rev.1, ORP-58289, Pacific Northwest National Laboratory, Richland, Washington.

Vienna JD, DS Kim, IS Muller, GF Piepel, and AA Kruger. 2014. “Toward Understanding the Effect of Low-Activity Waste Glass Composition on Sulfur Solubility.” *Journal of the American Ceramic Society* 97(10):3135-3142.

Vienna, JD, GF Piepel, DS Kim, JV Crum, CE Lonergan, BA Stanfill, BJ Riley, SK Cooley, and T Jin. 2016. *2016 Update of Hanford Glass Property Models and Constraints for Use in Estimating the Glass Mass to be Produced at Hanford by Implementing Current Enhanced Glass Formulation Efforts*. PNNL-25835, Pacific Northwest National Laboratory, Richland, Washington.

Vienna JD, A Heredia-Langner, SK Cooley, AE Holmes, DS Kim, NA Lumetta. 2020. *Glass Property-Composition Models for Support of Hanford WTP LAW Facility Operation*. PNNL-30932, Pacific Northwest National Laboratory, Richland, Washington.

Zhang J., AR Oganov, X Li, H Dong, Q Zeng.2015. “Novel compounds in the Zr–O system, their crystal structures, and mechanical properties.” *Phys.Chem.Chem.Phys.* 2015:17301.

Appendix A – Morphology/Color of Each Quenched Glass

The photographs in this appendix show each glass after melting in a platinum/rhodium crucible at the melt temperatures and times specified in Section 3.1.

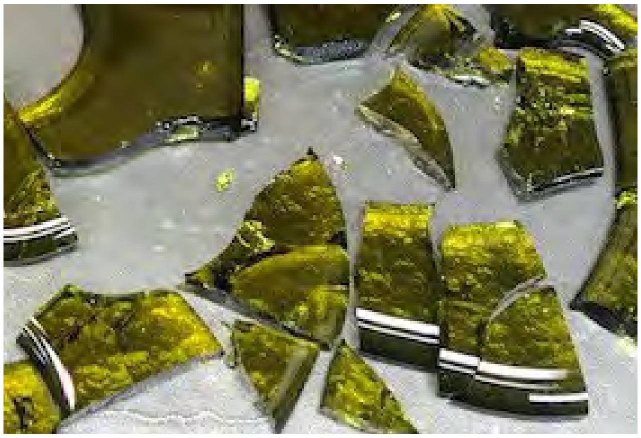

A.1 Glass LP4-1-3 Morphology after the First Melt

A.2. Glass LP4-2 Morphology after the Third Melt

A.3. Glass LP4-3 Morphology after the Third Melt

A.4. Glass LP4-1 Morphology after Second Melt

A.5. Glass LP4-5 Morphology after Second Melt

A.6. Glass LP4-6-2 Morphology after the Third Melt

A.7. Photo of Glass LP4-7-1 Morphology of the Second Melt

A.8. Photo of Glass LP4-8-1 Morphology of the Third Melt

A.9. Photo of Glass LP4-9 Morphology of the Second Melt

A.10. Photo of Glass LP4-10 Morphology of the Second Melt

A.11. Photo of Glass LP4-11 Morphology of the Third Melt

A.12. Photo of Glass LP4-12 Morphology of the Third Melt

A.13. Photo of Glass LP4-13 Morphology of the Air Quenched (left) and Annealed (right) for the Third Melt

A.14. Photo of Glass LP4-14 Morphology of the Second Melt

A.15. Photo of Glass LP4-15 Morphology of the Second Melt

A.16. Photo of Glass LP4-16 Morphology of the Second Melt

A.17. Photo of Glass LP4-17 Morphology of Second Melt

A.18. Photo of Glass LP4-18 Morphology of the Second Melt

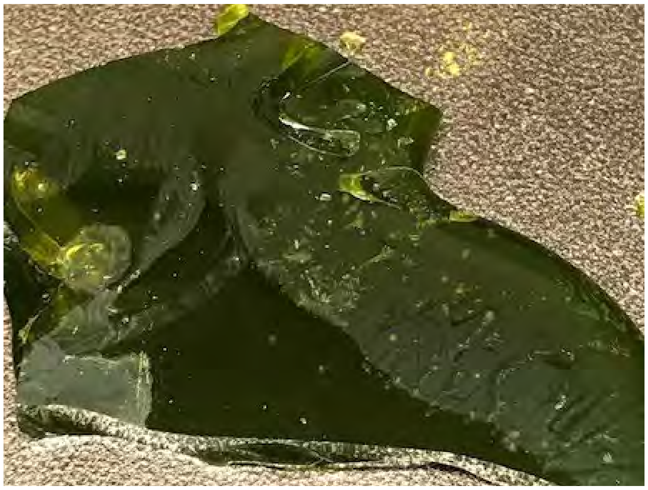

A.19. Photo of Glass LP4-19 Morphology of the Third Melt

A.20. Photo of Glass LP4-20 Morphology of the Third Melt

A.21. Photo of Glass LP4-21 Morphology of Third Melt

A.22. Photo of Glass LP4-22 Morphology of the Third Melt

A.23. Photo of Glass LP4-23-1 Morphology of the Second Melt

A.24. Photo of Glass LP4-24 Morphology of the Second Melt

A.25. Photo of Glass LP4-20 Morphology of Second Melt

Appendix B – Comparison Measured and Target Chemical Compositions

The data in this section compares the targeted glass compositions with the analyzed glass compositions and their percent differences. The measured sums of oxides for all glasses fall within the interval of 95 to 105 wt %, indicating acceptable recovery of the glass components. Percent differences of components with targeted concentrations of 5 wt% or more are reported. Relative differences are shaded if they are 10% or more. These criteria were selected arbitrarily for the purpose of highlighting differences from targeted concentrations that may be of practical concern.

Table B.1. Comparison of Targeted and Analyzed Low-Activity Waste (LAW) Glass Compositions

Sample ID	**LP4-01**			**LP4-2**			**LP4-3**			**LP4-4-1**		
Oxide	**Measured (wt%)**	**Target (wt%)**	**% Difference of Measured vs. Target**	**Measured (wt%)**	**Target (wt%)**	**% Difference of Measured vs. Target**	**Measured (wt%)**	**Target (wt%)**	**% Difference of Measured vs. Target**	**Measured (wt%)**	**Target (wt%)**	**% Difference of Measured vs. Target**
Al_2O_3	6.250	6.110	2.3%	12.924	13.760	-6.1%	9.622	9.860	-2.4%	12.480	13.250	-5.80%
B_2O_3	14.353	14.010	2.5%	7.019	7.220	-2.8%	13.644	13.910	-1.9%	5.603	6.240	-10.20%
CaO	2.707	2.630		1.539	1.520		5.751	5.750		6.821	7.110	-4.10%
Cl	0.076	0.060		0.384	0.510		0.090	0.150		0.242	0.470	
Cr_2O_3	0.302	0.310		0.161	0.170	-5.2%	0.535	0.550		0.146	0.020	
F	0.079	0.100		0.898	1.060		0.719	0.910		0.118	0.140	
Fe_2O_3	1.526	1.530		1.112	1.110		0.303	0.280	8.1%	0.171	0.160	6.90%
K_2O	0.120	0.000		3.367	3.400		4.785	4.810		5.165	5.440	-5.10%
Li_2O	0.215	0.000		4.645	4.660		4.446	4.460		5.119	5.050	1.40%
MgO	0.166	0.000		1.903	2.060	-7.6%	0.692	0.720		2.964	3.040	-2.50%
Na_2O	26.185	26.490	-1.2%	10.208	10.250	-0.4%	10.818	10.790	0.30%	11.027	10.730	2.80%
NiO	0.127	0.000		0.127	0.000		0.127	0.000		0.127	0.000	
P_2O_5	0.229	0.200		1.603	1.710	-6.2%	1.812	1.920	-5.60%	0.575	0.620	-7.30%
PbO	0.108	0.000		0.108	0.000		0.108	0.000		0.108	0.000	
SiO_2	34.550	35.570	-2.9%	42.465	43.310	-2.0%	37.224	37.110	0.30%	37.545	38.090	-1.40%
SnO_2	3.555	3.570		0.153	0.130		2.136	2.170		0.326	0.340	
SO_3	1.046	1.030		0.464	0.510		1.267	1.390	-8.90%	0.806	1.400	-42.40%
TiO_2	0.167	0.000		0.778	0.780		0.357	0.350		1.781	1.800	
V_2O_5	0.179	0.000		2.539	2.610		0.719	0.740		2.655	2.770	
ZnO	3.663	3.670		2.963	3.040		0.436	0.450		0.124	0.020	
ZrO_2	5.403	4.720	14.5%	2.445	2.190	11.6%	4.110	3.680	11.70%	3.012	3.310	-9.00%
Sum Oxide	101.006	100.000	1.0%	97.805	100.000	-2.2%	99.701	100.000	-0.30%	96.915	100.000	-3.10%

Table B.1. Comparison of Targeted and Analyzed LAW Glass Compositions (cont.)

Sample ID	**LP4-05**			**LP4-6-2**			**LP4-7-1**			**LP4-8-1**		
Oxide	**Measured (wt%)**	**Target (wt%)**	**% Difference of Measured vs. Target**	**Measured (wt%)**	**Target (wt%)**	**% Difference of Measured vs. Target**	**Measured (wt%)**	**Target (wt%)**	**% Difference of Measured vs. Target**	**Measured (wt%)**	**Target (wt%)**	**% Difference of Measured vs.Target**
Al_2O_3	10.378	10.250	1.30%	12.518	12.900	-3.00%	9.003	9.450	-4.70%	10.506	10.860	-3.30%
B_2O_3	12.477	12.150	2.70%	10.787	11.570	-6.80%	7.027	7.310	-3.90%	5.281	6.100	-13.40%
CaO	7.857	8.090	-2.90%	0.275	0.240	14.60%	10.319	11.650	-11.40%	1.175	1.150	
Cl	0.278	0.330		0.194	0.510		0.049	0.110		0.208	0.530	
Cr_2O_3	0.491	0.500		0.146	0.060		0.146	0.130		0.401	0.440	-8.90%
F	0.135	0.170		0.260	0.400		0.792	1.040		0.082	0.110	
Fe_2O_3	1.028	1.010		0.698	0.730		0.198	0.170	16.50%	1.413	1.470	
K_2O	0.176	0.160	10.10%	4.849	5.090	-4.70%	1.186	1.160		5.104	5.380	-5.10%
Li_2O	0.215	0.000		1.376	1.320		1.275	1.260		3.181	3.150	
MgO	0.972	1.010		3.113	3.230		3.109	3.120		0.745	0.760	
Na_2O	20.860	21.180	-1.50%	13.510	12.720	6.20%	14.693	14.470	1.50%	16.109	15.520	3.80%
NiO	0.127	0.040		0.127	0.000		0.127	0.000		0.127	0.000	
P_2O_5	0.274	0.290	-5.60%	0.755	0.820	-7.90%	1.543	1.690	-8.70%	1.749	1.910	-8.40%
PbO	0.108	0.010		0.108	0.000		0.108	0.000		0.108	0.000	
SiO_2	38.293	37.470	2.20%	36.849	37.400	-1.50%	34.443	34.630	-0.50%	38.561	39.790	-3.10%
SnO_2	0.127	0.000		3.558	3.680		3.948	4.080		2.381	2.500	-4.80%
SO_3	1.049	1.070		0.192	0.290	-33.80%	0.623	1.130	-44.90%	0.622	1.210	-48.60%
TiO_2	0.167	0.000		0.478	0.460		0.848	0.830		2.018	2.020	
V_2O_5	0.988	1.010		3.231	3.330		3.312	3.340		2.142	2.210	
ZnO	2.928	3.030		3.081	3.270	-5.80%	0.544	0.570	-4.60%	2.773	2.890	
ZrO_2	2.003	2.160	-7.30%	1.827	1.980	-7.70%	3.495	3.860	-9.50%	1.854	2.000	-7.30%
Sum Oxide	100.931	99.930	1.00%	97.932	100.000	-2.10%	96.788	100.000	-3.20%	96.540	100.000	-3.50%

Table B.1. Comparison of Targeted and Analyzed LAW Glass Compositions (cont.)

Sample ID	**LP4-09**			**LP4-10**			**LP4-11**			**LP4-12**		
Oxide	**Measured (wt%)**	**Target (wt%)**	**% Difference of Measured vs. Target**	**Measured (wt%)**	**Target (wt%)**	**% Difference of Measured vs. Target**	**Measured (wt%)**	**Target (wt%)**	**% Difference of Measured vs.Target**	**Measured (wt%)**	**Target (wt%)**	**% Difference of Measured vs.Target**
Al_2O_3	4.554	4.450	2.30%	4.204	4.080	3.00%	9.400	9.170	2.50%	4.185	3.910	7.00%
B_2O_3	13.041	12.960	0.60%	8.468	8.340	1.50%	13.234	12.750	3.80%	10.843	10.360	4.70%
CaO	0.318	0.330		4.778	4.780		0.635	0.630		0.787	0.740	6.40%
Cl	0.176	0.220		0.401	0.580		0.414	0.600		0.096	0.130	
Cr_2O_3	0.146	0.050		0.561	0.580		0.451	0.460		0.257	0.260	
F	0.680	0.820		0.396	0.460		0.118	0.170		0.352	0.490	
Fe_2O_3	0.143	0.050		1.188	1.180		0.143	0.060		0.365	0.360	
K_2O	5.767	5.770	-0.10%	5.794	5.830	-0.60%	4.267	4.330		5.424	5.560	-2.50%
Li_2O	3.342	3.510		4.424	4.410		1.332	1.440	-7.50%	2.108	2.150	
MgO	1.540	1.720	-10.50%	3.300	3.530	-6.50%	2.015	2.180	-7.60%	2.815	2.970	-5.20%
Na_2O	15.030	14.960	0.50%	13.581	13.930	-2.50%	14.356	14.470	-0.80%	11.691	11.480	1.80%
NiO	0.127	0.000		0.127	0.000		0.127	0.000		0.127	0.000	
P_2O_5	1.952	2.120	-7.90%	0.453	0.470		0.544	0.590	-7.90%	0.534	0.570	-6.20%
PbO	0.108	0.000		0.108	0.000		0.108	0.000		0.108	0.000	
SiO_2	36.368	36.620	-0.70%	46.530	44.850	3.80%	45.032	43.370	3.80%	48.509	46.550	4.20%
SnO_2	3.066	3.160		0.868	0.850		3.777	3.770		4.507	4.470	
SO_3	0.870	0.850		0.306	0.230	33.30%	0.153	0.110		0.418	0.480	-13.00%
TiO_2	1.636	1.740	-6.00%	1.835	1.870		1.636	1.680		0.704	0.680	
V_2O_5	3.320	3.540	-6.20%	0.179	0.050		0.732	0.770		4.088	4.050	
ZnO	2.623	2.760	-5.00%	0.205	0.210		0.973	1.010		0.746	0.740	
ZrO^2	3.873	4.370	-11.40%	4.208	3.770	11.60%	2.256	2.440	-7.60%	3.900	4.050	
Sum Oxide	98.680	100.000	-1.30%	101.914	100.000	1.90%	101.703	100.000	1.70%	102.564	100.000	2.60%

Table B.1.Comparison of Targeted and Analyzed LAW Glass Compositions (cont.)

Sample ID	**LP4-13**			**LP4-14**			**LP4-15**			**LP4-16**		
Oxide	**Measured (wt%)**	**Target (wt%)**	**% Difference of Measured vs. Target**	**Measured (wt%)**	**Target (wt%)**	**% Difference of Measured vs. Target**	**Measured (wt%)**	**Target (wt%)**	**% Difference of Measured vs. Target**	**Measured (wt%)**	**Target (wt%)**	**% Difference of Measured vs. Target**
Al_2O_3	3.718	3.880	-4.20%	5.961	5.990	-0.50%	10.506	10.120	3.80%	5.555	5.520	0.60%
B_2O_3	9.813	10.670	-8.00%	13.322	13.350	-0.20%	9.990	9.610	4.00%	11.849	11.900	-0.40%
CaO	7.391	8.300	-11.00%	10.445	10.810	-3.40%	4.908	5.060	-3.00%	0.457	0.440	
Cl	0.411	0.570	-27.90%	0.434	0.610		0.197	0.210		0.408	0.540	
Cr_2O_3	0.146	0.110		0.559	0.570		0.458	0.460		0.146	0.080	
F	0.819	0.940		0.172	0.220		0.285	0.320		0.848	1.020	
Fe_2O_3	0.956	0.990		1.449	1.440		0.613	0.610		0.520	0.500	
K_2O	3.141	3.190		3.397	3.470		1.043	1.010		2.117	2.070	
Li_2O	2.594	2.590		3.111	3.200		0.215	0.000		4.634	4.700	
MgO	0.844	0.830		2.678	2.870	-6.70%	0.633	0.660		1.223	1.330	-8.10%
Na_2O	17.794	17.670	0.70%	11.478	11.460	0.20%	22.377	23.270	-3.80%	13.355	13.320	0.30%
NiO	0.127	0.000		0.127	0.000		0.127	0.000		0.127	0.000	
P_2O_5	1.618	1.750	-7.50%	1.633	1.730	-5.60%	0.648	0.680		0.299	0.320	-6.60%
PbO	0.108	0.000		0.108	0.000		0.108	0.000		0.108	0.000	
SiO_2	34.389	35.760	-3.80%	36.956	36.200	2.10%	41.877	39.240	6.70%	45.407	44.980	1.00%
SnO_2	2.006	2.120	-5.40%	0.880	0.880		1.536	1.520		3.910	3.980	
SO_3	1.158	1.210		1.026	1.050		0.536	0.510	5.00%	0.618	0.630	
TiO_2	1.751	1.750		0.298	0.290		0.167	0.000		1.889	1.980	
V_2O_5	0.185	0.160		1.256	1.290		0.991	1.010		3.713	3.860	
ZnO	3.317	3.380		1.450	1.500		2.726	2.830		0.507	0.530	
ZrO_2	4.228	4.130		2.820	3.070	-8.20%	2.685	2.880	-6.80%	2.090	2.300	-9.10%
Sum Oxide	96.514	100.000	-3.50%	99.560	100.000	-0.40%	102.626	100.000	2.60%	99.780	100.000	-0.20%

Table B.1.Comparison of Targeted and Analyzed LAW Glass Compositions (cont.)

Sample ID	LP4-17			LP4-18			LP4-19			LP4-20		
Oxide	**Measured (wt%)**	**Target (wt%)**	**% Difference of Measured vs. Target**	**Measured (wt%)**	**Target (wt%)**	**% Difference of Measured vs. Target**	**Measured (wt%)**	**Target (wt%)**	**% Difference of Measured vs. Target**	**Measured (wt%)**	**Target (wt%)**	**% Difference of Measured vs. Target**
Al_2O_3	4.029	3.720	8.30%	4.365	4.160	4.90%	12.480	12.490	-0.10%	7.180	6.840	5.00%
B_2O_3	11.503	10.910	5.40%	6.722	6.400	5.00%	7.325	7.400	-1.00%	14.401	13.530	6.40%
CaO	7.986	8.580	-6.90%	11.886	12.230	-2.80%	2.910	2.950	-1.40%	1.966	1.870	5.10%
Cl	0.207	0.280		0.124	0.160		0.185	0.320		0.117	0.160	
Cr_2O_3	0.573	0.580		0.197	0.200		0.404	0.600	-32.70%	0.569	0.580	
F	0.885	1.110		0.267	0.360		0.739	0.860		0.556	0.700	
Fe_2O_3	0.612	0.590		0.498	0.480		0.710	0.730		1.423	1.440	
K_2O	2.945	2.920		0.120	0.080		3.255	3.390		3.894	3.900	
Li_2O	2.966	3.130	-5.30%	1.737	1.830	-5.10%	0.498	0.480		0.998	1.110	-10.10%
MgO	2.259	2.430	-7.00%	3.234	3.370		3.366	3.290		3.275	3.510	-6.70%
Na_2O	11.037	11.090	-0.50%	15.199	15.410	-1.40%	18.704	19.930	-6.20%	17.659	18.010	-2.00%
NiO	0.127	0.000		0.127	0.000		0.127	0.000		0.127	0.000	
P_2O_5	1.914	2.060	-7.10%	2.039	2.120		1.347	1.470	-8.40%	0.583	0.610	
PbO	0.108	0.000		0.108	0.000		0.108	0.000		0.108	0.000	
SiO_2	43.963	41.740	5.30%	46.637	44.370	5.10%	37.598	36.510	3.00%	37.438	35.090	6.70%
SnO_2	0.127	0.080		3.269	3.280		0.141	0.150	-6.00%	4.041	3.950	
SO_3	1.330	1.400	-5.00%	0.685	0.670		0.596	1.440	-58.60%	0.848	0.860	
TiO_2	1.160	1.210		1.939	1.950		1.613	1.610		1.485	1.510	
V_2O_5	3.789	3.920		0.906	0.900		0.970	1.280	-24.20%	3.847	3.870	
ZnO	0.233	0.240		0.124	0.050		0.441	0.460		0.643	0.660	
ZrO_2	3.637	4.010	-9.30%	1.878	1.980	-5.20%	4.248	4.640	-8.40%	1.699	1.800	-5.60%
Sum Oxide	101.390	100.000	1.40%	102.061	100.000	2.10%	97.765	100.000	-2.20%	102.857	100.000	2.90%

Table B.1. Comparison of Targeted and Analyzed LAW Glass Compositions (cont.)

Sample ID	LP4-21			LP4-22			LP4-23-1			LP4-24		
Oxide	Measured (wt%)	Target (wt%)	% Difference of Measured vs. Target	Measured (wt%)	Target (wt%)	% Difference of Measured vs. Target	Measured (wt%)	Target (wt%)	% Difference of Measured vs. Target	Measured (wt%)	Target (wt%)	% Difference of Measured vs. Target
Al_2O_3	4.412	4.300		9.225	9.470	-2.60%	5.909	6.070		12.967	13.260	-2.20%
B_2O_3	13.652	13.410	1.80%	12.300	12.820	-4.10%	5.715	6.460	-11.50%	9.362	9.600	-2.50%
CaO	5.142	5.430	-5.30%	0.140	0.110		4.103	4.400	-6.80%	2.288	2.340	
Cl	0.165	0.230		0.314	0.430		0.166	0.410		0.149	0.200	
Cr_2O_3	0.327	0.360		0.146	0.010		0.146	0.110		0.244	0.250	
F	0.266	0.350		0.573	0.760		0.221	0.270		0.514	0.590	
Fe_2O_3	1.146	1.110		1.272	1.340	-5.10%	0.796	0.830		0.894	0.940	-4.90%
K_2O	1.533	1.470		0.432	0.400	8.00%	3.942	4.120		4.641	4.660	
Li_2O	2.508	2.640	-5.00%	1.064	1.050		3.052	2.990		2.993	2.900	
MgO	0.235	0.230		0.388	0.410	-5.40%	2.541	2.630		2.400	2.420	
Na_2O	10.326	10.260	0.60%	19.041	20.510	-7.20%	16.783	16.570		16.816	16.050	4.80%
NiO	0.127	0.000		0.127	0.000		0.127	0.000		0.127	0.000	
P_2O_5	1.298	1.370	-5.30%	1.800	2.000	-10.00%	1.212	1.320	-8.20%	0.828	0.890	-7.00%
PbO	0.108	0.000		0.108	0.000		0.108	0.000		0.108	0.000	
SiO_2	47.439	47.310	0.30%	39.844	40.440		40.486	41.640	-2.80%	34.817	34.940	-0.40%
SnO_2	3.856	3.900		1.026	1.100	-6.70%	4.199	4.350		0.255	0.280	-8.90%
SO_3	1.081	1.460	-26.00%	0.906	1.030	-12.00%	0.765	0.950	-19.50%	0.332	0.320	
TiO_2	1.516	1.560		0.993	1.000		1.851	1.850		1.806	1.830	
V_2O_5	0.179	0.050		3.129	3.160		2.486	2.500		1.812	1.880	
ZnO	0.538	0.560		0.818	0.850		0.211	0.220		3.336	3.510	-5.00%
ZrO_2	3.644	4.000	-8.90%	2.786	3.110	-10.40%	2.060	2.310	-10.80%	2.837	3.140	-9.60%
Sum Oxide	99.498	100.000	-0.50%	96.432	100.000	-3.60%	96.879	100.000	-3.10%	99.526	100.000	-0.50%

Table B.1. Comparison of Targeted and Analyzed LAW Glass Compositions (cont.)

Sample ID	LP4-25-1		
Oxide	Measured (wt%)	Target (wt%)	% Difference of Measured vs. Target
Al_2O_3	7.289	7.420	-1.80%
B_2O_3	8.501	8.770	-3.10%
CaO	8.556	9.380	-8.80%
Cl	0.142	0.450	
Cr_2O_3	0.146	0.140	
F	0.756	0.970	
Fe_2O_3	1.449	1.500	
K_2O	2.512	2.620	
Li_2O	4.381	4.220	
MgO	3.230	3.220	
Na_2O	10.949	10.730	2.00%
NiO	0.127	0.000	
P_2O_5	1.743	1.860	-6.30%
PbO	0.108	0.000	
SiO_2	39.684	39.500	0.50%
SnO_2	3.555	3.750	-5.20%
SO_3	0.323	0.650	-50.30%
TiO_2	1.011	0.990	
V_2O_5	1.051	1.030	
ZnO	0.193	0.200	
ZrO_2	2.327	2.600	-10.50%
Sum Oxide	98.033	100.000	-2.00%

Table B.2. Comparison of Targeted and Analyzed High-Chromium Glass Compositions

Sample ID	**LP4-29**			**LP4-30**			**LP4-31**			**LP4-32**		
Oxide	**Measured (wt%)**	**Target (wt%)**	**% Difference of Measured vs. Target**	**Measured (wt%)**	**Target (wt%)**	**% Difference of Measured vs. Target**	**Measured (wt%)**	**Target (wt%)**	**% Difference of Measured vs. Target**	**Measured (wt%)**	**Target (wt%)**	**% Difference of Measured vs. Target**
Al_2O_3	2.121	2.000	6.05	6.382	6.600	-3.30	6.509	6.800	-4.28	2.419	2.400	0.79
B_2O_3	9.813	10.190	-3.70	13.870	15.230	-8.93	17.685	19.670	-10.09	15.673	16.800	-6.71
CaO	2.057	1.930	6.58	2.707	2.580	4.92	3.085	2.910	6.01	2.456	2.360	4.07
Cl	0.064	0.100	-36.00	<0.050	0.060	NA	<0.050	0.070	NA	<0.050	0.100	NA
Cr_2O_3	1.498	1.540	-2.73	1.619	1.680	-3.63	1.053	1.130	-6.81	1.926	2.020	-4.65
F	0.065	0.100	-35.00	<0.050	0.060	NA	<0.050	0.070	NA	0.058	0.100	-42.00
Fe_2O_3	3.170	3.270	-3.06	1.541	1.550	-0.58	5.544	6.020	-7.91	2.716	2.840	-4.37
K_2O	0.096	0.120	-20.00	7.562	8.840	-14.46	0.409	0.460	-11.09	2.213	2.370	-6.62
Li_2O	2.648	2.890	-8.37	0.480	0.600	-20.00	1.982	2.680	-26.04	2.492	2.680	-7.01
MnO	0.225	0.210	7.14	0.136	0.130	4.62	<0.131	0.130	NA	0.197	0.200	-15.00
Na_2O	19.512	20.870	-6.51	15.300	16.750	-8.66	18.131	18.420	-1.57	16.580	18.290	-9.35
NiO	<0.127	0.210	NA	<0.127	0.130	NA	<0.134	0.130	NA	0.174	0.200	-13.00
P_2O_5	0.282	0.310	-9.03	0.174	0.190	-8.42	0.181	0.200	-9.50	0.283	0.300	-5.67
PbO	0.191	0.210	-9.05	0.117	0.130	-10.00	0.121	0.130	-6.92	0.179	0.200	-10.50
SiO_2	56.852	55.600	2.25	45.567	45.280	0.63	40.807	41.120	-0.76	48.883	48.670	0.44
SO_3	0.205	0.350	-41.43	<0.125	0.120	NA	0.170	0.480	-64.58	0.164	0.340	-51.76
ZrO_2	0.097	0.100	-3.00	<0.068	0.060	NA	<0.068	0.070	NA	0.098	0.100	-2.00
Sum	99.024	100.000	-0.98	95.873	99.990	-4.12	96.110	100.000	-3.89	96.562	99.970	-3.41

Table B.2. Comparison of Targeted and Analyzed High-Chromium Glass Compositions (cont.)

Sample ID	**LP4-33**		
Oxide	**Measured (wt%)**	**Target (wt%)**	**% Difference of Measured vs. Target**
Al_2O_3	5.087	5.100	-0.25
B_2O_3	10.956	12.520	-12.49
CaO	1.445	1.190	21.43
Cl	<0.051	0.100	NA
Cr_2O_3	1.896	2.060	-7.96
F	0.064	0.100	-36.00
Fe_2O_3	6.312	6.830	-7.58
K_2O	8.236	9.690	-15.01
Li_2O	0.279	0.350	-20.29
MnO	0.197	0.200	-1.50
Na_2O	17.356	17.250	0.61
NiO	0.195	0.200	-2.50
P_2O_5	0.267	0.300	-11.00
PbO	0.184	0.200	-8.00
SiO_2	43.214	43.200	0.03
SO_3	0.353	0.620	-43.06
ZrO_2	0.099	0.100	-1.00
Sum	96.190	100.010	-3.82

Appendix C – Morphology/Color of Each CCC Glass

The photographs in this appendix show each glass after CCC as described in Section 4.2.

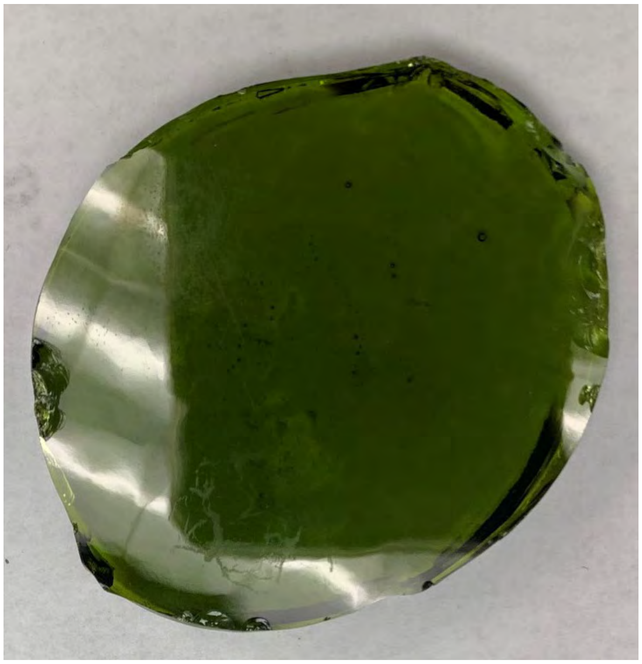

C.1. Glass LP4-01 Morphology after CCC

C.2. Glass LP4-02 Morphology after CCC

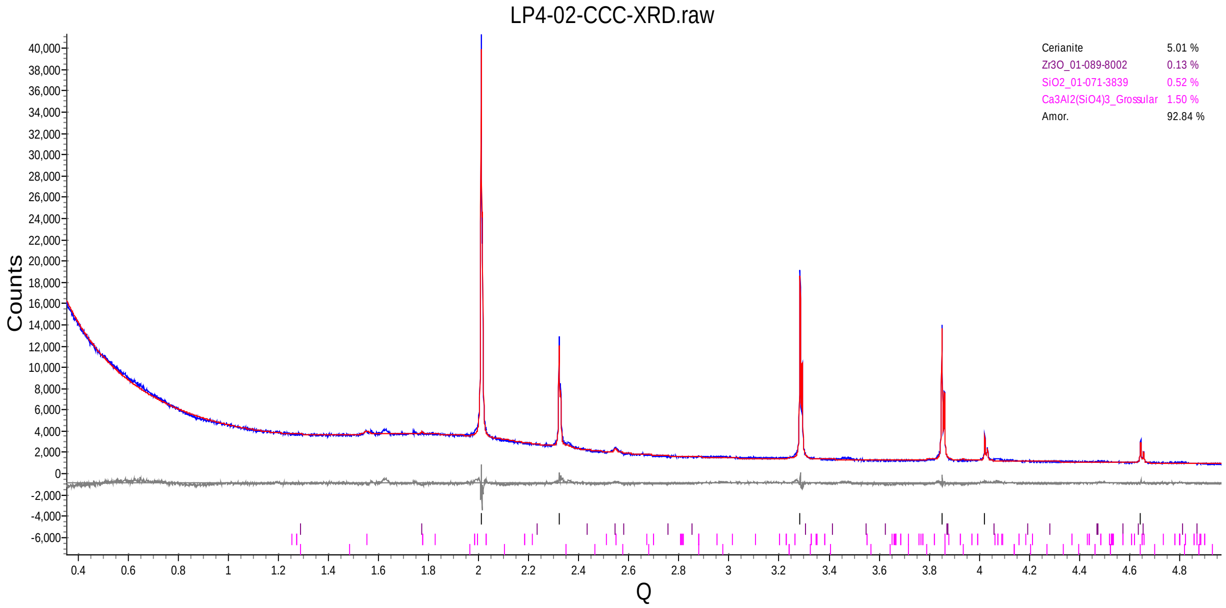
LP4-02-CCC-XRD.raw
Cerianite 5.01 %
Zr3O_01-089-8002 0.13 %
SiO2_01-071-3839 0.52 %
Ca3Al2(SiO4)3_Grossular 1.50 %
Amor. 92.84 %
Counts
40,000
38,000
36,000
34,000
32,000
30,000
28,000
26,000
24,000
22,000
20,000
18,000
16,000
14,000
12,000
10,000
8,000
6,000
4,000
2,000
0
-2,000
-4,000
-6,000
0.4
0.6
0.8
1
1.2
1.4
1.6
1.8
2
2.2
2.4
2.6
2.8
3
3.2
3.4
3.6
3.8
4
4.2
4.4
4.6
4.8
Q

C.3. Glass LP4-03 Morphology after CCC

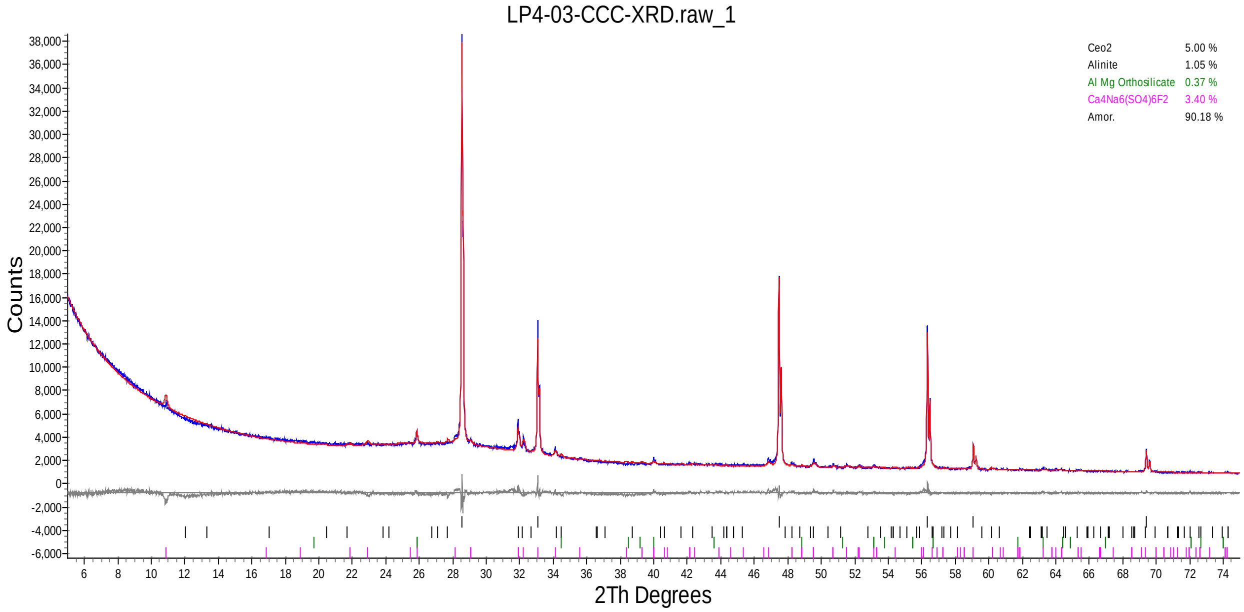

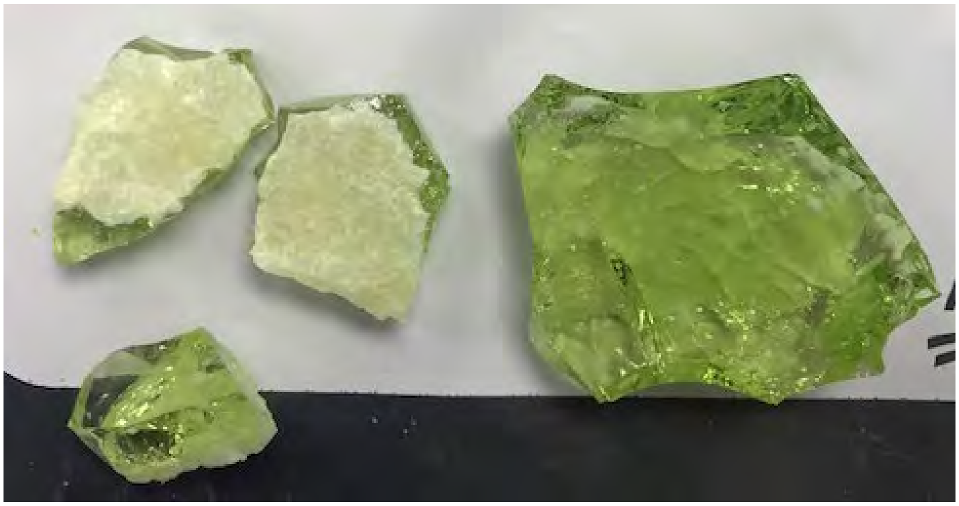

C.4. Glass LP4-01 Morphology after CCC

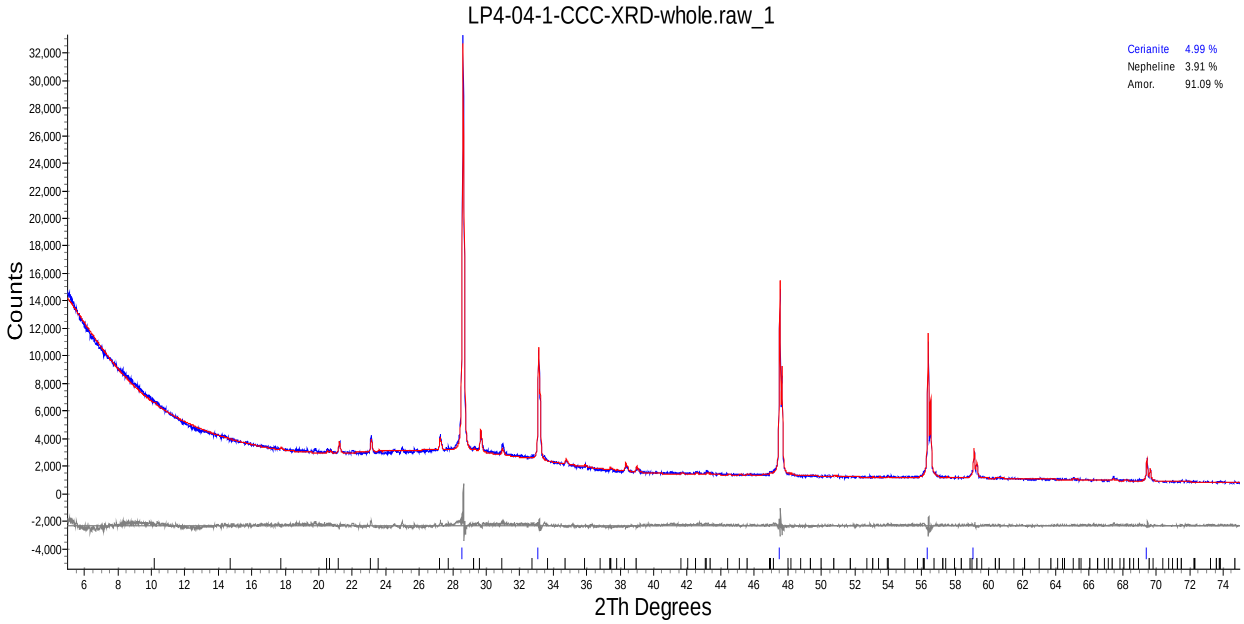

C.5. Glass LP4-05 Morphology after CCC

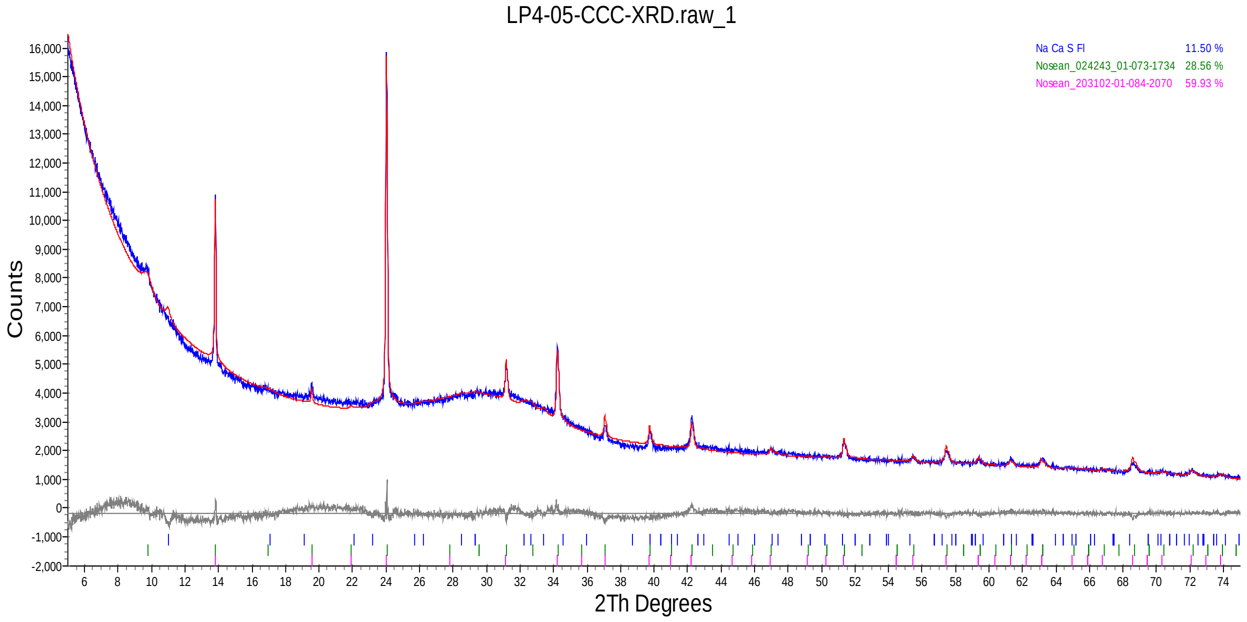

C.6. Glass LP4-06-1 Morphology after CCC

C.7. Glass LP4-07-1 Morphology after CCC

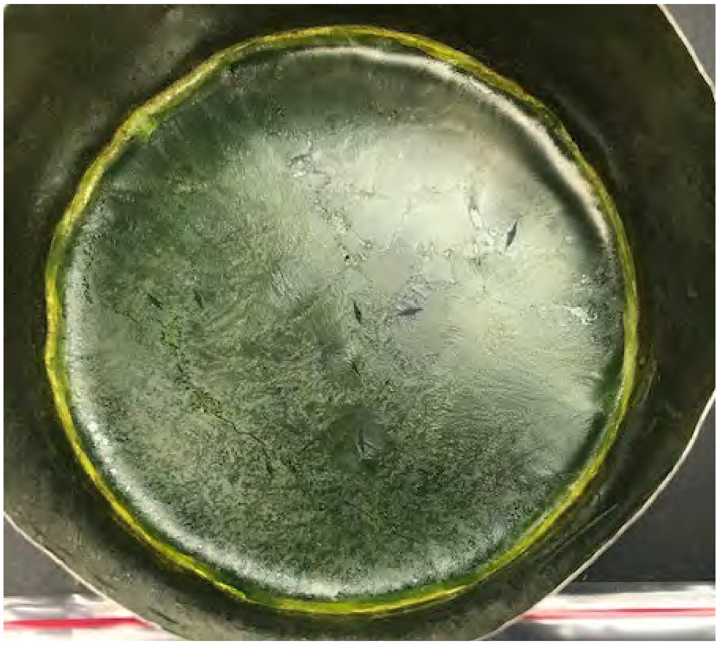

C.8. Glass LP4-08-1 Morphology after CCC

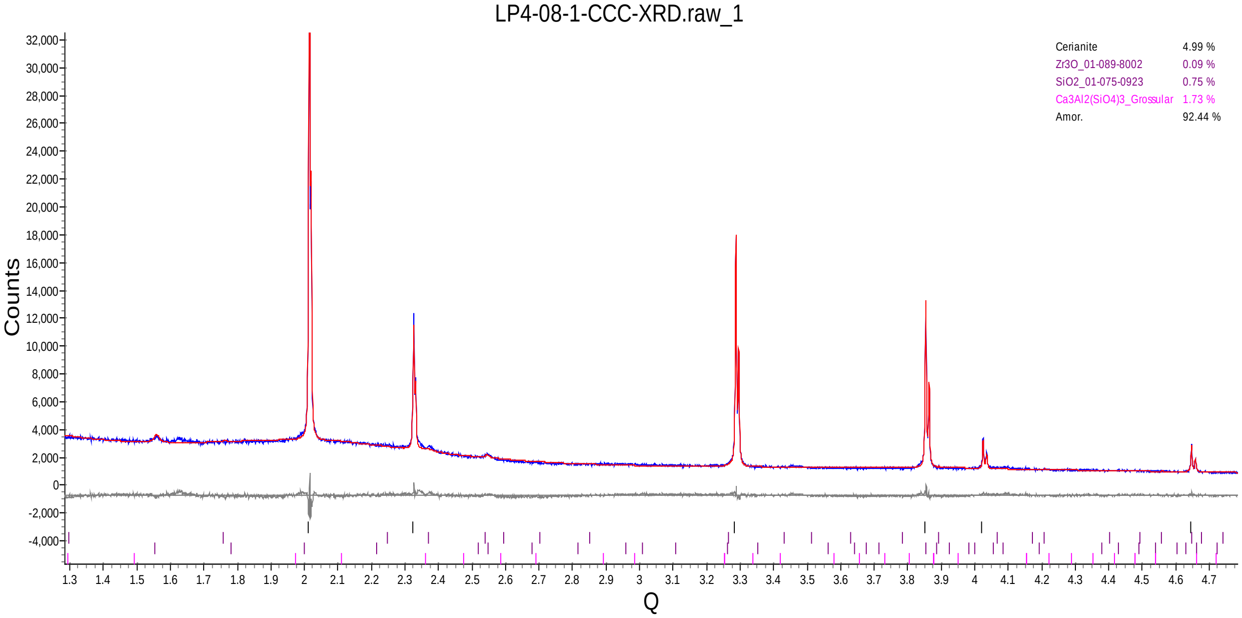

C.9. Glass LP4-09 Morphology after CCC

C.10. Glass LP4-10 Morphology after CCC

C.11. Glass LP4-11 Morphology after CCC

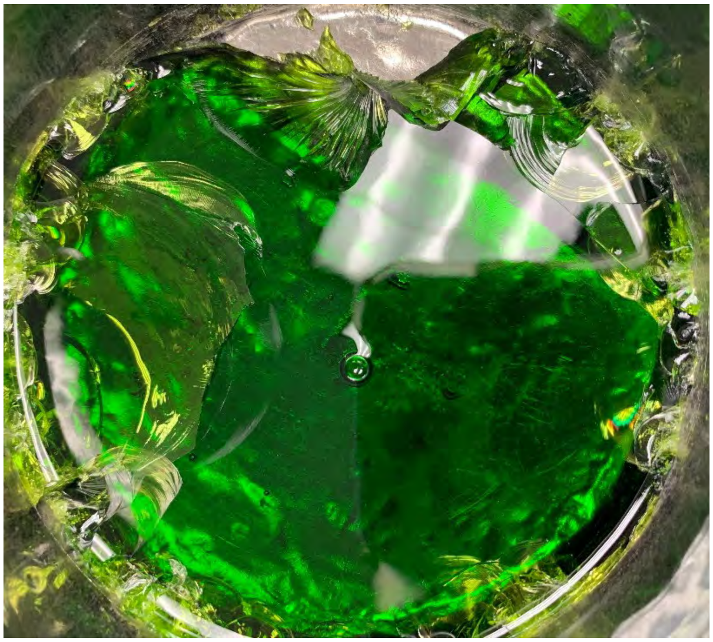

C.12. Glass LP4-12 Morphology after CCC

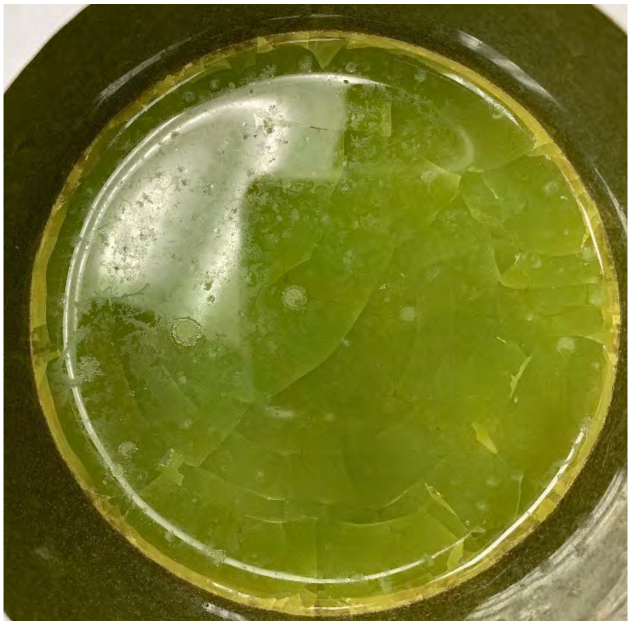

C.13. Glass LP4-13 Morphology after CCC

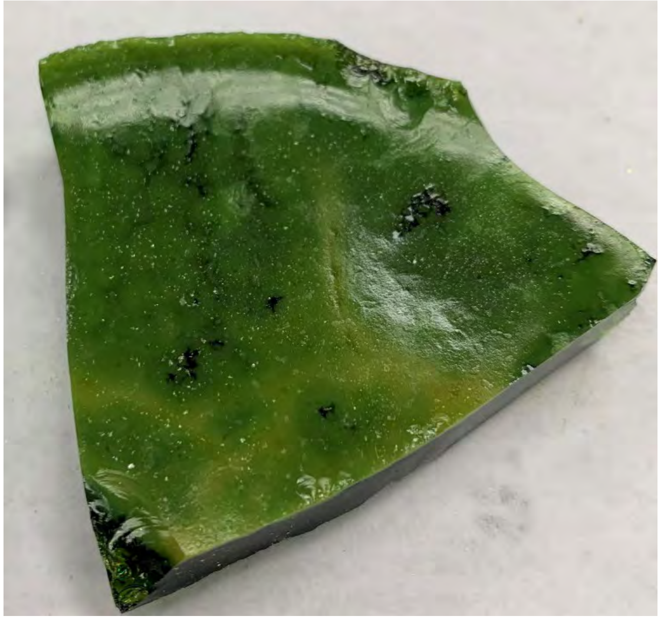

C.14. Glass LP4-14 Morphology after CCC

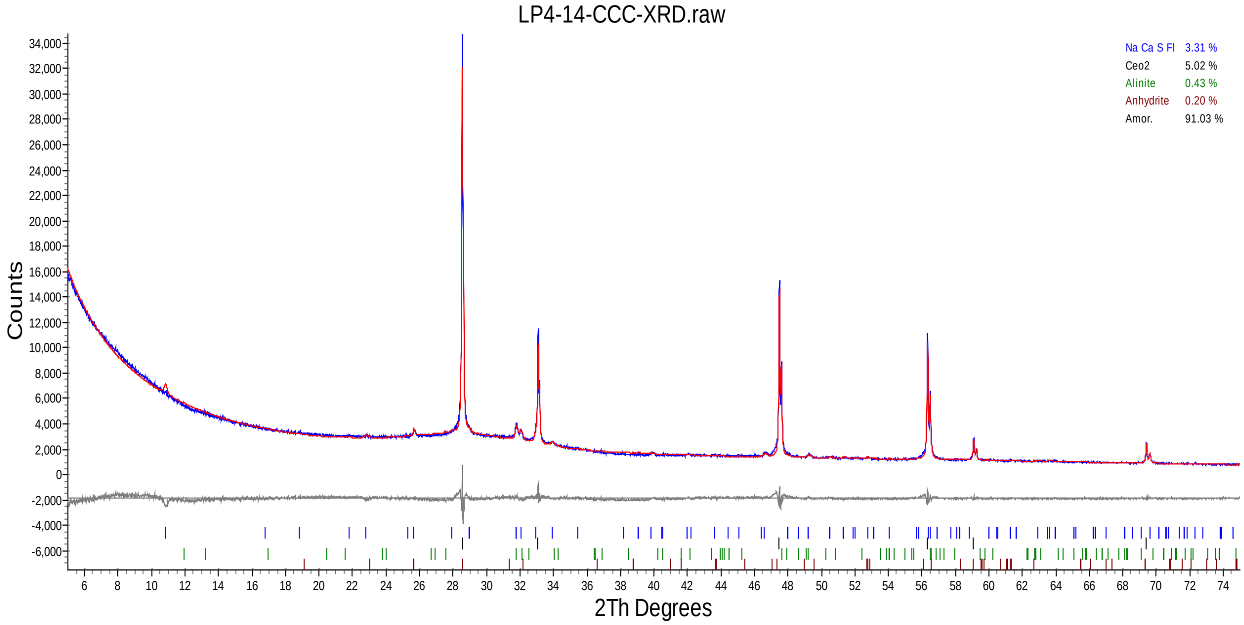
LP4-14-CCC-XRD.raw
Na Ca S Fl 3.31 %
Ceo2 5.02 %
Alinite 0.43 %
Anhydrite 0.20 %
Amor. 91.03 %
Counts
34,000
32,000
30,000
28,000
26,000
24,000
22,000
20,000
18,000
16,000
14,000
12,000
10,000
8,000
6,000
4,000
2,000
0
-2,000
-4,000
-6,000
6
8
10
12
14
16
18
20
22
24
26
28
30
32
34
36
38
40
42
44
46
48
50
52
54
56
58
60
62
64
66
68
70
72
74
2Th Degrees

C.15. Glass LP4-15 Morphology after CCC

C.16. Glass LP4-16 Morphology after CCC

C.17. Glass LP4-17 Morphology after CCC

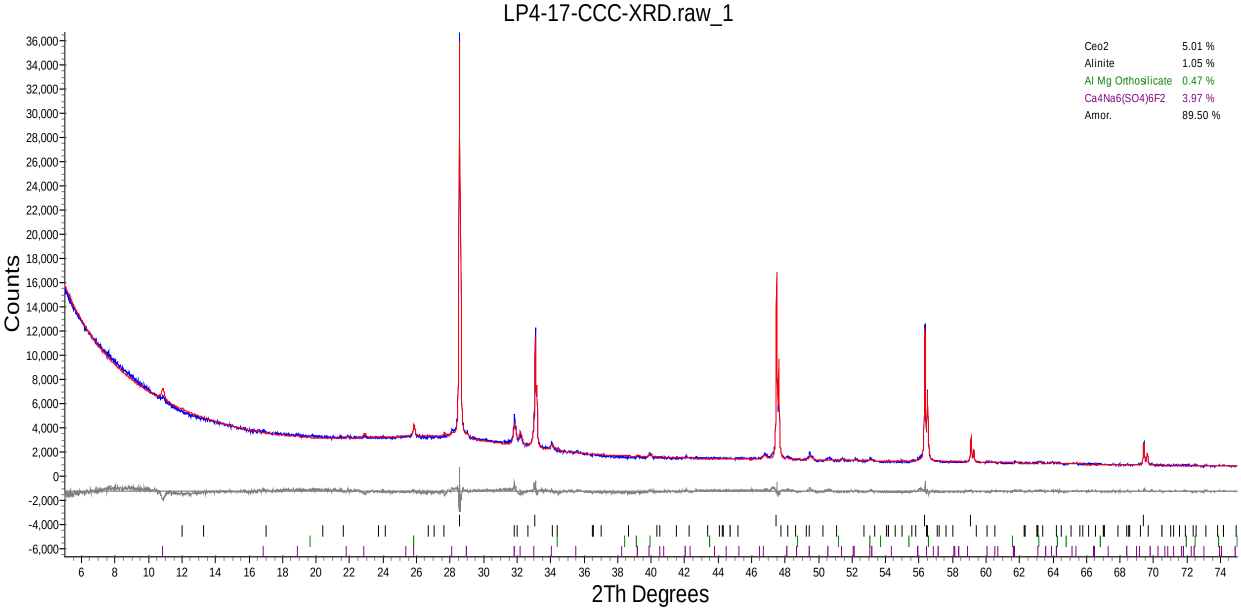

C.18. Glass LP4-18 Morphology after CCC

C.19. Glass LP4-19 Morphology after CCC

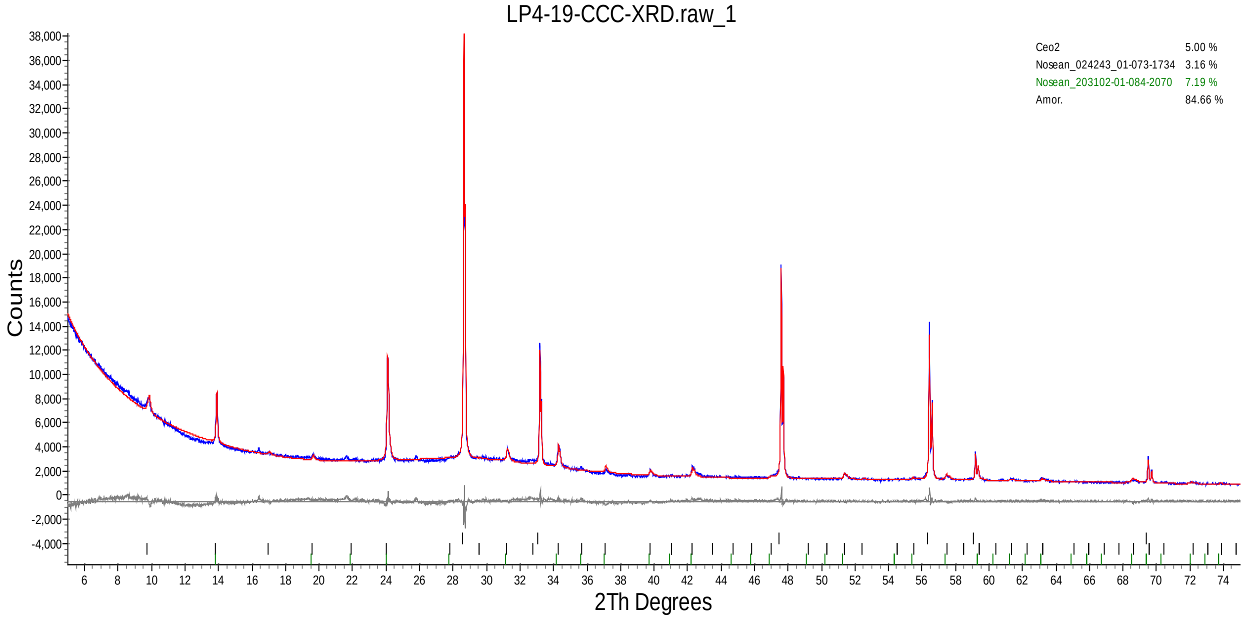
LP4-19-CCC-XRD.raw_1
Ceo2 5.00 %
Nosean_024243_01-073-1734 3.16 %
Nosean_203102-01-084-2070 7.19 %
Amor. 84.66 %
Counts
38,000
36,000
34,000
32,000
30,000
28,000
26,000
24,000
22,000
20,000
18,000
16,000
14,000
12,000
10,000
8,000
6,000
4,000
2,000
0
-2,000
-4,000
6 8 10 12 14 16 18 20 22 24 26 28 30 32 34 36 38 40 42 44 46 48 50 52 54 56 58 60 62 64 66 68 70 72 74
2Th Degrees

C.20. Glass LP4-20 Morphology after CCC

C.21. Glass LP4-21 Morphology after CCC

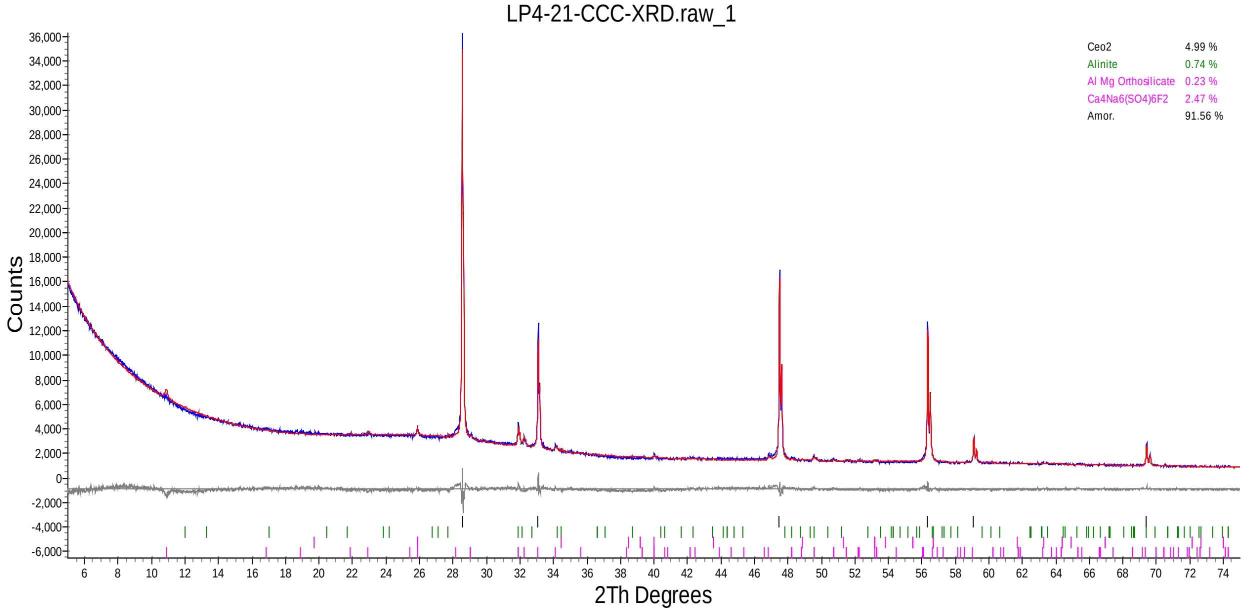

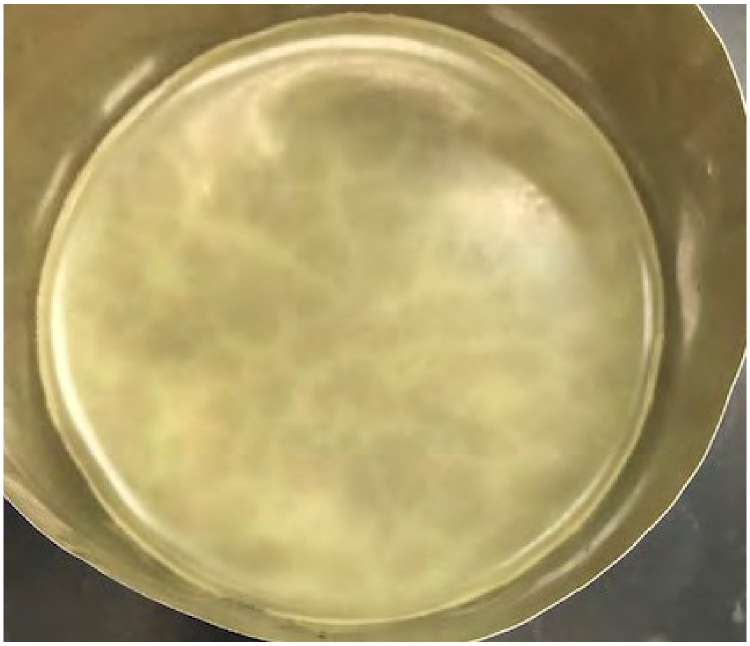

C.22. Glass LP4-22 Morphology after CCC

C.23. Glass LP4-23-1 Morphology after CCC

C.24. Glass LP4-24 Morphology after CCC

C.25. Glass LP4-25-1 Morphology after CCC

Appendix D – Crystal Fraction of Heat-Treated Glasses Photographs

This appendix contains photographs of the low-activity waste Phase 4 glasses after they were heat treated at 950 °C for 24 hours (crystal fraction [CF] heat treatment). As indicated by these photographs, each glass showed different responses to heat treatment.

D.1. Glass LP4-01 after CF Heat Treatment at 950 °C for 24 Hours

D.2. Glass LP4-02 after CF Heat Treatment at 950 °C for 24 Hours

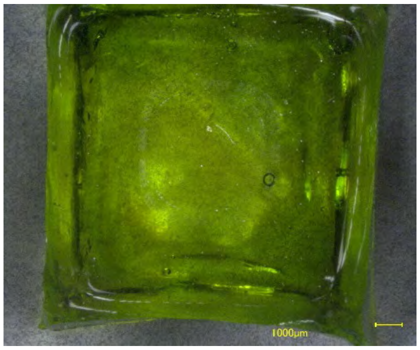

D.3. Glass LP4-03 after CF Heat Treatment at 950 °C for 24 Hours

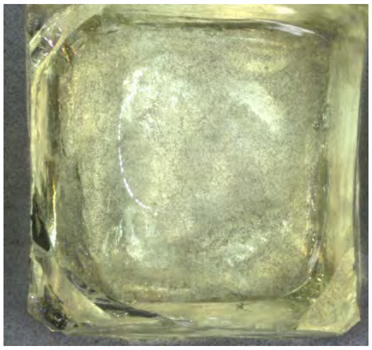

D.4. Glass LP4-04-1 after CF Heat Treatment at 950 °C for 24 Hours

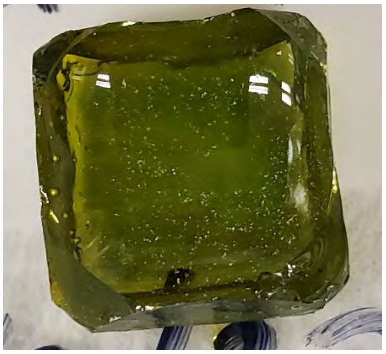

D.5. Glass LP4-05 after CF Heat Treatment at 950 °C for 24 Hours

D.6. Glass LP4-06-2 after CF Heat Treatment at 950 °C for 24 Hours

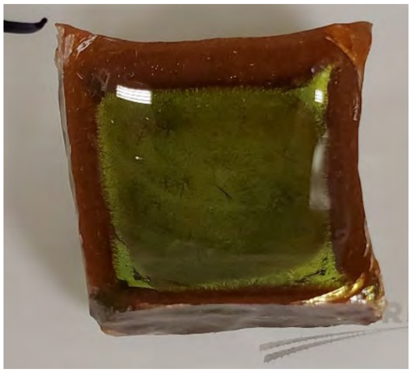

D.7. Glass LP4-07-1 after CF Heat Treatment at 950 °C for 24 Hours

D.8. Glass LP4-08-1 after CF Heat Treatment at 950 °C for 24 Hours

D.9. Glass LP4-09 after CF Heat Treatment at 950 °C for 24 Hours

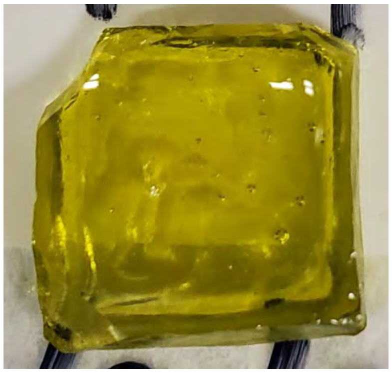

D.10. Glass LP4-10 after CF Heat Treatment at 950 °C for 24 Hours

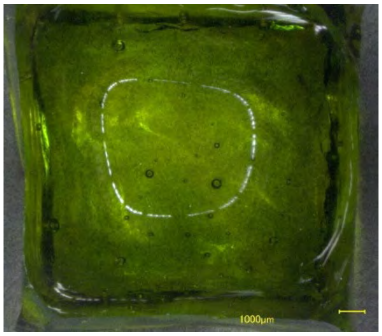

D.11. Glass LP4-11 after CF Heat Treatment at 950 °C for 24 Hours

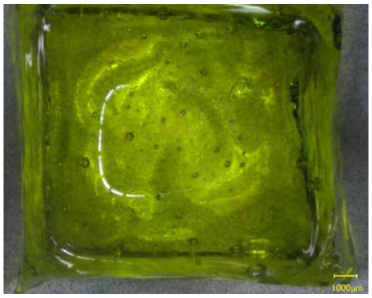

D.12. Glass LP4-12 after CF Heat Treatment at 950 °C for 24 Hours

D.13. Glass LP4-13 after CF Heat Treatment at 950 °C for 24 Hours

D.14. Glass LP4-14 after CF Heat Treatment at 950 °C for 24 Hours

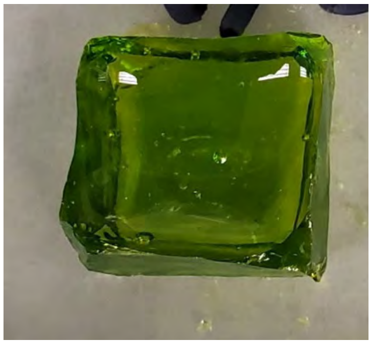

D.15. Glass LP4-15 after CF Heat Treatment at 950 °C for 24 Hours

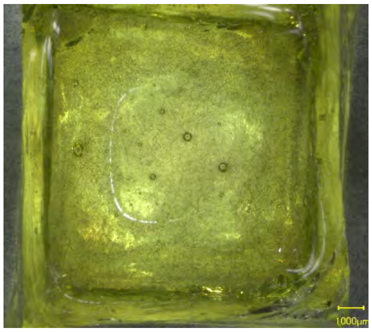

D.16. Glass LP4-16 after CF Heat Treatment at 950 °C for 24 Hours

D.17. Glass LP4-17 after CF Heat Treatment at 950 °C for 24 Hours

D.18. Glass LP4-18 after CF Heat Treatment at 950 °C for 24 Hours

D.19. Glass LP4-19 after CF Heat Treatment at 950 °C for 24 Hours

D.20. Glass LP4-20 after CF Heat Treatment at 950 °C for 24 Hours

D.21. Glass LP4-21 after CF Heat Treatment at 950 °C for 24 Hours

D.22. Glass LP4-22 after CF Heat Treatment at 950 °C for 24 Hours

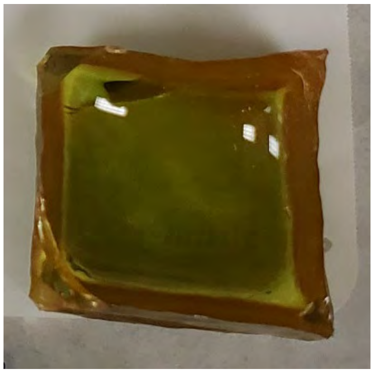

D.23. Glass LP4-23-1 after CF Heat Treatment at 950 °C for 24 Hours

D.24. Glass LP4-24 after CF Heat Treatment at 950 °C for 24 Hours

D.25. Glass LP4-25-1 after CF Heat Treatment at 950 °C for 24 Hours

Appendix E – Viscosity Data

This appendix contains the measured viscosity data for each of the glasses in this matrix. The plots shown in this appendix are fitted to the Arrhenius equation:

$$\ln(\eta) = A + \frac{B}{T_K} \qquad \text{(C.1)}$$

where A and B are independent of temperature and temperature (T_K) is in K (T(°C) + 273.15).

If the plots showed curvature, they would be better fit to the Vogel- Fulcher-Tamman (VFT) model

$$\ln(\eta) = E + \frac{F}{T_k - T_0} \qquad \text{(C.2)}$$

where E, F, and T_0 are temperature independent and composition dependent coefficients and T_K is the temperature in K (T(°C) + 273.15). The intent of the figures and Arrhenius equation fits shown in this appendix are mainly to assess trends of the data and provide some observations about whether there may be sufficient curvature in the data to consider VFT fits in the subsequent work that will decide between fitting the viscosity-temperature data to the Arrhenius or VFT equations. All the glasses in this matrix appear to have very good fits to the Arrhenius equation and do not show a need for fitting to the VFT model.

E.1 Glass LP4-01 Viscosity Data

Table E.1. Viscosity Data for Glass LP4-01

Measured Temp., °C	Viscosity, Pa-s	1/T x10000, K^{-1}	ln η, Pa-s
1150	1.107	7.027	0.101
1050	2.749	7.558	1.011
950	8.534	8.176	2.144
1150	1.094	7.027	0.089
1232	0.647	6.645	-0.436
1150	1.169	7.027	0.156

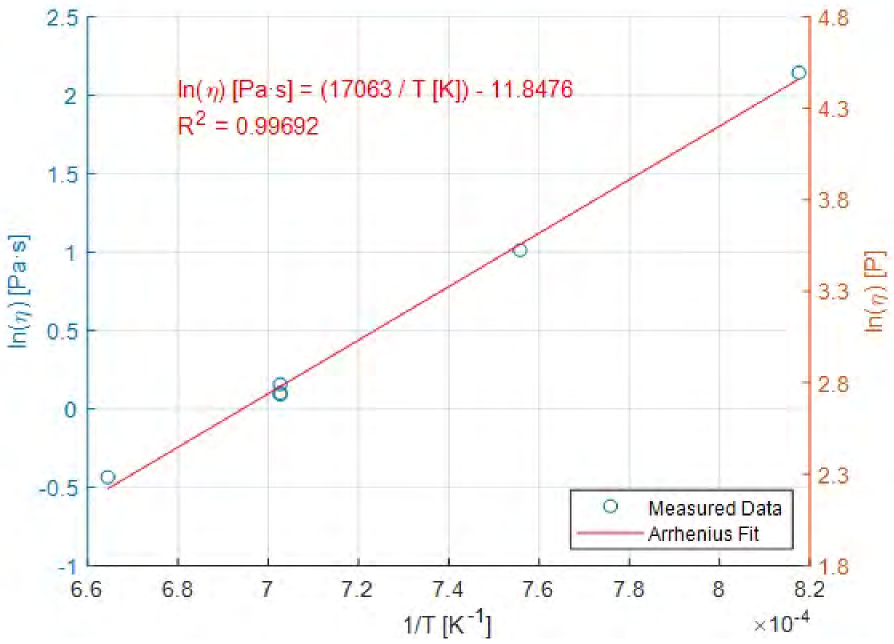

Figure E.1. Viscosity-Temperature Data and Arrhenius Equation Fit for Glass LP4-01

E.2 Glass LP4-02 Viscosity Data

Table E.2. Viscosity Data for Glass LP4-02

Measured Temp., °C	Viscosity, Pa-s	1/T x10000, K^{-1}	ln η, Pa-s
1150	6.672	7.027	1.898
1050	17.000	7.558	2.833
950	53.472	8.176	3.979
1150	6.668	7.027	1.897
1234	3.584	6.637	1.277
1150	7.096	7.027	1.960

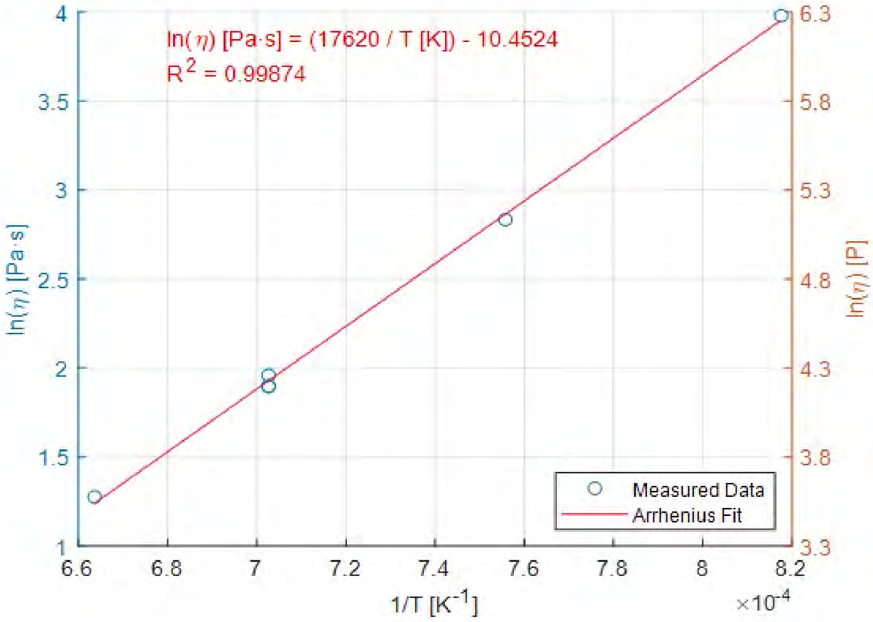

Figure E.2. Viscosity-Temperature Data and Arrhenius Equation Fit for Glass LP4-02

E.3 Glass LP4-03 Viscosity Data

Table E.3. Viscosity Data for Glass LP4-03

Measured Temp., °C	Viscosity, Pa-s	1/T x10000, K^{-1}	ln η, Pa-s
1150	1.915	7.027	0.650
1050	4.344	7.558	1.469
950	12.000	8.176	2.485
1150	1.720	7.027	0.542
1228	1.044	6.662	0.043
1150	1.995	7.027	0.691

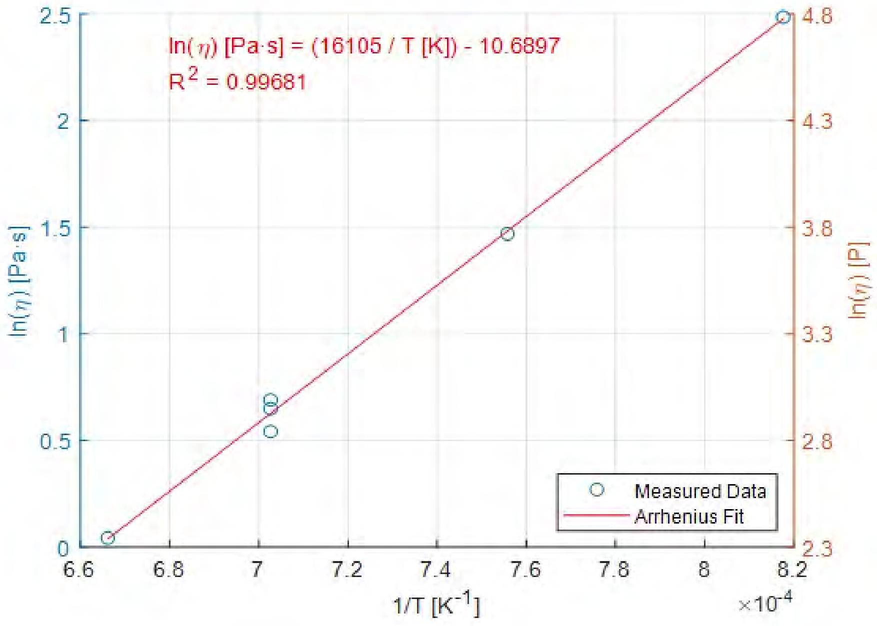

Figure E.3. Viscosity-Temperature Data and Arrhenius Equation Fit for Glass LP4-03

E.4 Glass LP4-04-1 Viscosity Data

Table E.4. Viscosity Data for Glass LP4-04-1

Measured Temp., °C	Viscosity, Pa-s	1/T x10000, K^{-1}	ln η, Pa-s
1150	3.096	7.027	1.130
1050	7.286	7.558	1.986
950	24.970	8.176	3.218
1150	3.038	7.027	1.111
1250	1.386	6.565	0.327
1150	3.063	7.027	1.119

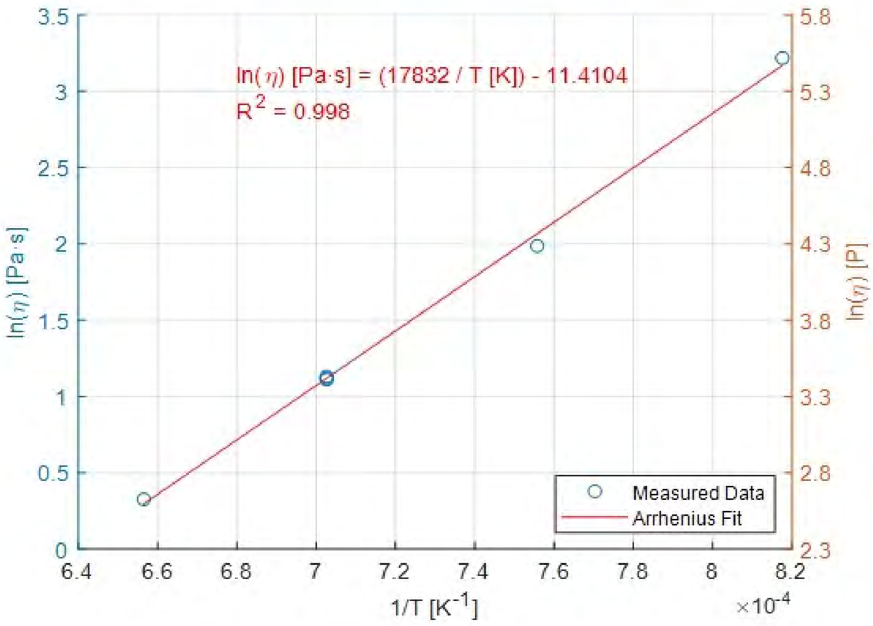

Figure E.4. Viscosity-Temperature Data and Arrhenius Equation Fit for Glass LP4-04-1

E.5 Glass LP4-05 Viscosity Data

Table E.5. Viscosity Data for Glass LP4-05

Measured Temp., °C	Viscosity, Pa-s	1/T x10000, K^{-1}	ln η, Pa-s
1150	2.652	7.027	0.975
1050	6.360	7.558	1.850
950	20.859	8.176	3.038
1150	2.510	7.027	0.920
1225	1.487	6.674	0.396
1150	2.737	7.027	1.007

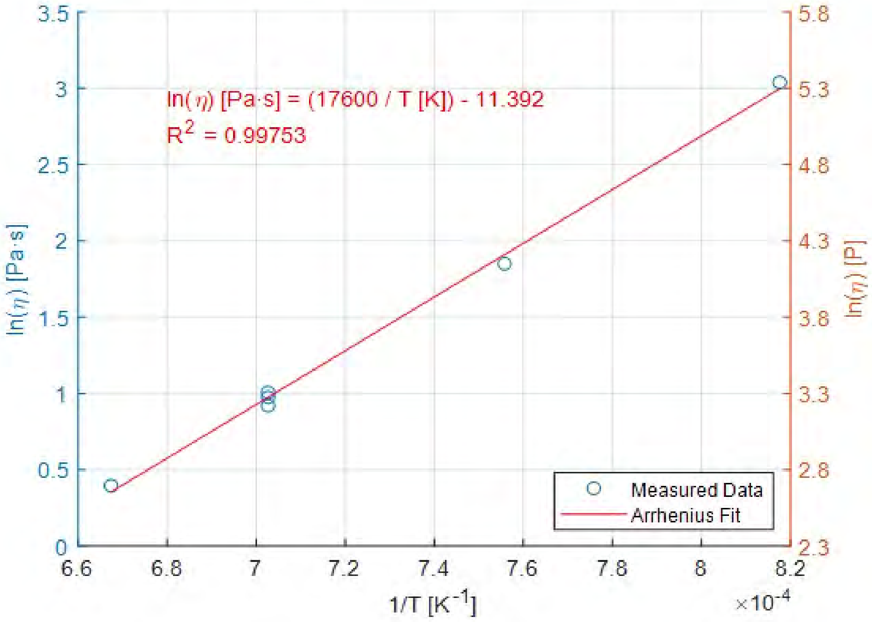

Figure E.5. Viscosity-Temperature Data and Arrhenius Equation Fit for Glass LP4-05

E.6 Glass LP4-06-2 Viscosity Data

Table E.6. Viscosity Data for Glass LP4-06-2

Measured Temp., °C	Viscosity, Pa-s	1/T x10000, K^{-1}	ln η, Pa-s
1150	13.811	7.027	2.625
1050	35.467	7.558	3.569
950	117.600	8.176	4.767
1150	12.551	7.027	2.530
1197	7.621	6.803	2.031
1150	11.642	7.027	2.455

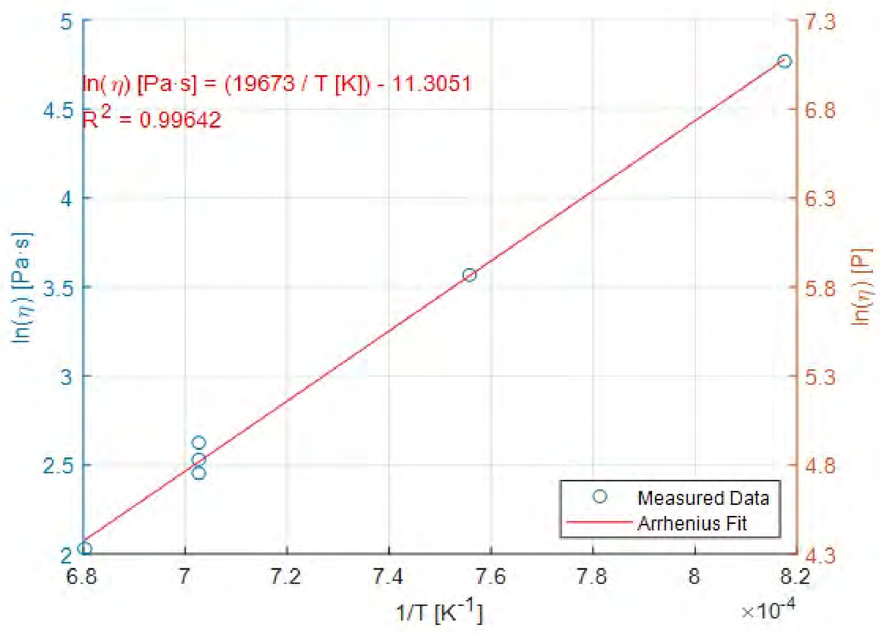

Figure E.6. Viscosity-Temperature Data and Arrhenius Equation Fit for Glass LP4-06-2

E.7 Glass LP4-07-1 Viscosity Data

Table E.7. Viscosity Data for Glass LP4-07-1

Measured Temp., °C	Viscosity, Pa-s	1/T x10000, K^{-1}	ln η, Pa-s
1150	3.317	7.027	1.199
1050	10.200	7.558	2.322
950	36.480	8.176	3.597
1150	3.085	7.027	1.127
1229	1.271	6.658	0.240
1150	3.602	7.027	1.282

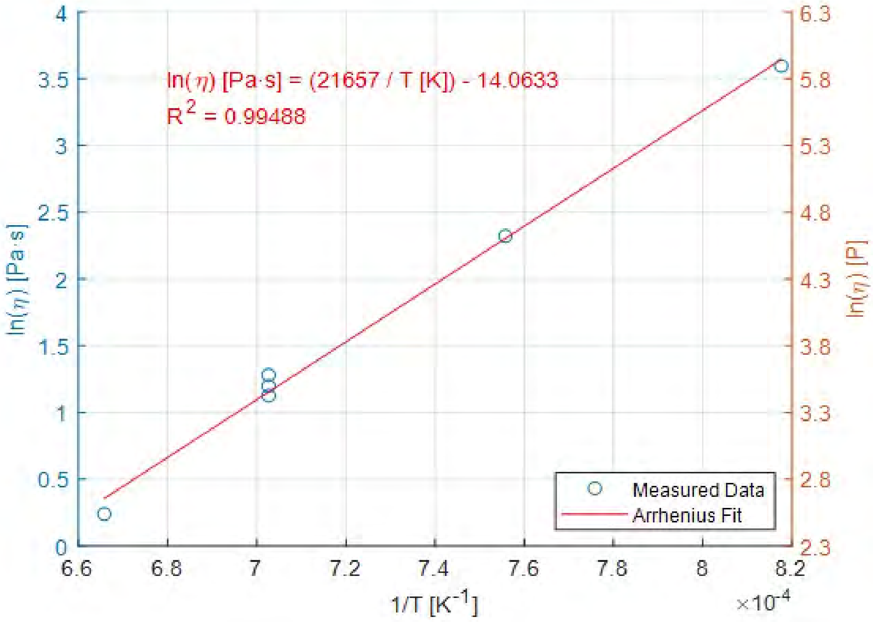

Figure E.7. Viscosity-Temperature Data and Arrhenius Equation Fit for Glass LP4-07-1

E.8 Glass LP4-08-1 Viscosity Data

Table E.8. Viscosity Data for Glass LP4-08-1

Measured Temp., °C	Viscosity, Pa-s	1/T x10000, K^{-1}	ln η, Pa-s
1150	5.404	7.027	1.687
1050	14.034	7.558	2.641
950	49.340	8.176	3.899
1150	5.369	7.027	1.681
1250	2.434	6.565	0.890
1150	5.353	7.027	1.678

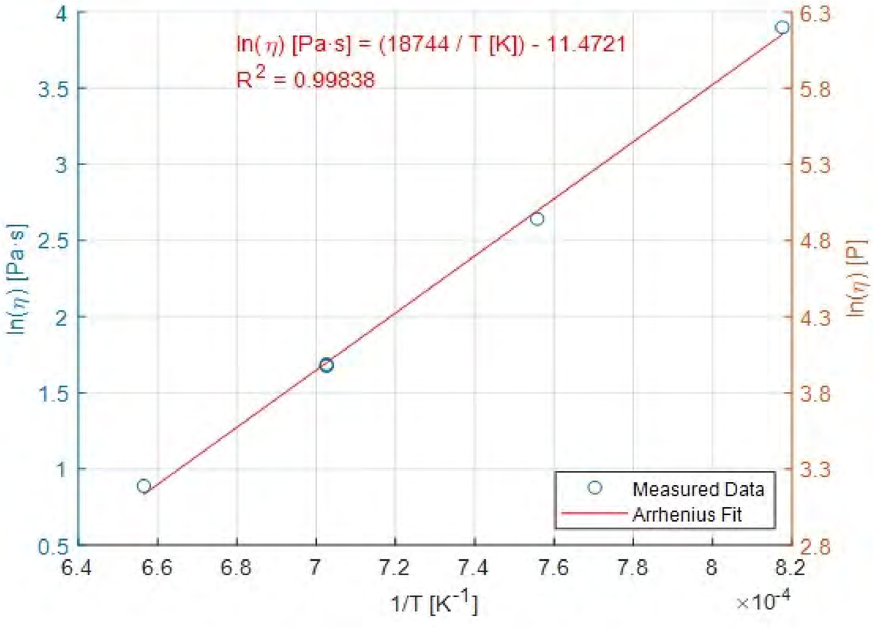

Figure E.8. Viscosity-Temperature Data and Arrhenius Equation Fit for Glass LP4-08-1

E.9 Glass LP4-09 Viscosity Data

Table E.9. Viscosity Data for Glass LP4-09

Measured Temp., °C	Viscosity, Pa-s	1/T x10000, K^{-1}	ln η, Pa-s
1150	1.687	7.027	0.523
1050	3.306	7.558	1.196
950	9.819	8.176	2.284
1150	1.663	7.027	0.508
1250	0.857	6.565	-0.155
1150	1.797	7.027	0.586

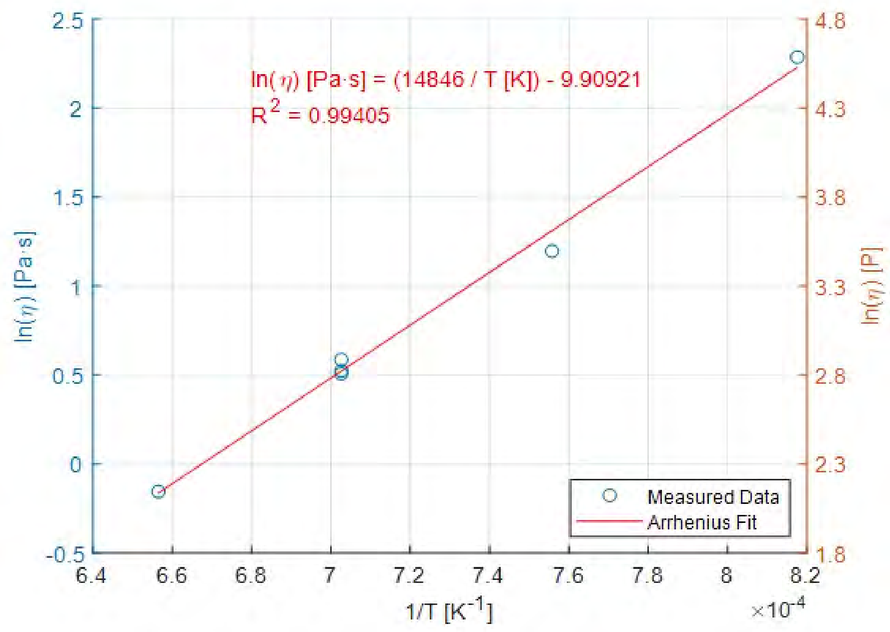

Figure E.9. Viscosity-Temperature Data and Arrhenius Equation Fit for Glass LP4-09

E.10 Glass LP4-10 Viscosity Data

Table E.10. Viscosity Data for Glass LP4-10

Measured Temp., °C	Viscosity, Pa-s	1/T x10000, K^{-1}	ln η, Pa-s
1150	1.878	7.027	0.630
1050	4.228	7.558	1.442
950	12.158	8.176	2.498
1150	1.809	7.027	0.593
1249	0.875	6.568	-0.134
1150	1.794	7.027	0.584

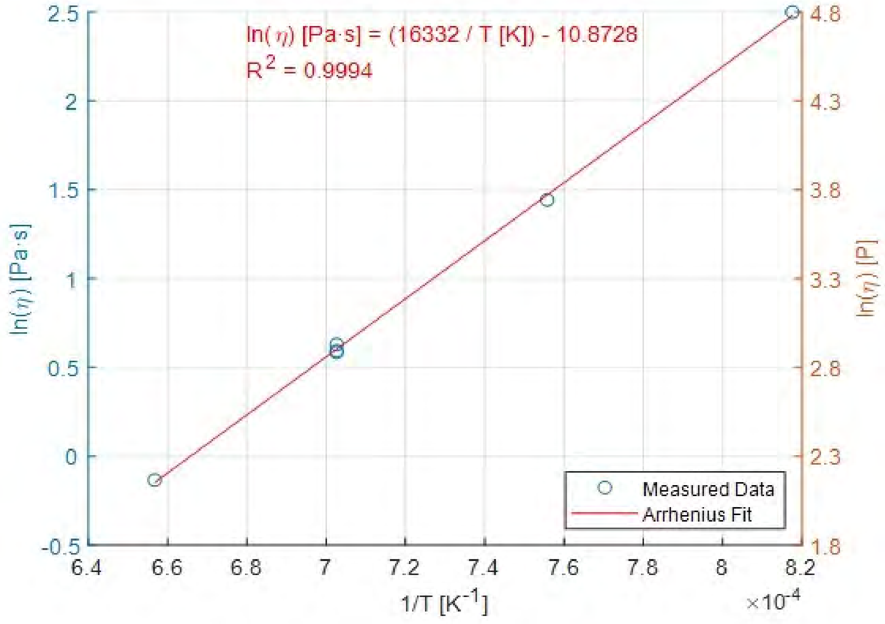

Figure E.10. Viscosity-Temperature Data and Arrhenius Equation Fit for Glass LP4-10

E.11 Glass LP4-11 Viscosity Data

Table E.11. Viscosity Data for Glass LP4-11

Measured Temp., °C	Viscosity, Pa-s	1/T x10000, K^{-1}	ln η, Pa-s
1150	8.880	7.027	2.184
1050	25.146	7.558	3.225
950	101.135	8.176	4.616
1150	9.170	7.027	2.216
1199	5.714	6.791	1.743
1150	8.829	7.027	2.178

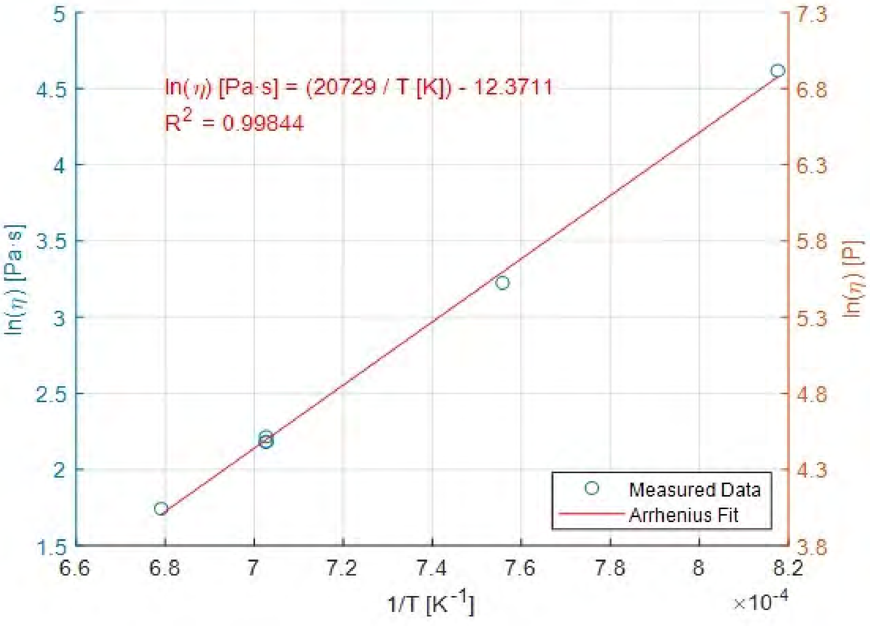

Figure E.11. Viscosity-Temperature Data and Arrhenius Equation Fit for Glass LP4-11

E.12 Glass LP4-12 Viscosity Data

Table E.12. Viscosity Data for Glass LP4-12

Measured Temp., °C	Viscosity, Pa-s	1/T x10000, K^{-1}	ln η, Pa-s
1150	7.182	7.027	1.972
1050	20.404	7.558	3.016
950	79.575	8.176	4.377
1150	7.343	7.027	1.994
1240	3.325	6.605	1.202
1150	7.083	7.027	1.958

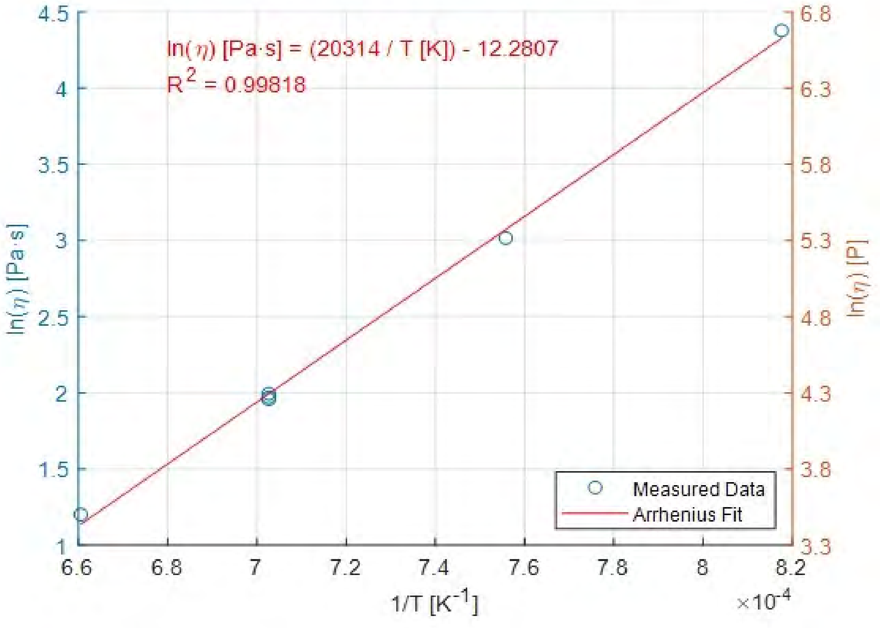

Figure E.12. Viscosity-Temperature Data and Arrhenius Equation Fit for Glass LP4-12

E.13 Glass LP4-13 Viscosity Data

Table E.13. Viscosity Data for Glass LP4-13

Measured Temp., °C	Viscosity, Pa-s	1/T x10000, K^{-1}	ln η, Pa-s
1150	1.126	7.027	0.118
1050	2.590	7.558	0.952
950	7.282	8.176	1.985
1150	1.236	7.067	0.212
1184	0.882	6.865	-0.126
1150	1.128	7.027	0.120

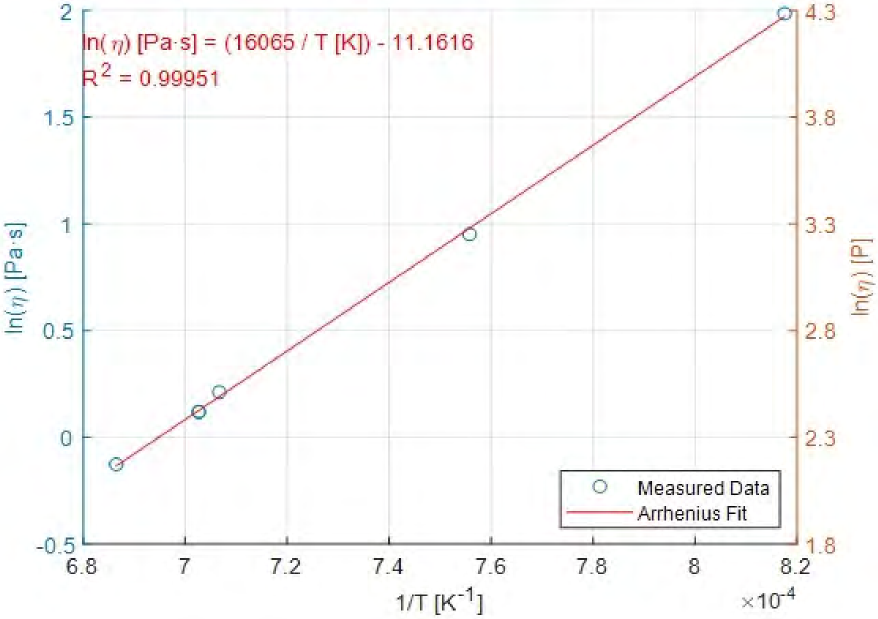

Figure E.13. Viscosity-Temperature Data and Arrhenius Equation Fit for Glass LP4-13

E.14 Glass LP4-14 Viscosity Data

Table E.14. Viscosity Data for Glass LP4-14

Measured Temp., °C	Viscosity, Pa-s	1/T x10000, K^{-1}	ln η, Pa-s
1150	1.182	7.027	0.167
1050	2.980	7.558	1.092
950	9.462	8.176	2.247
1150	1.231	7.027	0.208
1189	0.866	6.838	-0.143
1150	1.175	7.027	0.161

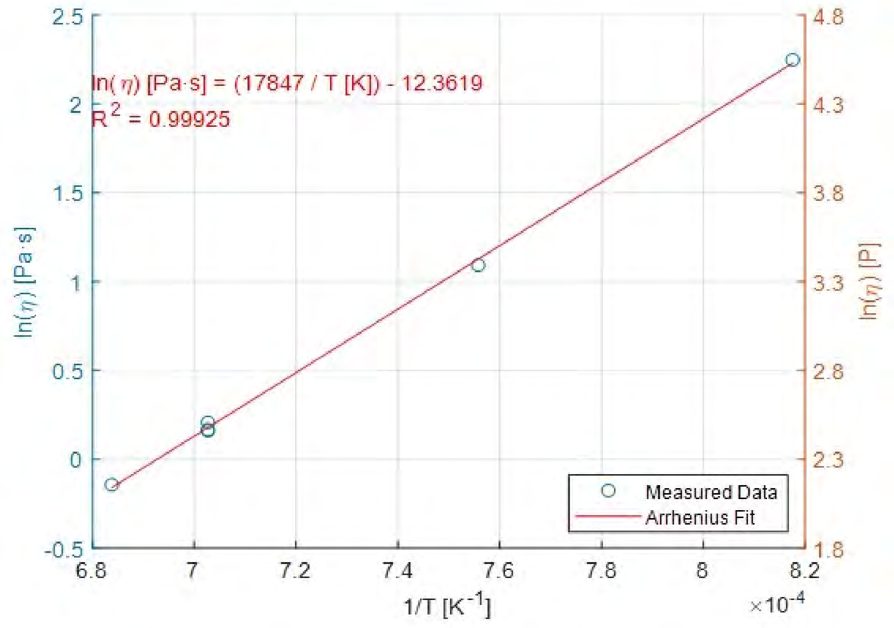

Figure E.14. Viscosity-Temperature Data and Arrhenius Equation Fit for Glass LP4-14

E.15 Glass LP4-15 Viscosity Data

Table E.15. Viscosity Data for Glass LP4-15

Measured Temp., °C	Viscosity, Pa-s	1/T x10000, K^{-1}	ln η, Pa-s
1150	4.641	7.027	1.535
1050	12.484	7.558	2.524
950	44.089	8.176	3.786
1150	5.142	7.041	1.637
1183	3.649	6.870	1.294
1150	4.817	7.027	1.572

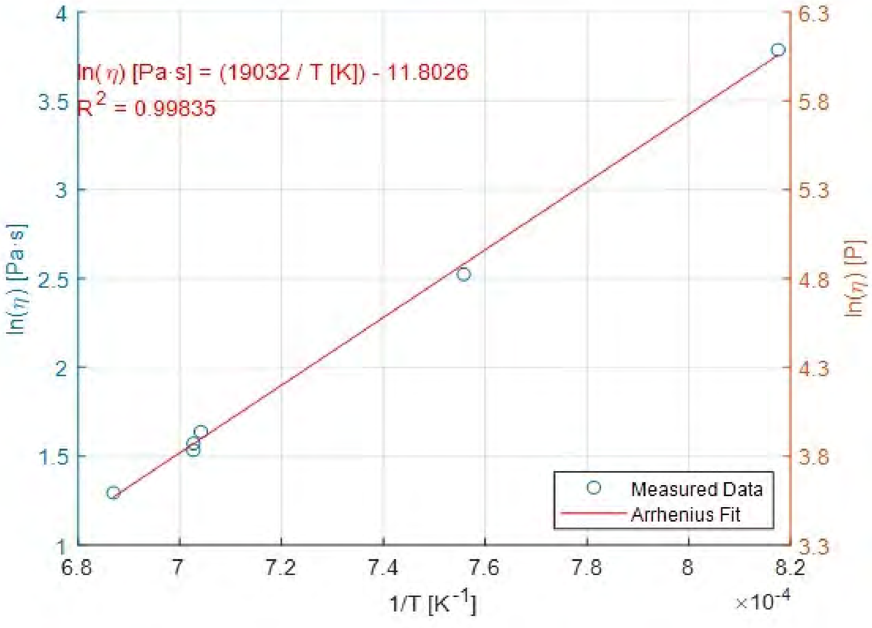

Figure E.15. Viscosity-Temperature Data and Arrhenius Equation Fit for Glass LP4-15

E.16 Glass LP4-16 Viscosity Data

Table E.16. Viscosity Data for Glass LP4-16

Measured Temp., °C	Viscosity, Pa-s	1/T x10000, K^{-1}	ln η, Pa-s
1150	2.831	7.027	1.040
1050	6.867	7.558	1.927
950	21.715	8.176	3.078
1150	3.301	7.063	1.194
1180	2.299	6.883	0.833
1150	2.881	7.027	1.058

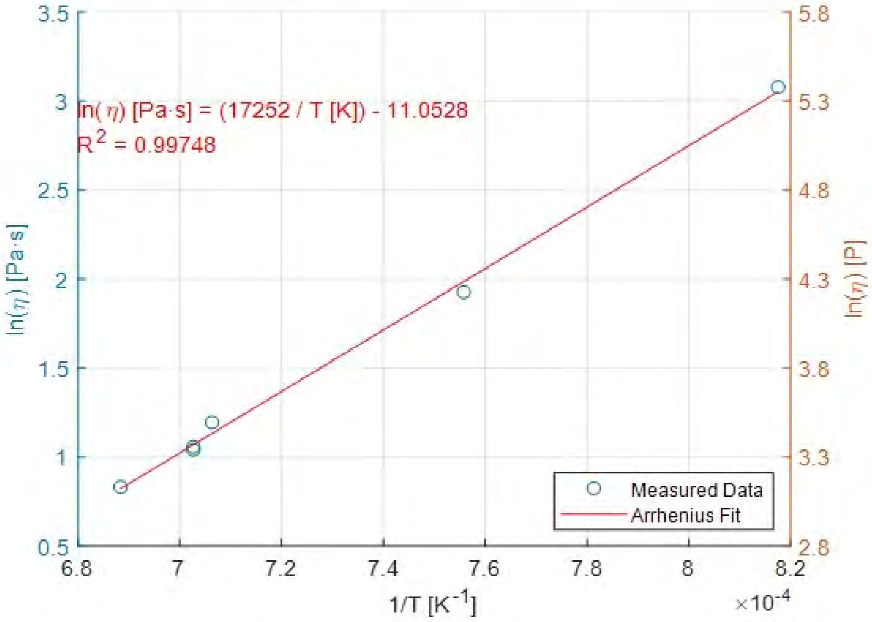

Figure E.16. Viscosity-Temperature Data and Arrhenius Equation Fit for Glass LP4-16

E.17 Glass LP4-17 Viscosity Data

Table E.17. Viscosity Data for Glass LP4-17

Measured Temp., °C	Viscosity, Pa-s	1/T x10000, K^{-1}	ln η, Pa-s
1150	2.051	7.027	0.718
1050	4.898	7.558	1.589
950	16.148	8.176	2.782
1150	2.127	7.027	0.755
1198	1.449	6.796	0.371
1150	2.042	7.027	0.714

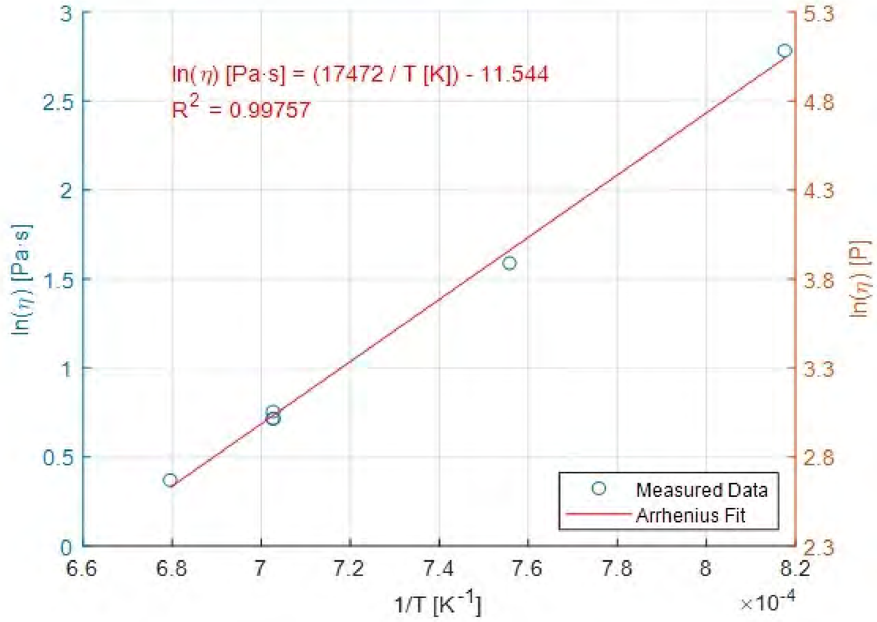

Figure E.17. Viscosity-Temperature Data and Arrhenius Equation Fit for Glass LP4-17

E.18 Glass LP4-18 Viscosity Data

Table E.18. Viscosity Data for Glass LP4-18

Measured Temp., °C	Viscosity, Pa-s	1/T x10000, K^{-1}	ln η, Pa-s
1150	3.470	7.027	1.244
1050	9.190	7.558	2.218
950	36.280	8.176	3.591
1150	3.647	7.027	1.294
1205	2.514	6.767	0.922
1150	3.454	7.027	1.239

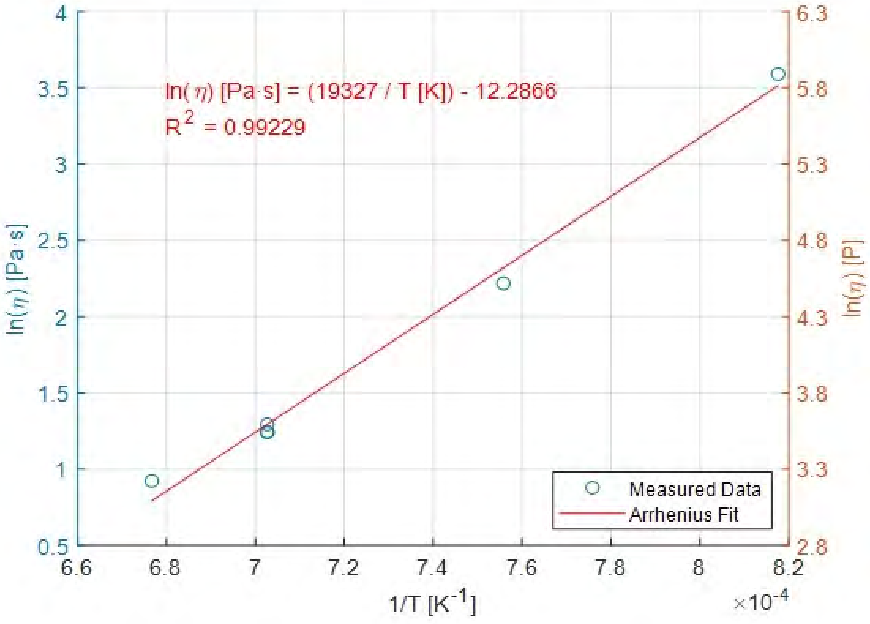

Figure E.18. Viscosity-Temperature Data and Arrhenius Equation Fit for Glass LP4-18

E.19 Glass LP4-19 Viscosity Data

Table E.19. Viscosity Data for Glass LP4-19

Measured Temp., °C	Viscosity, Pa-s	1/T x10000, K^{-1}	ln η, Pa-s
1150	8.186	7.027	2.102
1050	23.797	7.558	3.170
950	95.734	8.176	4.562
1150	8.351	7.027	2.122
1213	4.919	6.730	1.593
1150	8.077	7.027	2.089

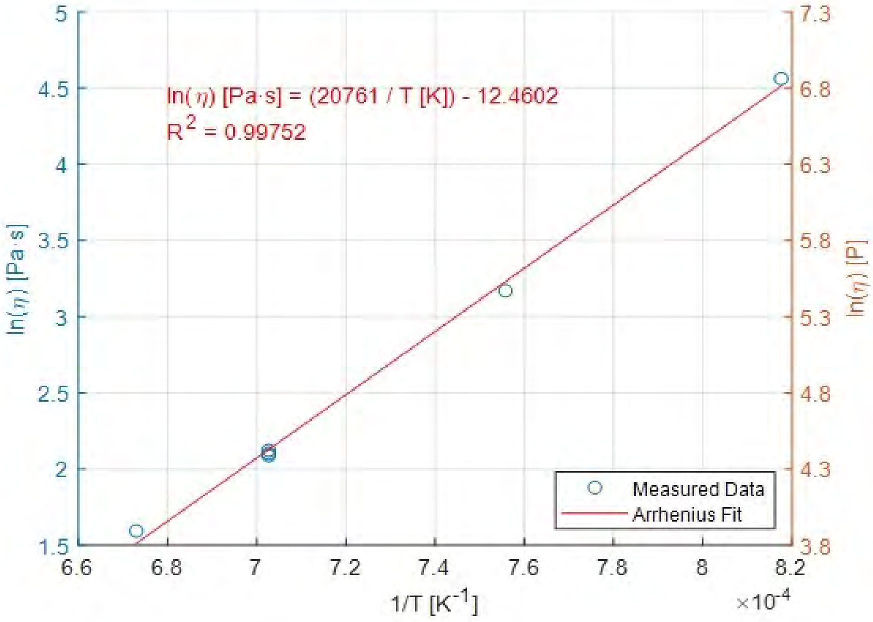

Figure E.19. Viscosity-Temperature Data and Arrhenius Equation Fit for Glass LP4-19

E.20 Glass LP4-20 Viscosity Data

Table E.20. Viscosity Data for Glass LP4-20

Measured Temp., °C	Viscosity, Pa-s	1/T x10000, K^{-1}	ln η, Pa-s
1150	1.834	7.027	0.606
1050	4.196	7.558	1.434
950	13.595	8.176	2.610
1150	1.818	7.027	0.597
1193	1.277	6.817	0.245
1150	1.761	7.027	0.566

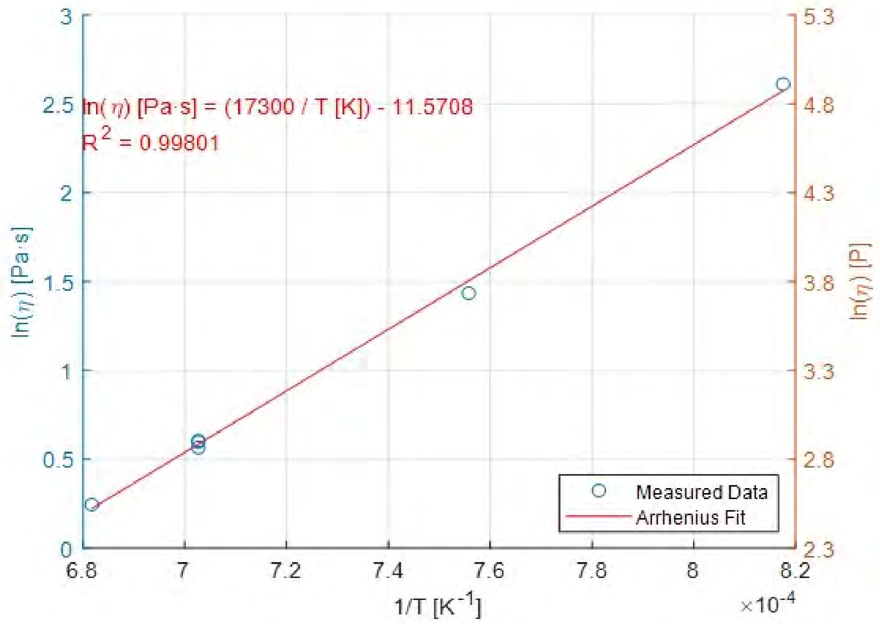

Figure E.20. Viscosity-Temperature Data and Arrhenius Equation Fit for Glass LP4-20

E.21 Glass LP4-21 Viscosity Data

Table E.21. Viscosity Data for Glass LP4-21

Measured Temp., °C	Viscosity, Pa-s	1/T x10000, K^{-1}	ln η, Pa-s
1150	7.793	7.027	2.053
1050	23.818	7.558	3.170
950	108.960	8.176	4.691
1150	7.905	7.027	2.067
1204	4.645	6.768	1.536
1150	7.465	7.027	2.010

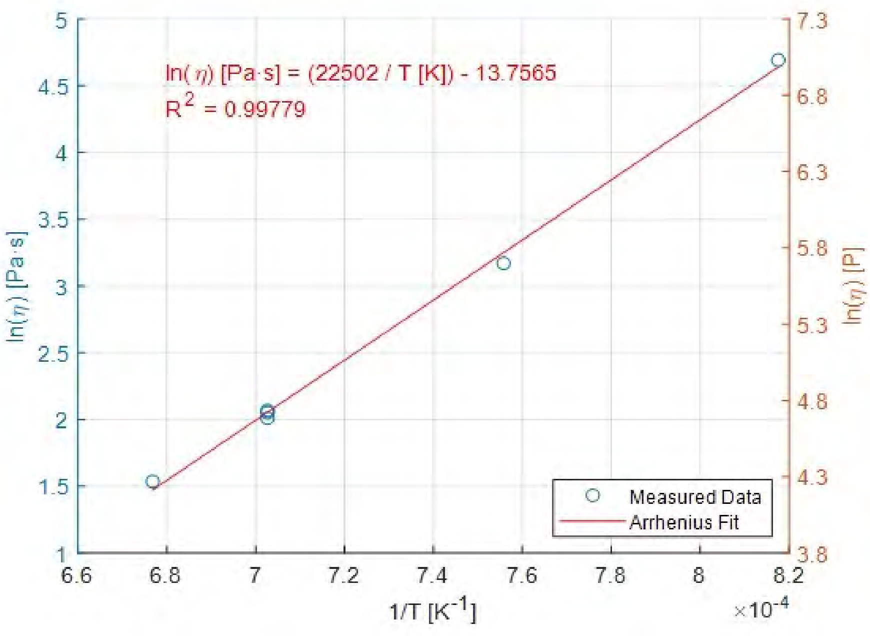

Figure E.21. Viscosity-Temperature Data and Arrhenius Equation Fit for Glass LP4-21

E.22 Glass LP4-22 Viscosity Data

Table E.22. Viscosity Data for Glass LP4-22

Measured Temp., °C	Viscosity, Pa-s	1/T x10000, K^{-1}	ln η, Pa-s
1150	4.868	7.027	1.583
1050	11.619	7.558	2.453
950	36.824	8.176	3.606
1150	4.905	7.027	1.590
1198	3.387	6.795	1.220
1150	4.863	7.027	1.582

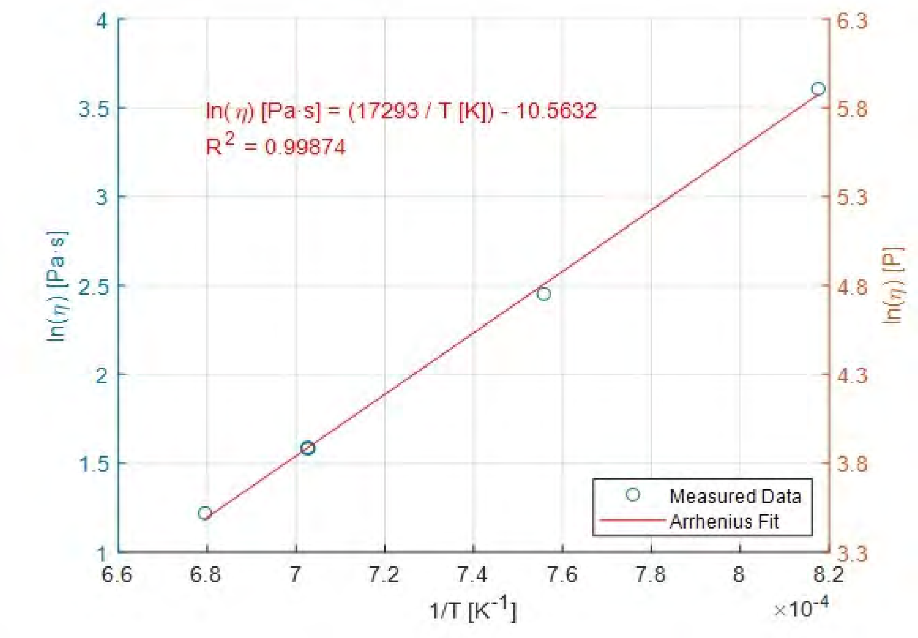

Figure E.22. Viscosity-Temperature Data and Arrhenius Equation Fit for Glass LP4-22

E.23 Glass LP4-23-1 Viscosity Data

Table E.23. Viscosity Data for Glass LP4-23-1

Measured Temp., °C	Viscosity, Pa-s	1/T x10000, K^{-1}	ln η, Pa-s
1150	3.498	7.027	1.252
1050	8.928	7.558	2.189
950	30.589	8.176	3.421
1150	3.527	7.027	1.261
1198	2.355	6.797	0.856
1150	3.398	7.027	1.223

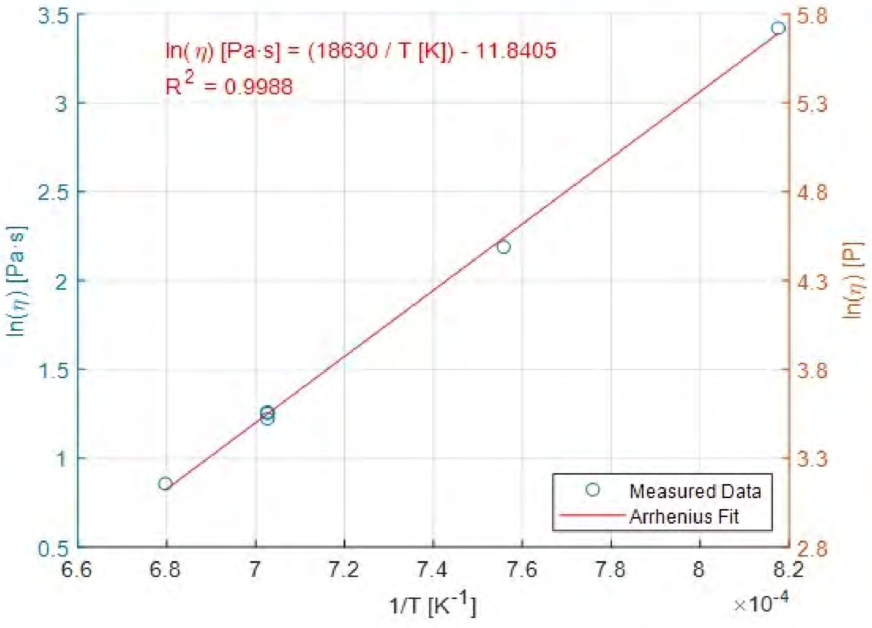

Figure E.23. Viscosity-Temperature Data and Arrhenius Equation Fit for Glass LP4-23-1

E.24 Glass LP4-24 Viscosity Data

Table E.24. Viscosity Data for Glass LP4-24

Measured Temp., °C	Viscosity, Pa-s	1/T x10000, K^{-1}	ln η, Pa-s
1150	3.005	7.027	1.100
1050	7.231	7.558	1.978
950	21.621	8.176	3.074
1150	3.039	7.027	1.111
1201	2.044	6.784	0.715
1150	3.011	7.027	1.102

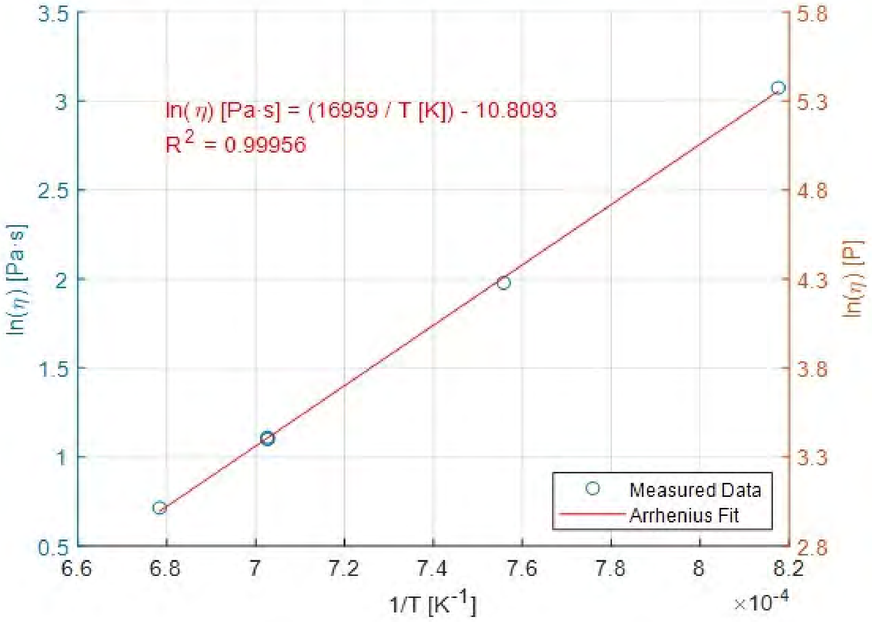

Figure E.24. Viscosity-Temperature Data and Arrhenius Equation Fit for Glass LP4-24

E.25 Glass LP4-25-1 Viscosity Data

Table E.25. Viscosity Data for Glass LP4-25-1

Measured Temp., °C	Viscosity, Pa-s	1/T x10000, K^{-1}	ln η, Pa-s
1150	2.366	7.027	0.861
1050	5.532	7.558	1.710
950	19.009	8.176	2.945
1150	2.460	7.027	0.900
1206	1.604	6.760	0.473
1150	2.341	7.027	0.850

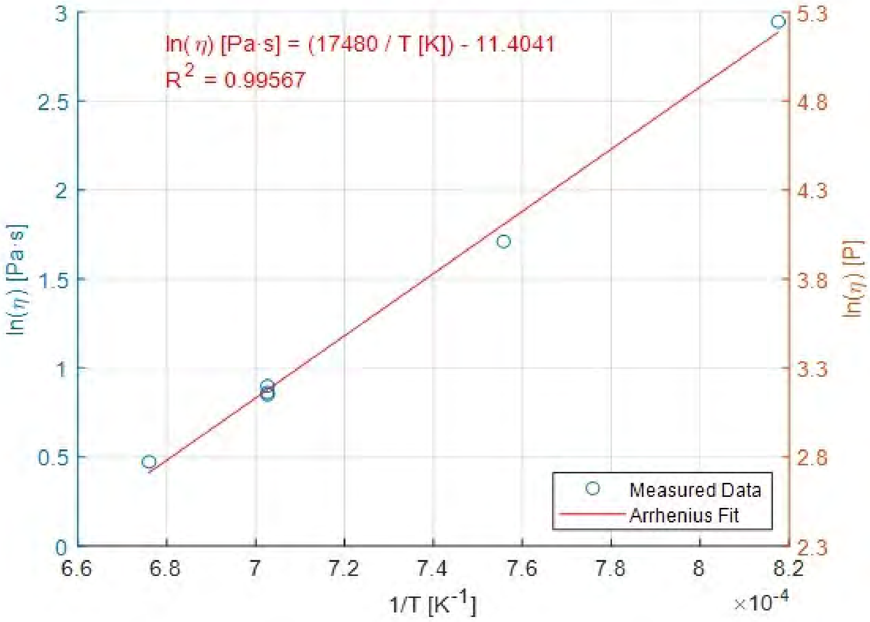

Figure E.25. Viscosity-Temperature Data and Arrhenius Equation Fit for Glass LP4-25-1

Appendix F – Electrical Conductivity Data

This appendix contains the measured electrical conductivity data for each of the glasses in this matrix.

The plots shown in this appendix are fitted to the Arrhenius equation, which is shown below:

$$\ln(\varepsilon) = A + B/T_K \qquad \text{(F.1)}$$

where *A* and *B* are independent of temperature and temperature (T_K) is in K (T(°C) + 273.15).

However, some of the plots showed curvature and would be better fit to the Vogel-Fulcher-Tamman (VFT) model:

$$\ln(\varepsilon) = \mathrm{A} + \frac{\mathrm{B}}{T_K\text{-}T_0} \qquad \text{(F.2)}$$

where A, B, and T_0 are temperature independent and composition-dependent coefficients and T_K is in °K (T(°C) + 273.15). The intent of the figures and Arrhenius equation fits shown in this appendix are mainly to assess trends of the data and provide some observations about whether there may be sufficient curvature in the data to consider VFT fits in the subsequent work that will decide between fitting the data to the Arrhenius or VFT equations for the electrical conductivity-temperature data for each glass that is being made.

F.1 Glass LP4-01 Electrical Conductivity Data

Table F.1. Electrical Conductivity Data for Glass LP4-01

Temperature, °C	Conductivity, S/m	1/(T+273.15), K^{-1}	ln ε (S/m)
950	34.53	8.18E-04	3.54
950	34.50	8.18E-04	3.54
1050	48.55	7.56E-04	3.88
1150	62.76	7.03E-04	4.14
1250	76.62	6.57E-04	4.34

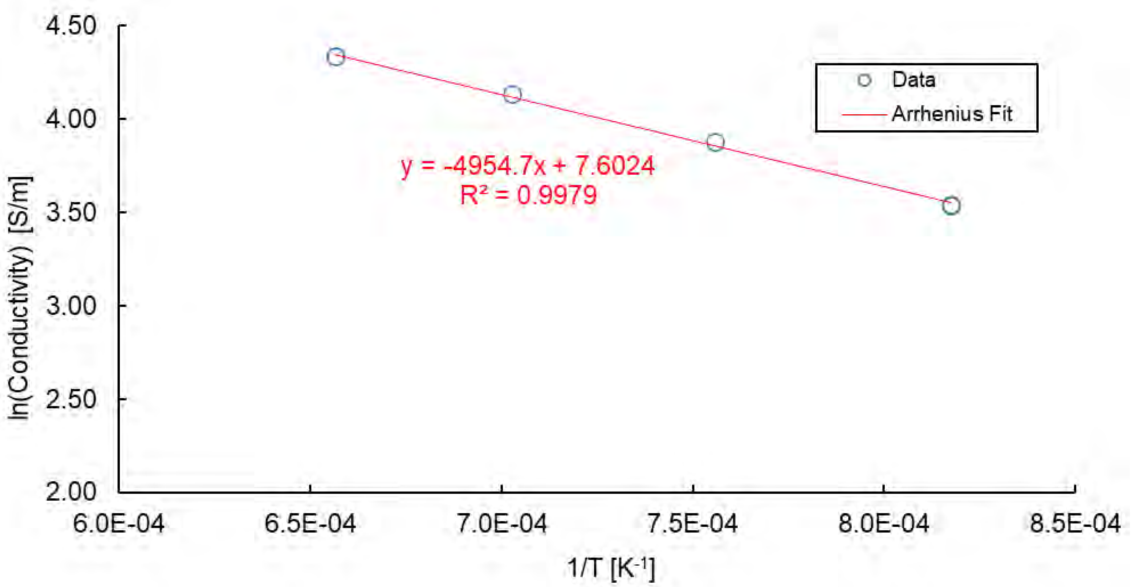

Figure F.1. Electrical Conductivity-Temperature Data and Arrhenius Equation Fit for Glass LP4-01

F.2 Glass LP4-02 Electrical Conductivity Data

Table F.2.Electrical Conductivity Data for Glass LP4-02

Temperature, °C	Conductivity, S/m	1/(T+273.15), K^{-1}	ln(ε, S/m)
950	17.06	8.18E-04	2.84
950	17.03	8.18E-04	2.83
1050	26.55	7.56E-04	3.28
1050	26.52	7.56E-04	3.28
1150	36.86	7.03E-04	3.61
1150	36.82	7.03E-04	3.61
1250	47.82	6.57E-04	3.87

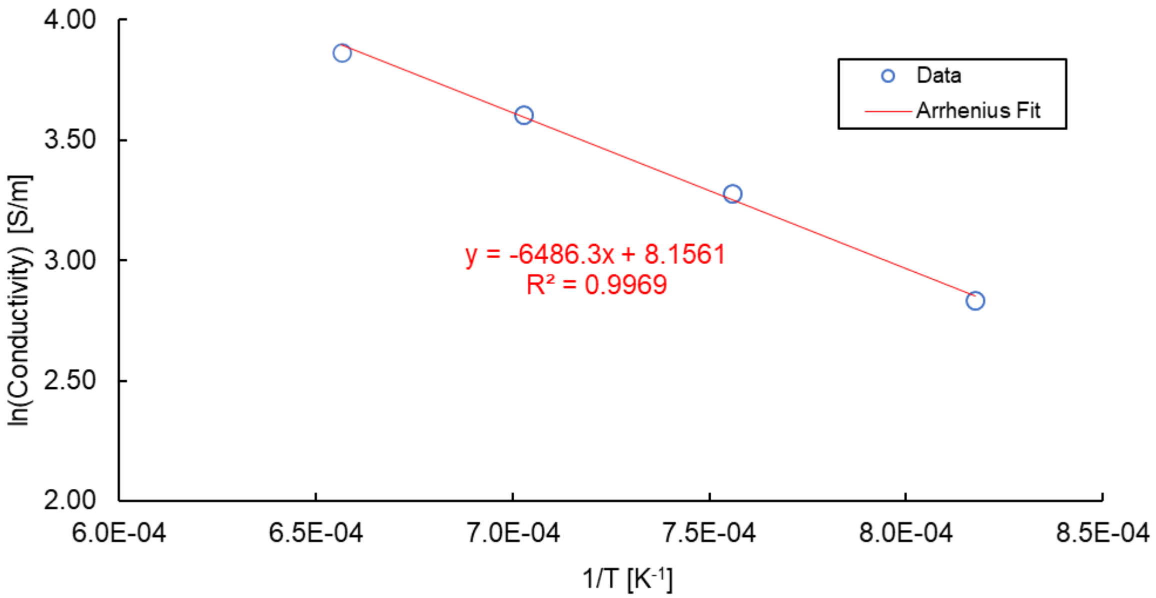

Figure F.2. Electrical Conductivity-Temperature Data and Arrhenius Equation Fit for Glass LP4-02

F.3 Glass LP4-03 Electrical Conductivity Data

Table F.3.Electrical Conductivity Data for Glass LP4-03

Temperature, °C	Conductivity, S/m	1/(T+273.15), K^{-1}	ln(ε, S/m)
950	15.71	8.18E-04	2.75
950	15.67	8.18E-04	2.75
1050	26.02	7.56E-04	3.26
1150	37.85	7.03E-04	3.63
1150	37.78	7.03E-04	3.63
1250	50.57	6.57E-04	3.92
1250	50.62	6.57E-04	3.92

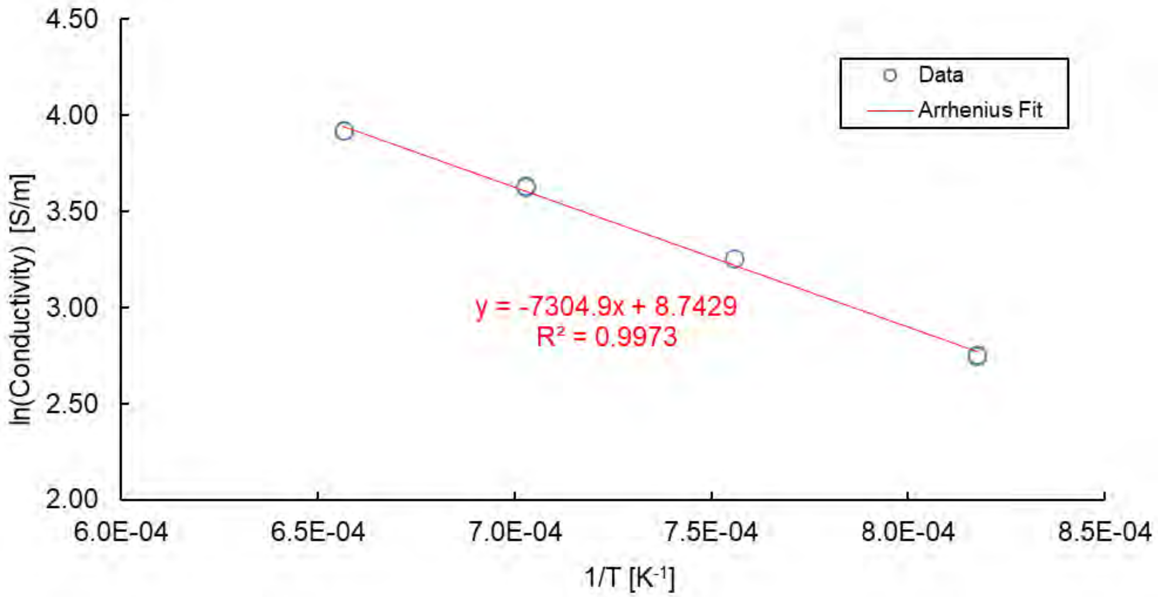

Figure F.3. Electrical Conductivity-Temperature Data and Arrhenius Equation Fit for Glass LP4-03

F.4 Glass LP4-04-1 Electrical Conductivity Data

Table F.4.Electrical Conductivity Data for Glass LP4-04-1

Temperature, °C	Conductivity, S/m	1/(T+273.15), K^{-1}	ln(ε, S/m)
950	11.13	8.18E-04	2.41
950	11.00	8.18E-04	2.40
1050	18.68	7.56E-04	2.93
1050	18.64	7.56E-04	2.93
1150	28.52	7.03E-04	3.35
1250	39.32	6.57E-04	3.67
1250	39.22	6.57E-04	3.67

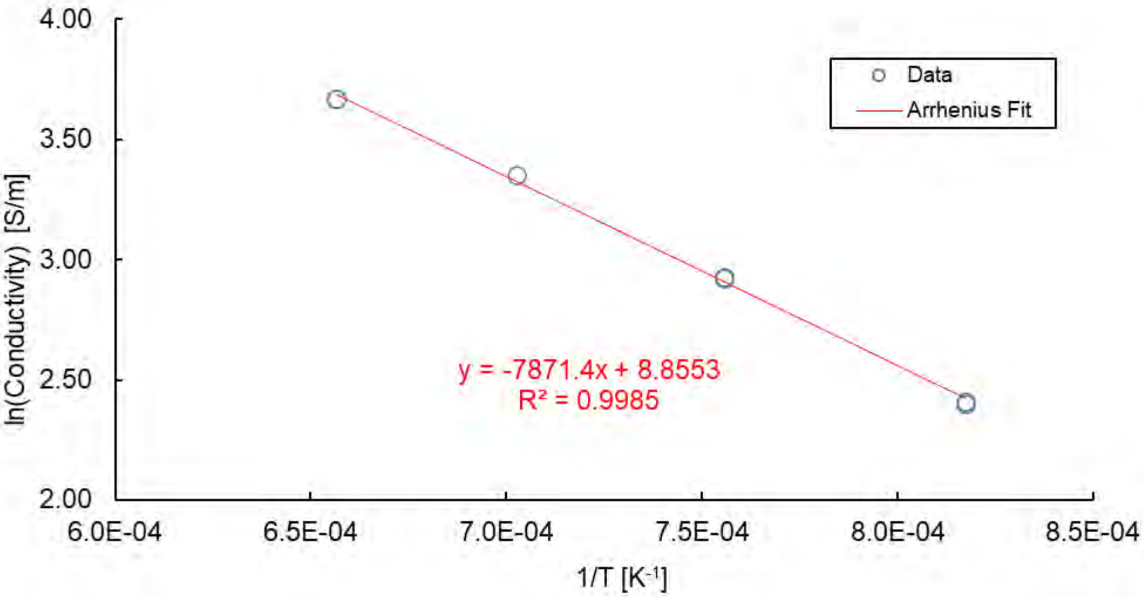

Figure F.4. Electrical Conductivity-Temperature Data and Arrhenius Equation Fit for Glass LP4-04-1

F.5 Glass LP4-05 Electrical Conductivity Data

Table F.5.Electrical Conductivity Data for Glass LP4-05

Temperature, °C	Conductivity, S/m	1/(T+273.15), K^{-1}	ln(ε, S/m)
950	21.54	8.18E-04	3.07
950	21.53	8.18E-04	3.07
1050	32.36	7.56E-04	3.48
1050	32.28	7.56E-04	3.47
1150	43.59	7.03E-04	3.77
1150	43.48	7.03E-04	3.77
1250	57.01	6.57E-04	4.04

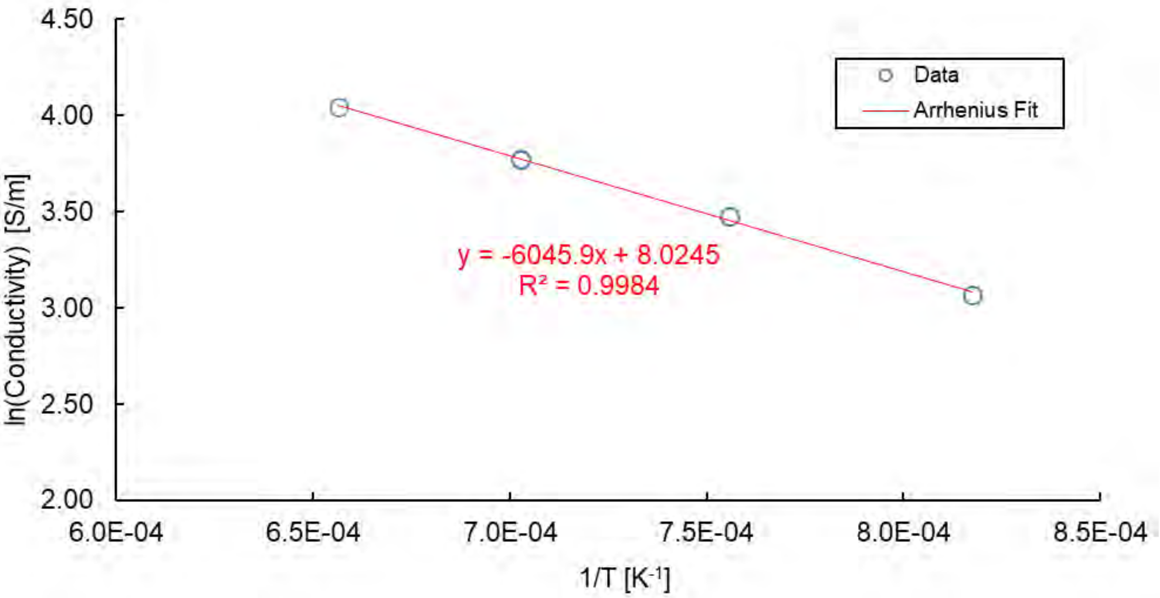

Figure F.5. Electrical Conductivity-Temperature Data and Arrhenius Equation Fit for Glass LP4-05

F.6 Glass LP4-06 Electrical Conductivity Data

Table F.6.Electrical Conductivity Data for Glass LP4-06

Temperature, °C	Conductivity, S/m	1/(T+273.15), K^{-1}	ln(ε, S/m)
950	11.47	8.18E-04	2.44
950	11.45	8.18E-04	2.44
1050	18.70	7.56E-04	2.93
1050	18.69	7.56E-04	2.93
1150	27.07	7.03E-04	3.30
1250	35.94	6.57E-04	3.58

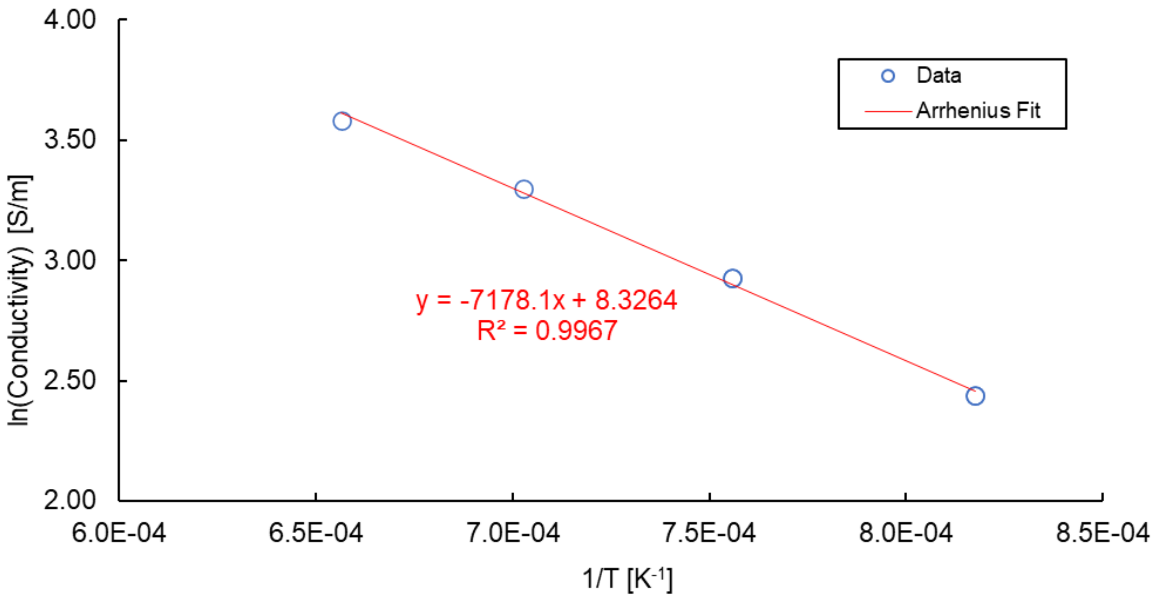

Figure F.6. Electrical Conductivity -Temperature Data and Arrhenius Equation Fit for Glass LP4-06

F.7 Glass LP4-07-1 Electrical Conductivity Data

Table F.7. Electrical Conductivity Data for Glass LP4-07-1

Temperature, °C	Conductivity, S/m	1/(T+273.15), K^{-1}	ln(ε, S/m)
950	7.99	8.18E-04	2.08
950	7.97	8.18E-04	2.08
1050	14.30	7.56E-04	2.66
1050	14.27	7.56E-04	2.66
1150	22.66	7.03E-04	3.12
1150	22.61	7.03E-04	3.12
1250	32.23	6.57E-04	3.47
1250	32.18	6.57E-04	3.47

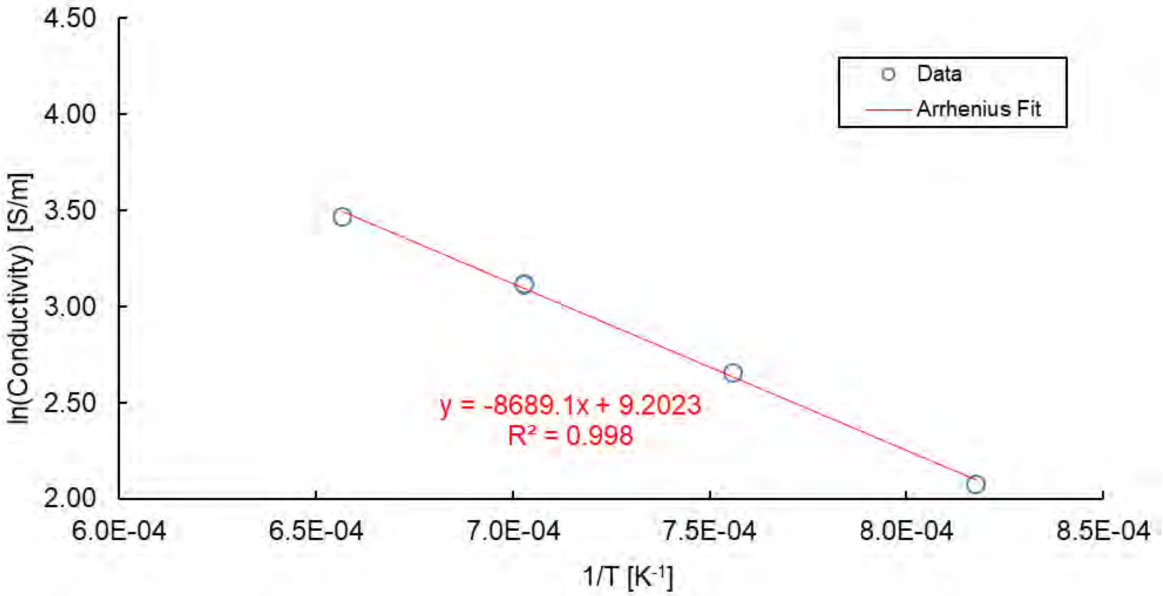

Figure F.7. Electrical Conductivity-Temperature Data and Arrhenius Equation Fit for Glass LP4-07-1

F.8 Glass LP4-08-1 Electrical Conductivity Data

Table F.8.Electrical Conductivity Data for Glass LP4-08-1

Temperature, °C	Conductivity, S/m	1/(T+273.15), K^{-1}	ln(ε, S/m)
950	14.25	8.18E-04	2.66
950	14.22	8.18E-04	2.65
1050	21.91	7.56E-04	3.09
1150	30.86	7.03E-04	3.43
1150	30.83	7.03E-04	3.43
1250	41.02	6.57E-04	3.71
1250	41.02	6.57E-04	3.71

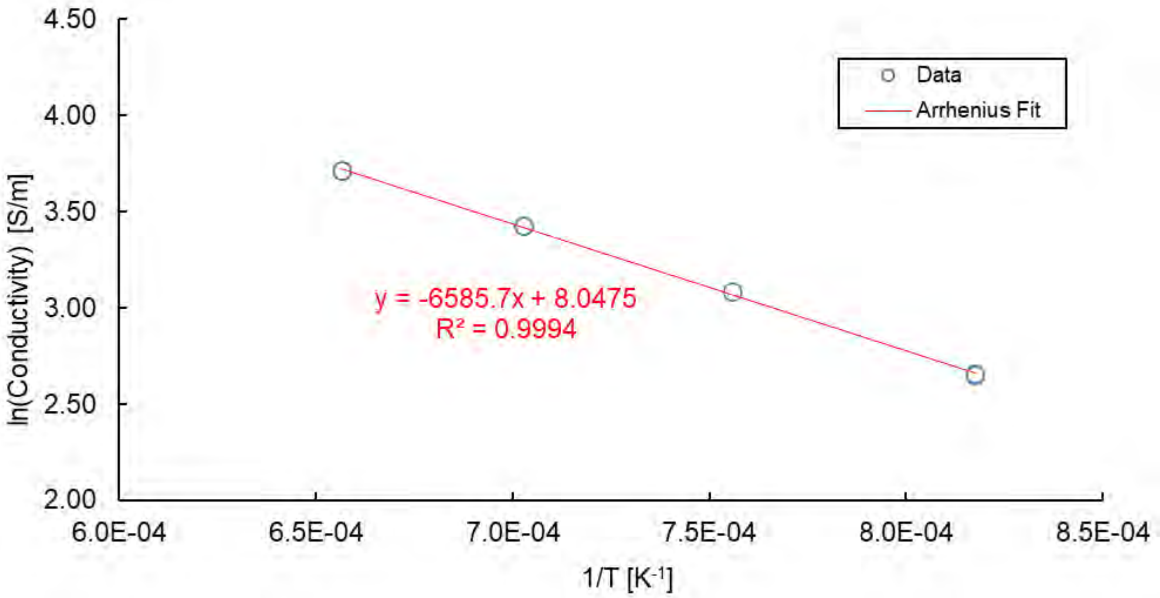

Figure F.8. Electrical Conductivity-Temperature Data and Arrhenius Equation Fit for Glass LP4-08-1

F.9 Glass LP4-09 Electrical Conductivity Data

Table F.9. Electrical Conductivity Data for Glass LP4-09

Temperature, °C	Conductivity, S/m	1/(T+273.15), K^{-1}	ln(ε, S/m)
950	25.45	8.18E-04	3.24
950	25.40	8.18E-04	3.23
1050	38.16	7.56E-04	3.64
1050	38.14	7.56E-04	3.64
1150	51.92	7.03E-04	3.95
1150	51.79	7.03E-04	3.95
1250	64.39	6.57E-04	4.16
1250	64.32	6.57E-04	4.16

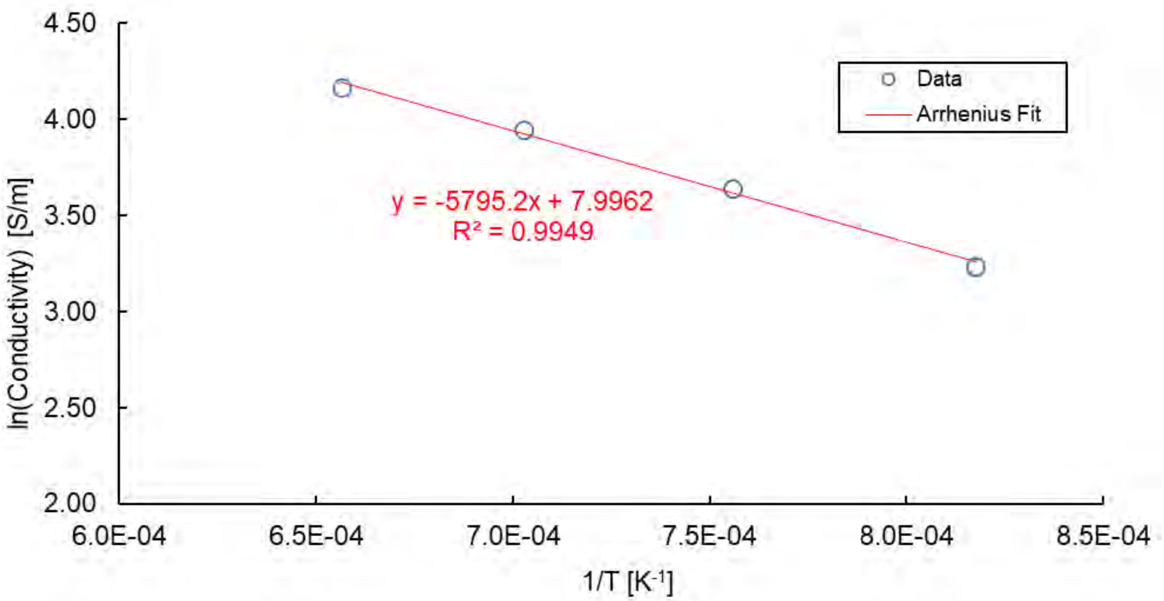

Figure F.9. Electrical Conductivity-Temperature Data and Arrhenius Equation Fit for Glass LP4-09

F.10 Glass LP4-10 Electrical Conductivity Data

Table F.10. Electrical Conductivity Data for Glass LP4-10

Temperature, °C	Conductivity, S/m	1/(T+273.15), K^{-1}	ln(ε, S/m)
950	25.93	8.18E-04	3.26
950	25.81	8.18E-04	3.25
1050	36.97	7.56E-04	3.61
1050	36.89	7.56E-04	3.61
1150	47.46	7.03E-04	3.86
1150	47.36	7.03E-04	3.86
1250	55.66	6.57E-04	4.02
1250	55.06	6.57E-04	4.01

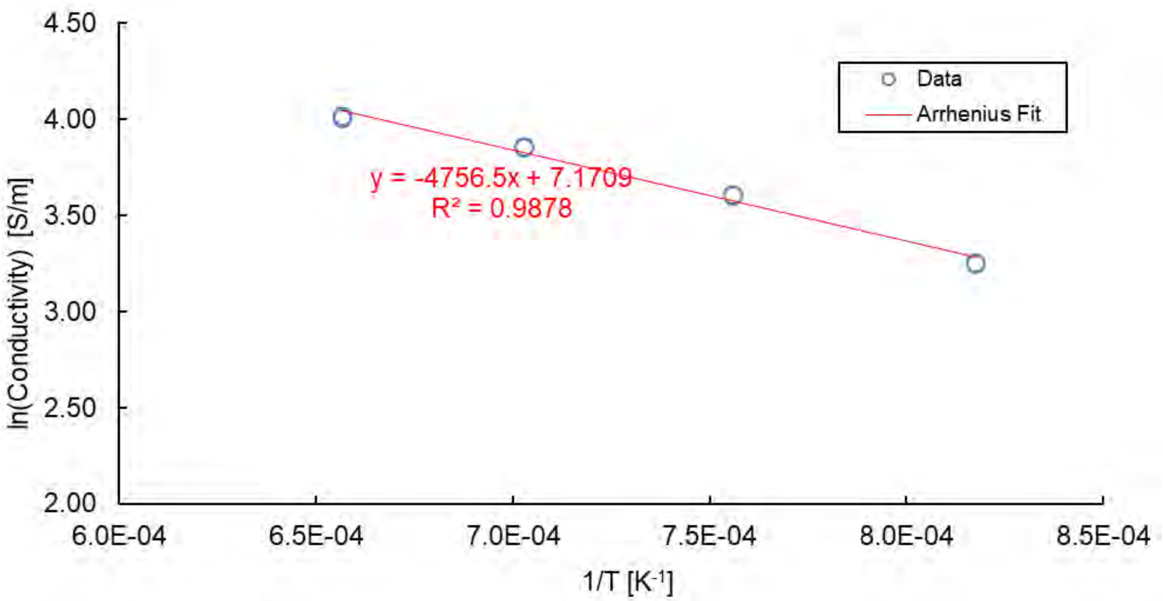

Figure F.10. Electrical Conductivity-Temperature Data and Arrhenius Equation Fit or Glass LP4-10

F.11 Glass LP4-11 Electrical Conductivity Data

Table F.11. Electrical Conductivity Data for Glass LP4-11

Temperature, °C	Conductivity, S/m	1/(T+273.15), K^{-1}	ln(ε, S/m)
950	11.93	8.18E-04	2.48
950	11.87	8.18E-04	2.47
1050	18.23	7.56E-04	2.90
1050	18.20	7.56E-04	2.90
1150	25.16	7.03E-04	3.23
1250	32.53	6.57E-04	3.48

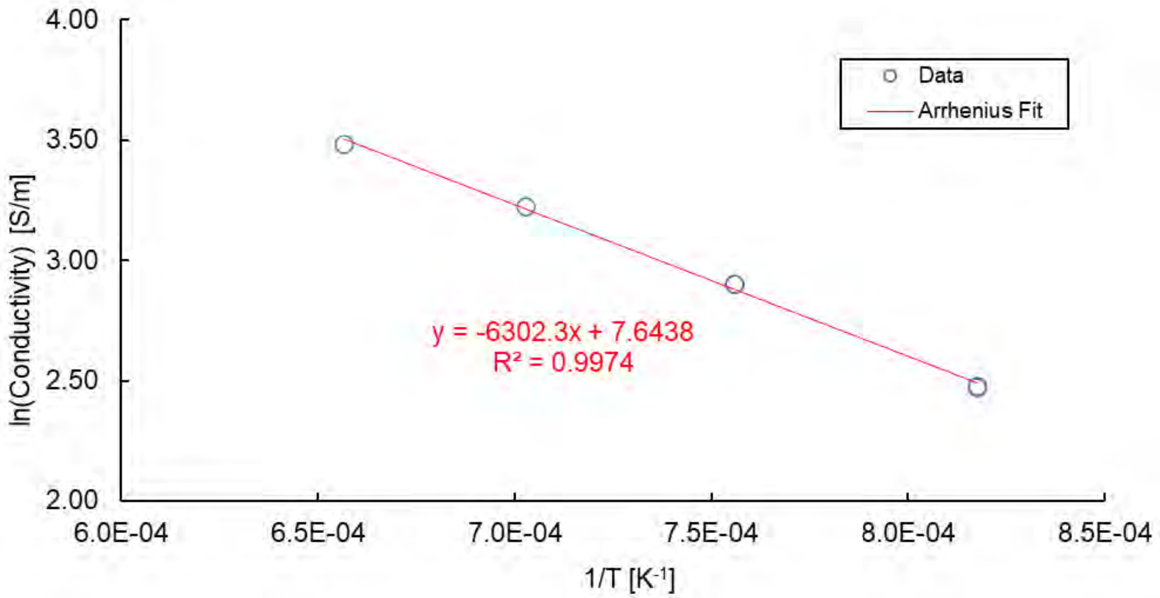

Figure F.11. Electrical Conductivity-Temperature Data and Arrhenius Equation Fit for Glass LP4-11

F.12 Glass LP4-12 Electrical Conductivity Data

Table F.12.Electrical Conductivity Data for Glass LP4-12

Temperature, °C	Conductivity, S/m	1/(T+273.15), K^{-1}	ln(ε, S/m)
950	13.12	8.18E-04	2.57
950	13.06	8.18E-04	2.57
1050	20.66	7.56E-04	3.03
1050	20.60	7.56E-04	3.03
1150	29.28	7.03E-04	3.38
1250	38.37	6.57E-04	3.65
1250	38.48	6.57E-04	3.65

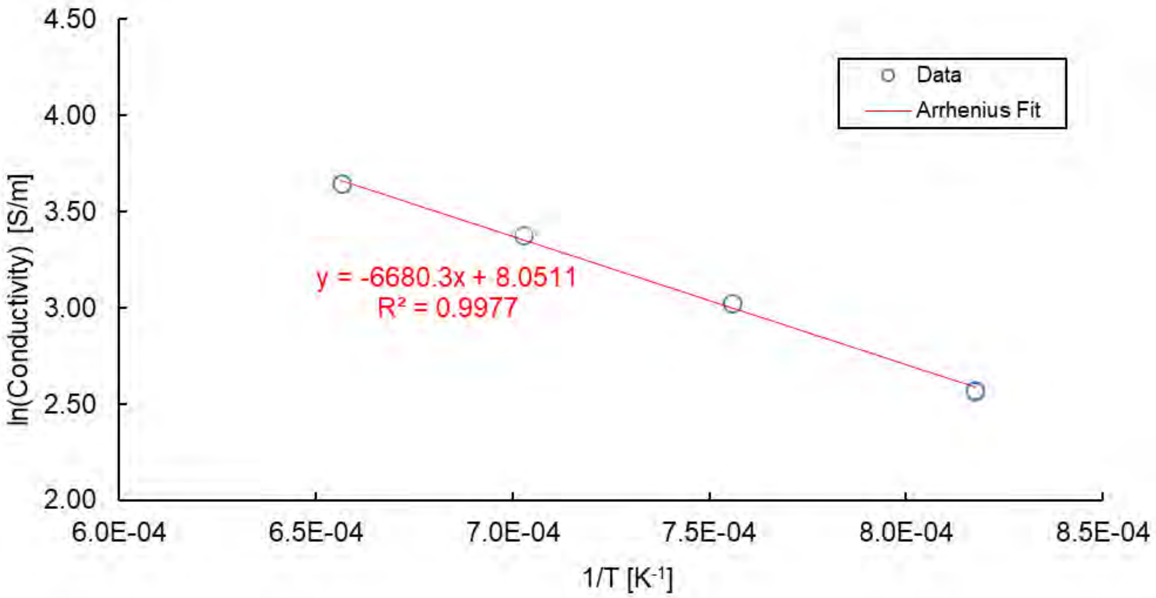

Figure F.12. Electrical Conductivity-Temperature Data and Arrhenius Equation Fit for Glass LP4-12

F.13 Glass LP4-13 Electrical Conductivity Data

Table F.13.Electrical Conductivity Data for Glass LP4-13

Temperature, °C	Conductivity, S/m	1/(T+273.15), K^{-1}	ln(ε, S/m)
950	26.27	8.18E-04	3.27
950	26.19	8.18E-04	3.27
1050	39.21	7.56E-04	3.67
1050	39.10	7.56E-04	3.67
1150	52.42	7.03E-04	3.96
1250	65.75	6.57E-04	4.19
1250	65.76	6.57E-04	4.19

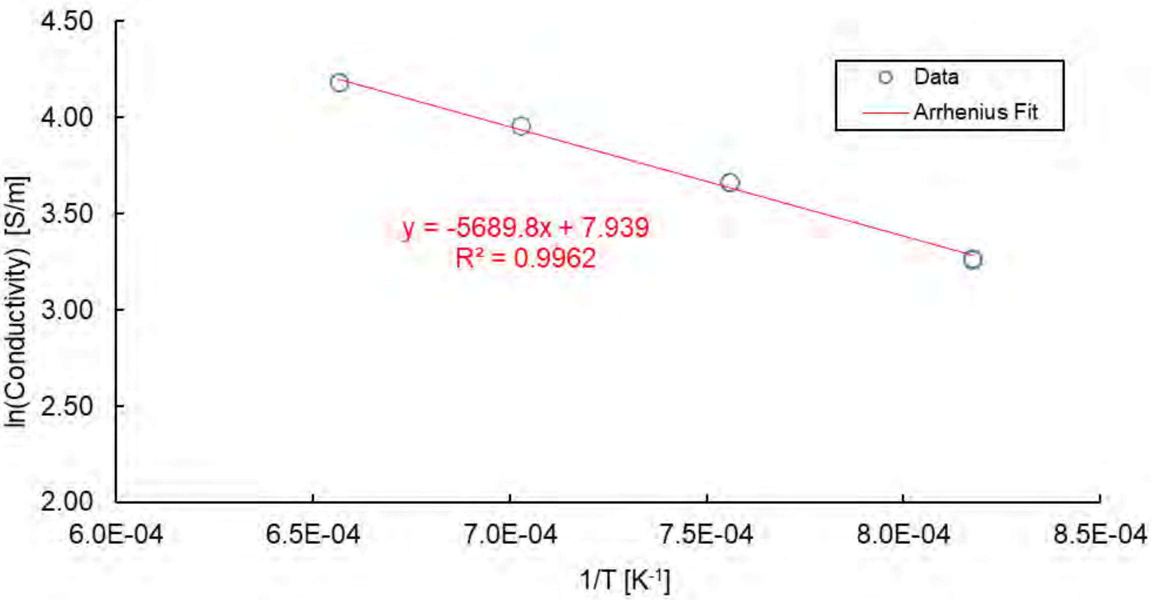

Figure F.13. Electrical Conductivity-Temperature Data and Arrhenius Equation Fit for Glass LP4-13

F.14 Glass LP4-14 Electrical Conductivity Data

Table F.14.Electrical Conductivity Data for Glass LP4-14

Temperature, °C	Conductivity, S/m	1/(T+273.15), K^{-1}	ln(ε, S/m)
950	27.09	8.18E-04	3.30
950	27.01	8.18E-04	3.30
1050	40.36	7.56E-04	3.70
1050	40.25	7.56E-04	3.70
1150	54.11	7.03E-04	3.99
1250	68.07	6.57E-04	4.22
1250	68.05	6.57E-04	4.22

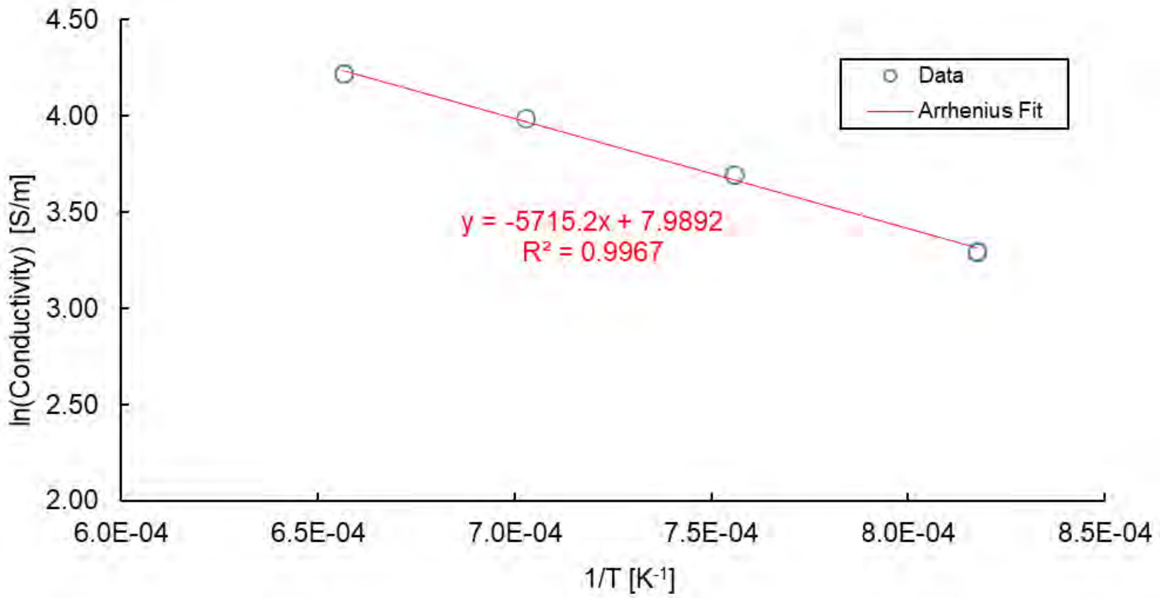

Figure F.14. Electrical Conductivity-Temperature Data and Arrhenius Equation Fit for Glass LP4-14

F.15 Glass LP4-15 Electrical Conductivity Data

Table F.15. Electrical Conductivity Data for Glass LP4-15

Temperature, °C	Conductivity, S/m	1/(T+273.15), K^{-1}	ln(ε, S/m)
950	27.95	8.18E-04	3.33
950	27.90	8.18E-04	3.33
1050	38.76	7.56E-04	3.66
1050	38.64	7.56E-04	3.65
1150	49.67	7.03E-04	3.91
1150	49.62	7.03E-04	3.90
1250	60.27	6.57E-04	4.10
1250	60.27	6.57E-04	4.10

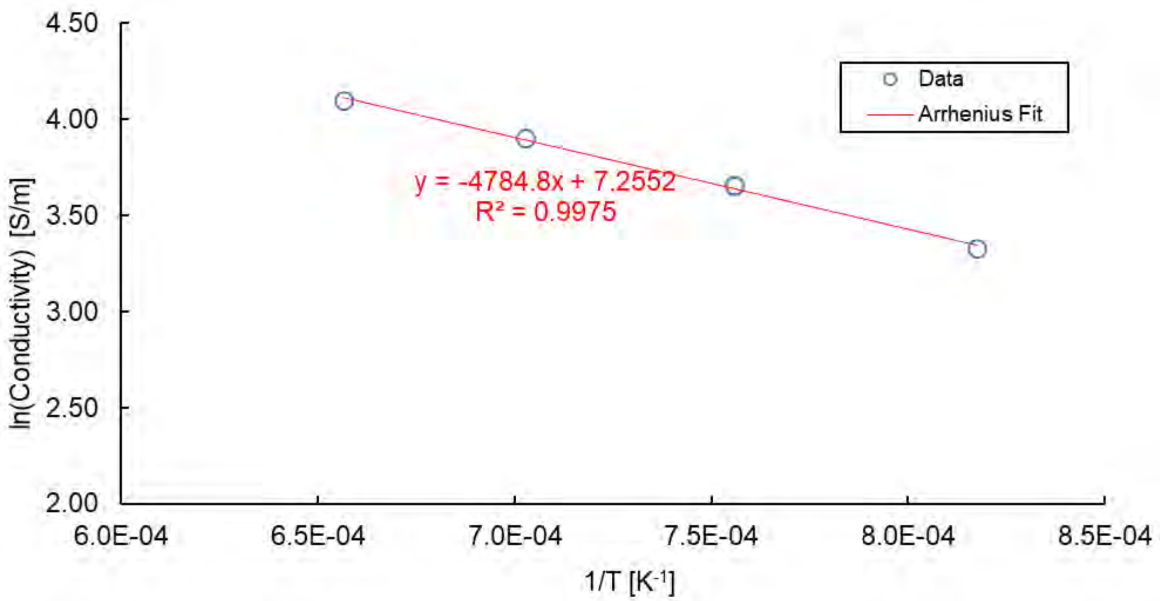

Figure F.15. Electrical Conductivity-Temperature Data and Arrhenius Equation Fit for Glass LP4-15

F.16 Glass LP4-16 Electrical Conductivity Data

Table F.16.Electrical Conductivity Data for Glass LP4-16

Temperature, °C	Conductivity, S/m	1/(T+273.15), K^{-1}	ln(ε, S/m)
950	21.25	8.18E-04	3.06
950	21.20	8.18E-04	3.05
1050	31.17	7.56E-04	3.44
1050	31.08	7.56E-04	3.44
1150	42.29	7.03E-04	3.74
1250	53.68	6.57E-04	3.98
1250	53.69	6.57E-04	3.98

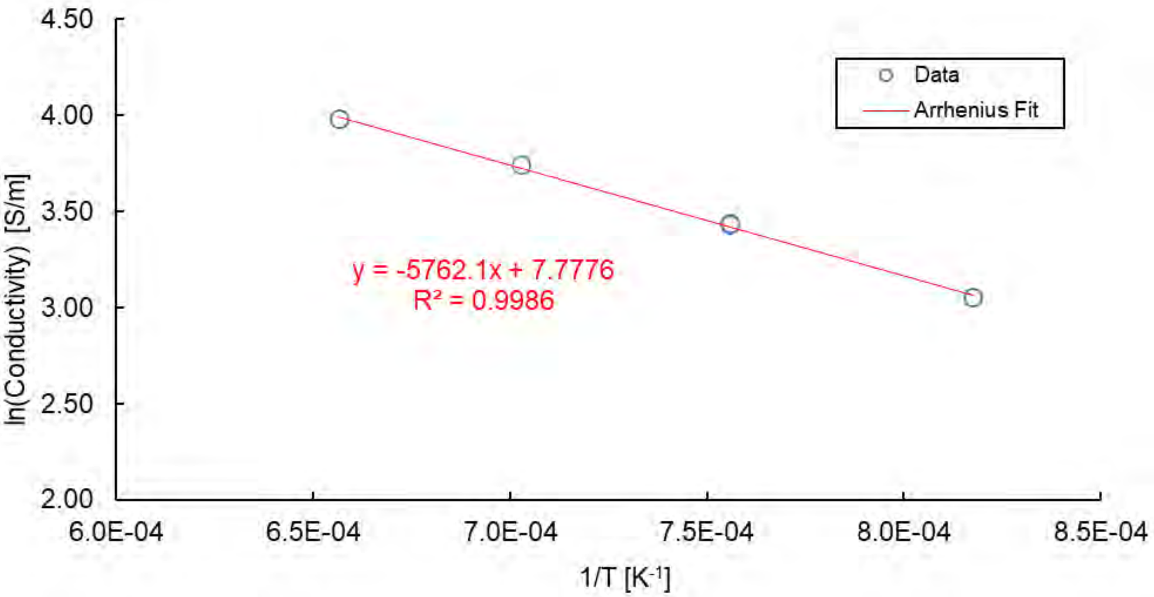

Figure F.16. Electrical Conductivity-Temperature Data and Arrhenius Equation Fit for Glass LP4-16

F.17 Glass LP4-17 Electrical Conductivity Data

Table F.17. Electrical Conductivity Data for Glass LP4-17

Temperature, °C	Conductivity, S/m	1/(T+273.15), K^{-1}	ln(ε, S/m)
950	15.56	8.18E-04	2.74
950	15.50	8.18E-04	2.74
1050	24.92	7.56E-04	3.22
1050	24.84	7.56E-04	3.21
1150	35.51	7.03E-04	3.57
1150	35.45	7.03E-04	3.57
1250	46.56	6.57E-04	3.84
1250	46.70	6.57E-04	3.84

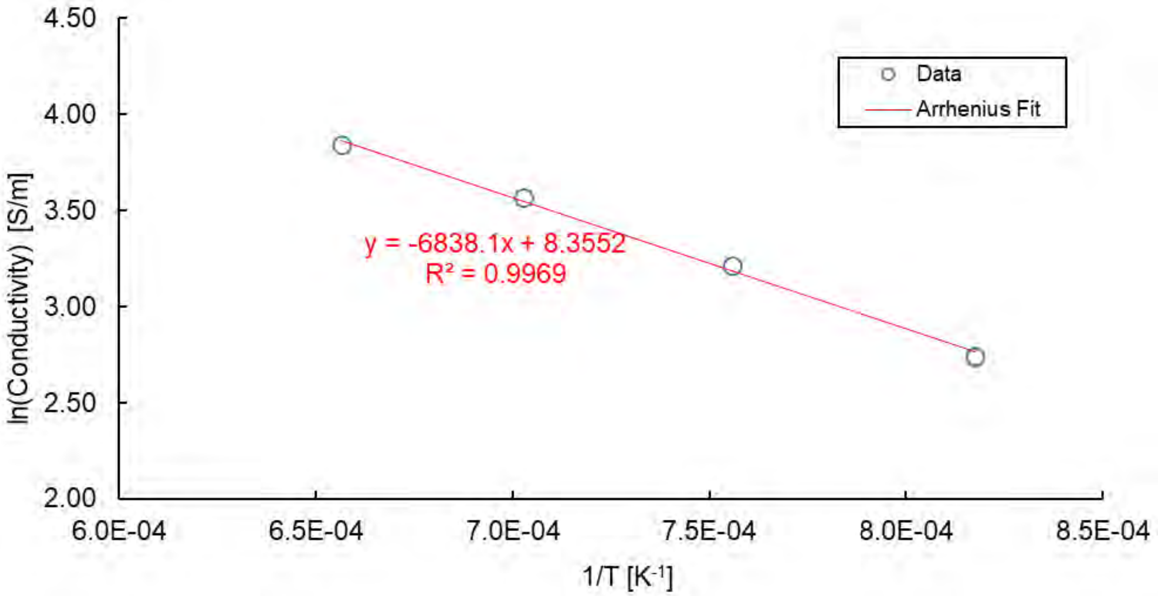

Figure F.17. Electrical Conductivity-Temperature Data and Arrhenius Equation Fit for Glass LP4-17

F.18 Glass LP4-18 Electrical Conductivity Data

Table F.18.Electrical Conductivity Data for Glass LP4-18

Temperature, °C	Conductivity, S/m	1/(T+273.15), K^{-1}	ln(ε, S/m)
950	13.45	8.18E-04	2.60
950	13.40	8.18E-04	2.60
1050	22.32	7.56E-04	3.11
1050	22.28	7.56E-04	3.10
1150	33.24	7.03E-04	3.50
1150	33.11	7.03E-04	3.50
1250	45.39	6.57E-04	3.82
1250	45.52	6.57E-04	3.82

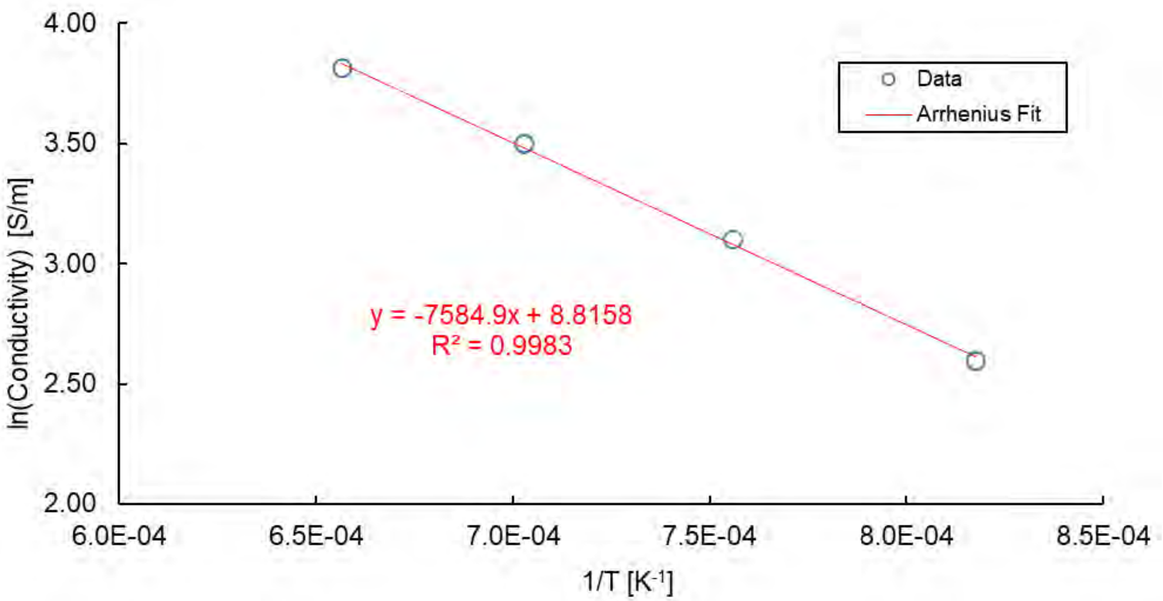

Figure F.18. Electrical Conductivity-Temperature Data and Arrhenius Equation Fit for Glass LP4-18

F.19 Glass LP4-19 Electrical Conductivity Data

Table F.19.Electrical Conductivity Data for Glass LP4-19

Temperature, °C	Conductivity, S/m	1/(T+273.15), K^{-1}	ln(ε, S/m)
950	23.00	8.18E-04	3.14
950	22.91	8.18E-04	3.13
1050	33.26	7.56E-04	3.50
1050	33.10	7.56E-04	3.50
1150	44.01	7.03E-04	3.78
1150	43.96	7.03E-04	3.78
1250	54.67	6.57E-04	4.00
1250	54.71	6.57E-04	4.00

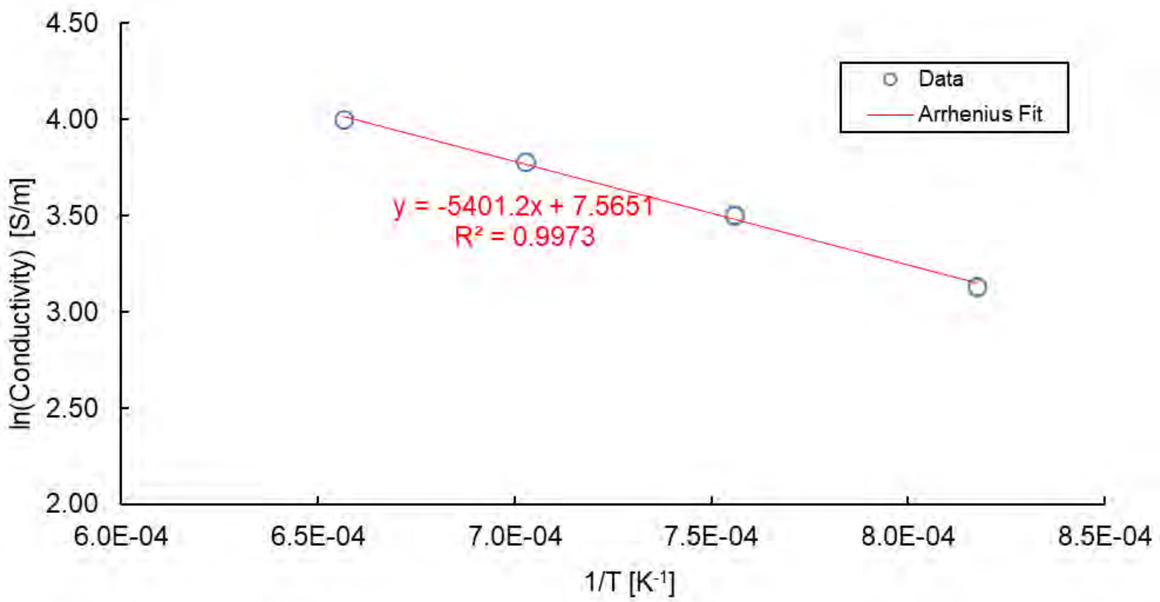

Figure F.19. Electrical Conductivity-Temperature Data and Arrhenius Equation Fit for Glass LP4-19

F.20 Glass LP4-20 Electrical Conductivity Data

Table F.20. Electrical Conductivity Data for Glass LP4-20

Temperature, °C	Conductivity, S/m	1/(T+273.15), K^{-1}	ln(ε, S/m)
950	23.65	8.18E-04	3.16
950	23.57	8.18E-04	3.16
1050	34.76	7.56E-04	3.55
1050	34.64	7.56E-04	3.54
1150	46.58	7.03E-04	3.84
1250	59.06	6.57E-04	4.08

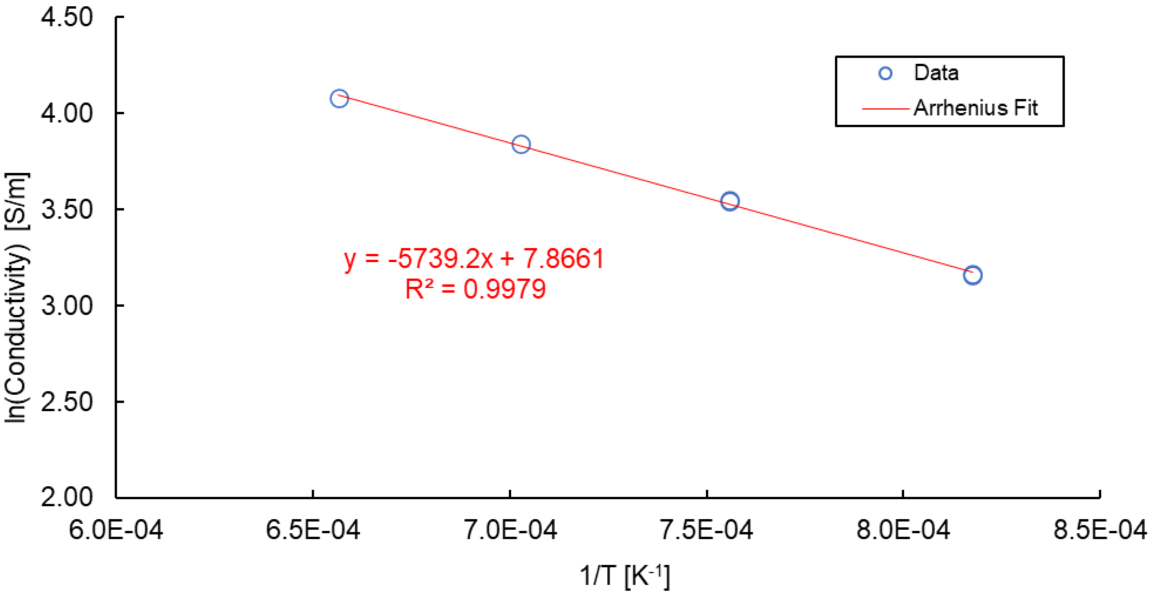

Figure F.20. Electrical Conductivity-Temperature Data and Arrhenius Equation Fit for Glass LP4-20

F.21 Glass LP4-21 Electrical Conductivity Data

Table F.21.Electrical Conductivity Data for Glass LP4-21

Temperature, °C	Conductivity, S/m	1/(T+273.15), K^{-1}	ln(ε, S/m)
950	9.22	8.18E-04	2.22
950	9.18	8.18E-04	2.22
1050	15.92	7.56E-04	2.77
1050	15.89	7.56E-04	2.77
1150	24.31	7.03E-04	3.19
1250	32.93	6.57E-04	3.49
1250	33.02	6.57E-04	3.50

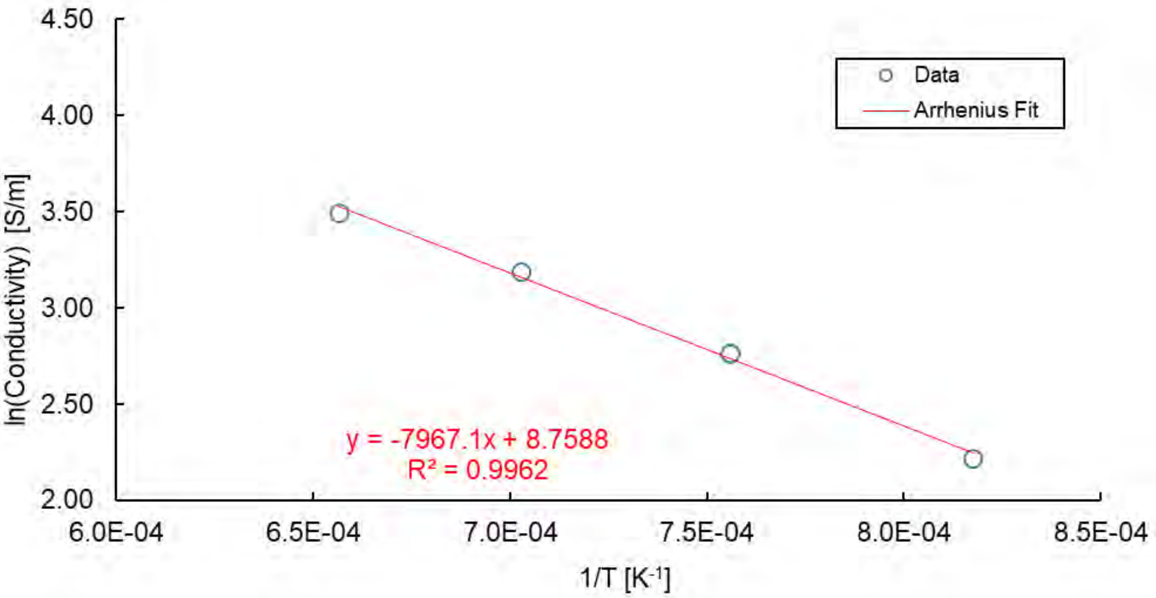

Figure F.21. Electrical Conductivity-Temperature Data and Arrhenius Equation Fit for Glass LP4-21

F.22 Glass LP4-22 Electrical Conductivity Data

Table F.22.Electrical Conductivity Data for Glass LP4-22

Temperature, °C	Conductivity, S/m	1/(T+273.15), K^{-1}	ln(ε, S/m)
950	25.09	8.18E-04	3.22
950	25.02	8.18E-04	3.22
1050	34.93	7.56E-04	3.55
1050	34.83	7.56E-04	3.55
1150	44.93	7.03E-04	3.81
1250	54.95	6.57E-04	4.01
1250	54.88	6.57E-04	4.01

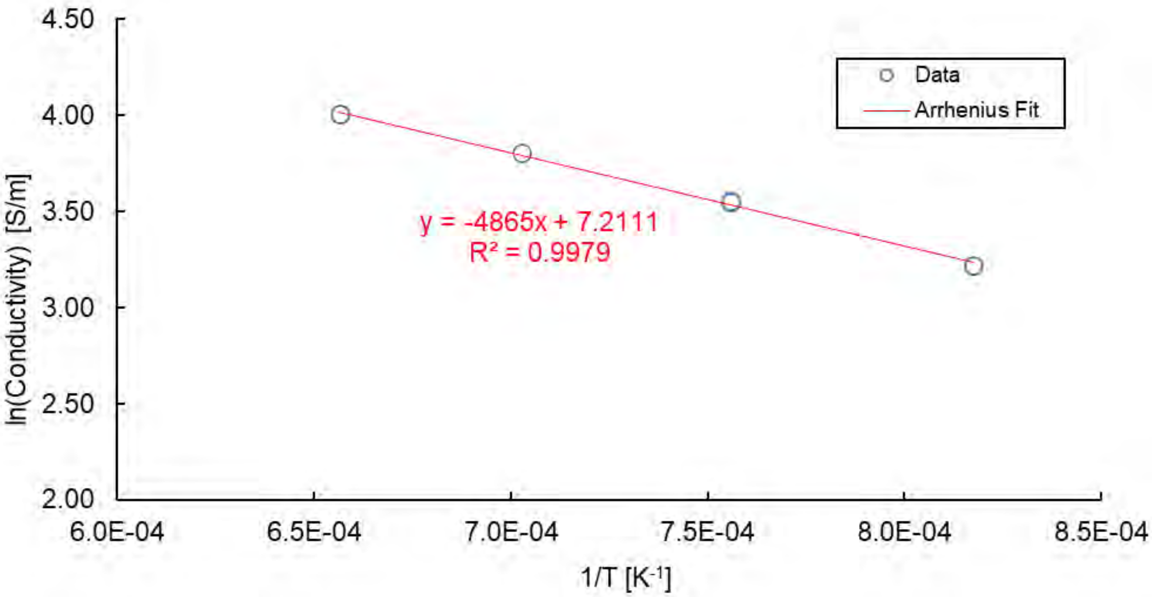

Figure F.22. Electrical Conductivity-Temperature Data and Arrhenius Equation Fit for Glass LP4-22

F.23 Glass LP4-23-1 Electrical Conductivity Data

Table F.23.Electrical Conductivity Data for Glass LP4-23-1

Temperature, °C	Conductivity, S/m	1/(T+273.15), K^{-1}	ln(ε, S/m)
950	21.45	8.18E-04	3.07
950	21.37	8.18E-04	3.06
1050	32.56	7.56E-04	3.48
1050	32.49	7.56E-04	3.48
1150	44.60	7.03E-04	3.80
1250	57.18	6.57E-04	4.05
1250	57.20	6.57E-04	4.05

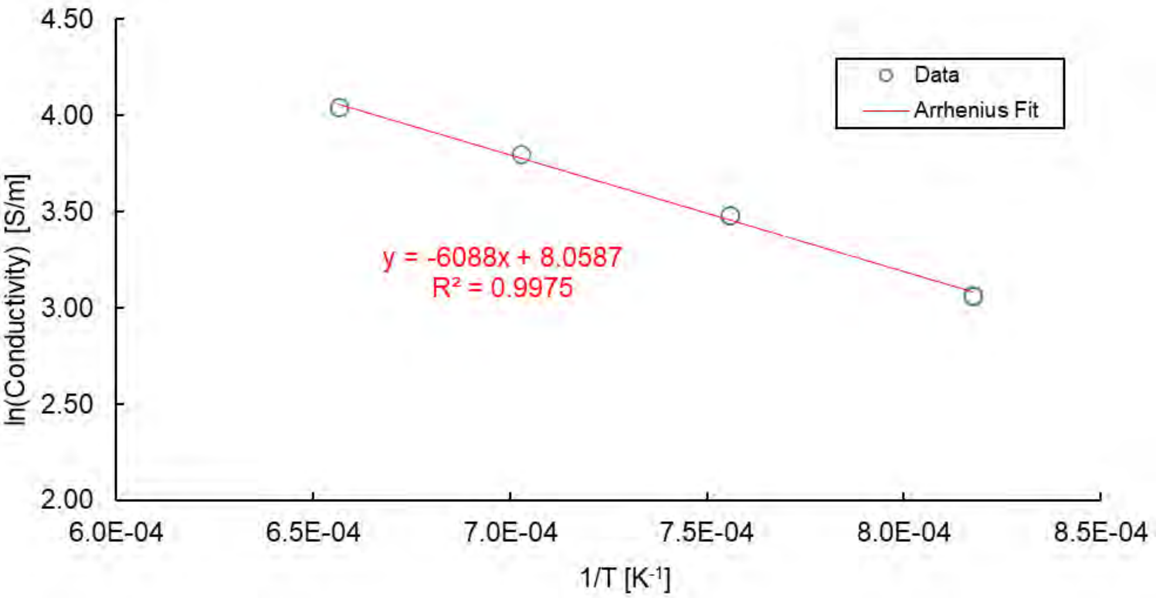

Figure F.23. Electrical Conductivity-Temperature Data and Arrhenius Equation Fit for Glass LP4-23-1

F.24 Glass LP4-24 Electrical Conductivity Data

Table F.24.Electrical Conductivity Data for Glass LP4-24

Temperature, °C	Conductivity, S/m	1/(T+273.15), K^{-1}	ln(ε, S/m)
950	23.07	8.18E-04	3.14
950	23.00	8.18E-04	3.14
1050	33.92	7.56E-04	3.52
1050	33.74	7.56E-04	3.52
1150	45.06	7.03E-04	3.81
1150	45.08	7.03E-04	3.81
1250	56.43	6.57E-04	4.03
1250	56.45	6.57E-04	4.03

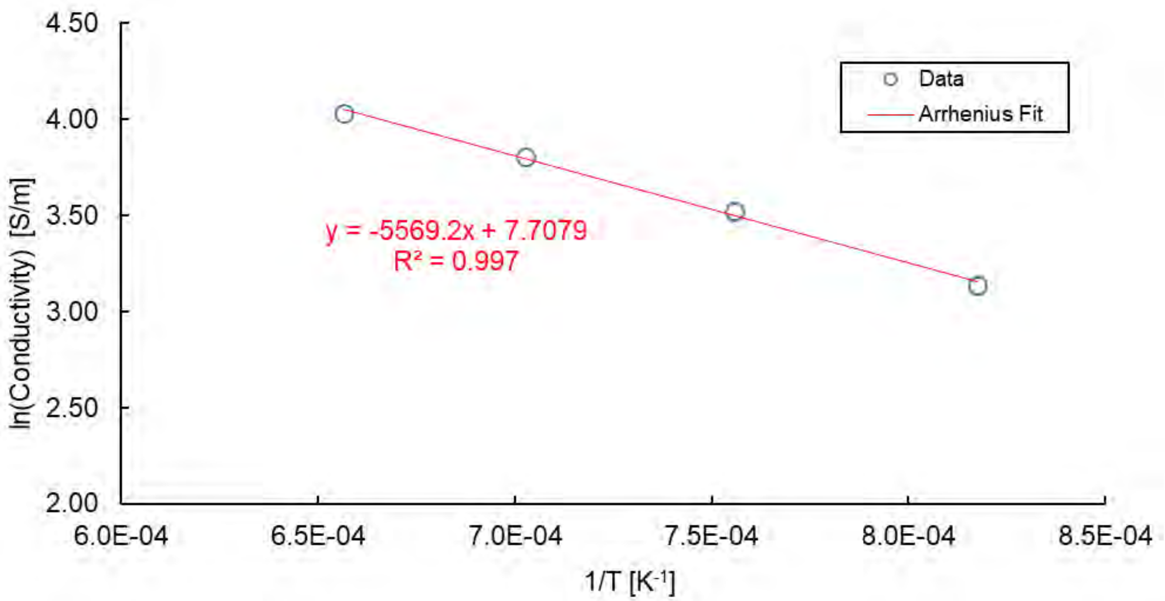

Figure F.24. Electrical Conductivity-Temperature Data and Arrhenius Equation Fit for Glass LP4-24

F.25 Glass LP4-25-1 Electrical Conductivity Data

Table F.25. Electrical Conductivity Data for Glass LP4-25-1

Temperature, °C	Conductivity, S/m	1/(T+273.15), K^{-1}	ln(ε, S/m)
950	12.57	8.18E-04	2.53
950	11.91	8.18E-04	2.48
1050	22.71	7.56E-04	3.12
1050	22.53	7.56E-04	3.11
1150	35.38	7.03E-04	3.57
1250	49.32	6.57E-04	3.90
1250	49.45	6.57E-04	3.90

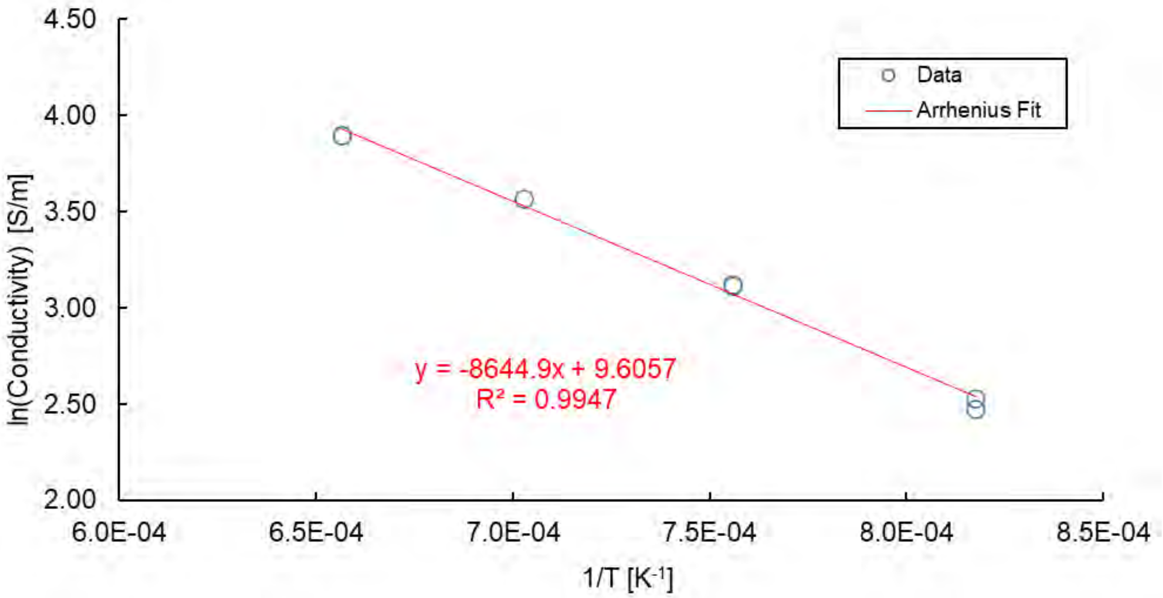

Figure F.25. Electrical Conductivity-Temperature Data and Arrhenius Equation Fit

Pacific Northwest
National Laboratory

902 Battelle Boulevard
P.O. Box 999
Richland, WA 99354
1-888-375-PNNL (7665)

www.pnnl.gov